TENNESSEE VALLEY AUTHORITY - BROWNS FERRY NUCLEAR PLANT (BFN) -
TECHNICAL SPECIFICATIONS (TS) CHANGES TS-431 AND TS-418
EXTENDED POWER UPRATE (EPU) - UNITS 1, 2, and 3

ENCLOSURE 2

GE-NE-0000-0049-6652-01NP
General Electric Boiling Water Reactor Steam Dryer Scale Model Test Based Fluctuating Load Definition Methodology - March 2006 Benchmark Report

- NON-PROPRIETARY VERSION -

GE Energy
Nuclear
1989 Little Orchard Road
San Jose, CA 95125

GE-NE-0000-0049-6652-01NP
Revision 0
Class I
March 2006

Non-Proprietary Information

General Electric Boiling Water Reactor Steam Dryer Scale Model Test Based Fluctuating Load Definition Methodology – March 2006 Benchmark Report

Principal Contributor

Daniel Sommerville

INFORMATION NOTICE

This document is the GE non-proprietary version of GE-NE-0000-0049-6652-01P which has the proprietary information removed.

Portions of the document that have been removed are indicated by white space with open and closed bracket as shown here [[ ]].

IMPORTANT NOTICE REGARDING CONTENTS OF THIS REPORT PLEASE READ CAREFULLY

The information contained in this document is furnished for the purpose of obtaining NRC approval of the licensing requirements to expand the power/flow operating range to allow operation with the licensed thermal power up to 120% of original thermal power. The only undertakings of General Electric Company with respect to information in this document are contained in contracts between General Electric Company and participating utilities, and nothing contained in this document shall be construed as changing those contracts. The use of this information by anyone other than that for which it is intended is not authorized; and with respect to **any unauthorized use**, General Electric Company makes no representation or warranty, and assumes no liability as to the completeness, accuracy, or usefulness of the information contained in this document.

ACKNOWLEDGEMENTS

The BWR scale model test program is a first of a kind effort that has involved a substantial amount of discovery and effort. The team assembled to solve this problem was truly multi-disciplinary. Without the assistance and support of the entire team this effort could not have been a success. We wish to thank and acknowledge the following people for their substantial contributions to this effort.

Technical Guidance and Review:	Dr. Robert Blevins, Consultant Mr. John Lynch, GE Energy Dr. Fred Moody, Consultant Mr. Daniel Pappone, GE Energy
Acoustic Modeling:	Dr. Eike Brechlin, LMS Mr. David Galbally, GE Energy Mr. Mathieu Jonckheere, LMS
Testing and Data Analysis:	Mr. Tom DeBrabandere, LMS Mr. Greg Falbo, LMS Mr. Quentin Guzek, LMS Mr. Michael Nieheisel, LMS Mr. Matthew O'Connor, GE Energy Mr. Elijio Prado, GE Energy
CFD Analysis:	Dr. Robert Malone, GE Energy
Test Setup & Support:	Mr. Steve DelGrande, GE Energy Mr. Henry Domec, GE Energy Mr. Teddy McDowell, GE Energy Mr. Richard Turnwall, GE Energy Mr. Dwight Springer, GE Energy Mr. Steve Wilson, GE Energy
Mechanical Design & Drafting:	Mr. Tom Lewis, GE Energy Mr. Paul Ng, GE Energy Mr. Jonathon Quach, GE Energy Mr. Jeff Sanders, GE Energy Mr. Ralph Walker, GE Energy
Project Management:	Mr. Alton Jenkins, GE Energy Mr. Edward Skeehan, GE Energy

Table of Contents

List of Tables

List of Figures

Nomenclature

ABWR	Advanced Boiling Water Reactor
AC	Alternating Current
BWR	Boiling Water Reactor
CFD	Computational Fluid Dynamics
CFM	Cubic Feet per Minute
DC	Direct Current
DRF	Design Record File
EPU	Extended Power Uprate
ERV	Electromatic Relief Valve
FEM	Finite Element Model
FIV	Flow Induced Vibration
FRF	Frequency Response Function
FSI	Fluid-Structure Interaction
GE	General Electric Company
GENE	General Electric Nuclear Energy
HPCI	High Pressure Coolant Injection
ID	Inner Diameter
IGSCC	Intergranular Stress Corrosion Cracking
IVVI	In Vessel Visual Examination
LES	Large Eddy Simulation

Nomenclature, contd.

LMS	Lueven Measurement Systems
MDOF	Multiple Degree of Freedom System
MS	Main Steam
MSIV	Main Steam Isolation Valves
MSL	Main Steam Line
ODS	Operational Deflection Shape
OLTP	Original Licensed Thermal Power
PC	Personal Computer
PSD	Power Spectral Density
QC	Quad Cities
QC1	Quad Cities Unit 1
QC2	Quad Cities Unit 2
RANS	Reynolds Averaged Navier Stokes
RCIC	Reactor Core Isolation Cooling
RMS	Root Mean Square
RPM	Revolutions per Minute
RPV	Reactor Pressure Vessel
SDOF	Single Degree of Freedom System
SMT	Scale Model Test

Nomenclature, contd.

S/RV	Safety and Relief Valves
SV	Safety Valve
TCV	Turbine Control Valves
TRV	Target Rock Valve
TSV	Turbine Stop Valves
VPF	Vane Passing Frequency
1-D	One Dimensional
3-D	Three Dimensional
c	Speed of sound in media
[c]	Damping matrix
d	Diameter of branch line and/or cavity width
E	Energy
f	Frequency of acoustic oscillation
F	Body force
[k]	Stiffness matrix
L	Length of resonating chamber
[m]	Mass matrix
M	Mach Number
n	Shear wave mode
P	Pressure

Nomenclature, contd.

P'	Fluctuating Pressure
Re	Reynolds Number
Re_p	Reynolds number using main steam line ID as the characteristic dimension
Re_v	Reynolds number using reactor pressure vessel ID as the characteristic dimension
St	Strouhal Number
t	Time
U	Mean fluid velocity
V	Velocity
X	Geometric scaling factor and/or displacement
X''	Acceleration
y	Displacement
y'	Velocity
y''	Acceleration
λ	Wavelength
ρ	Fluid Density
ω	Circular Frequency

Subscripts

A	Plant A
m	Model
QC	Quad Cities
p	Plant

Executive Summary

Several incidences of high cycle fatigue cracking have been observed in the steam dryers at Dresden and Quad Cities following operation at extended power uprate conditions for a relatively short period of time. The field experience exhibited at the Quad Cities and Dresden power plants suggests that the steam dryers at these power plants experience substantial loading during normal operation. GE has developed a scale model testing based steam dryer fluctuating load definition methodology to assist in creating load definitions for BWR steam dryers. The QC2 steam system was used as the pilot application of this methodology. GE has recently installed an instrumented steam dryer into QC2 and performed power ascension testing with this dryer. This document summarizes the conclusions made from review of currently available in-vessel data as well as the results of multiple tests performed with scale models of the QC plant configuration. Both the original and replacement dryer designs were tested. The scale model test data is benchmarked against the QC2 plant data to illustrate the ability of the GE SMT methodology to provide useful steam dryer fluctuating load definitions.

The following conclusions are made from the plant data review:

1. The fluctuating pressure load spectra shown by the in-plant measurements from four separate BWRs and the inherent similarity in BWR steam system design suggests that all BWRs can be expected to contain similar sources and exhibit steady state fluctuating load frequency content in each of the four frequency bands discussed in this document [[
   ]]. The frequencies and amplitudes exhibited by a plant specific configuration will depend primarily on the plant specific configuration. In other words, each BWR is expected to have the potential to possess frequency content in the four frequency bands listed above; however, the load amplitudes for each plant are not expected to be identical for all plants.

2. Acoustic pressure loading is considered to be the dominant excitation mechanism for steam dryer vibrations.

3. Flow turbulence and shear layer instabilities are each separately responsible for exciting portions of the frequency content observed in the vessels of four separate BWRs.

[[

]]

10. The steam dryers instrumented with strain gauges demonstrate that the dryer panels will respond to frequencies across the entire bandwidth monitored. Significant response is observed at the high frequency S/RV aero-acoustic resonance frequencies.

The following conclusions are made from the QC SMT and SMT benchmark:

1. The scale model test data matches well with the available in-plant data; therefore,

    a. The scale model test apparatus and methodology are viable tools to predict fluctuating pressure loads on the steam dryer.

    b. The conclusion that acoustic loads are the primary contribution to the fluctuating loads on the BWR steam dryer is validated.

    c. The model fluctuating pressure amplitude predictions bound the plant measurements in the 1-100 Hz frequency band at the plant scale.

d. The model can predict the onset of S/RV standpipe acoustic resonances; however, the quality of the comparison between the predicted SMT amplitude and the measured plant amplitude exhibits substantial variability.

2. The sources for the fluctuating pressures acting on the dryer can be explained by the following:

[[

3. The acoustic finite element method is a viable tool for predicting the normal modes of the steam plenum and these normal modes can be used to infer the spatial pressure distribution of the fluctuating loads acting on the steam dryer.

Additional work is on-going to improve the understanding of the excitation mechanisms and source locations as well as to improve the accuracy of the load predictions by removing conservatism in the 1-100 Hz frequency band and removing variability in the [[ ]]

1.0 Scope

This report provides the engineering basis for the scale model test apparatus and methodology used to provide BWR steam dryer load predictions. This document is intended to provide the reader with an understanding of the following items:

- General characteristics of the unsteady fluid loading observed in BWR steam systems
- Technical basis for investigating acoustic induced vibration as the dominant flow induced vibration load mechanism
- General understanding of the GE scale model test apparatus and methodology
- Use of acoustic finite element modeling to interpret SMT data
- Summary of the research findings from testing performed on a representative BWR model
- Benchmark of the GE scale model test apparatus and methodology
- Experimental uncertainty associated with the SMT predicted BWR steam dryer normal operation fluctuating loads

This document is not intended to be a detailed test report for every test performed. All scale model test data are archived at the GENE San Jose site and the test procedures are contained in the applicable design record files.

2.0 Background

This section provides background information addressing the following items:

- BWR Steam dryer failures
- Metallurgical analysis of initial steam dryer failure
- General BWR configuration
- General steam dryer configuration

2.1 Quad Cities Unit 2 Steam Dryer Failure - 2002

On July 11, 2002, Quad Cities Unit 2 (QC2) was shut down due to degradation of the steam dryer. QC2 had operated approximately 90 days under Extended Power Uprate (EPU) conditions. The plant was licensed to operate at up to 117% of original licensed thermal power (OLTP). At full power, this would increase steam flow to approximately 120% of previous OLTP flow. During the end of that 90-day period, QC2 experienced several anomalous readings related to reactor pressure, reactor water level, steam flow, and steam line moisture content.

Following plant shutdown, an inspection of the QC2 plant revealed that a steam dryer cover plate had failed (See Figure 1), allowing steam to bypass the dryer flow path. The root cause investigation of the QC2 cover plate failure identified a potential cause to be high cycle fatigue generated by the near coincidence of an acoustic natural frequency in the steam plenum and the mechanical natural frequency of the cover plate.

Subsequent to the failure observed in 2002, additional failures were observed during 2003 in the dryer outer hoods of both Quad Cities Units 1 and 2. These failures were also associated with high cycle fatigue caused by fluctuating pressure load. Figures 1 through 3 are photographs of some of the observed failures. The steam dryers at Dresden Units 2 and 3 also showed incipient cracking at the same initiation sites as the hood

cracking observed in the Quad Cities dryers, though the cracks at the Dresden units did not grow to failure.

In response to these failures, GE has initiated a development program to investigate the nature of the steam dryer loading. This effort includes model testing as well as development of acoustic and computational fluid dynamics models.

2.2 Analysis of initial steam dryer failure

A metallurgical evaluation of the fracture surfaces of the 2003 Quad Cities Unit 2 failure was performed to obtain additional information regarding the failure mechanism. The results of this evaluation support the following conclusions and observations:

1. The failure was a result of high cycle fatigue
2. Intergranular Stress Corrosion Cracking (IGSCC) was not evident
3. No chemistry, material, or manufacturing deficiencies were observed
4. The observed cracks initiated at the local stress concentration adjacent to a diagonal brace attachment weld beneath the horizontal cover plate

2.3 General BWR and Steam Dryer Configuration

Figures 4 and 5 describe the general BWR nuclear boiler arrangement. The steam dryer, shown to the right of the reactor pressure vessel in Figure 4, is located in the top of the vessel. Steam is generated in the reactor core then passes through the steam separators and steam dryer prior to leaving the vessel through the main steam nozzles. The general flow path of the reactor coolant is shown is Figure 5. The black arrows in this figure identify the water flow path and the white arrows depict the steam flow path. Figure 6 is a section view of the steam dryer from which the orientation of the internal dryer banks can be seen. The chevron flow paths through the dryer vane banks remove moisture from the steam.

Liquid is removed from the steam as the flow passes through the steam separators and steam dryer; the steam leaves the dryer with a quality of approximately 99.9%. The steam exits the reactor pressure vessel through each of four separate main steam nozzles. The orientation of the main steam nozzles with respect to the steam dryer is shown in Figure 7. This figure illustrates one side of the steam dryer; as can be seen in the previous figures, the steam dryer is symmetric and the other two main steam nozzles are diametrically opposed to those shown in Figure 7. Once the steam leaves the reactor pressure vessel it is routed to the turbine through the main steam piping. The piping contains multiple elbows and flow restrictions such as: venturis, Main Steam Isolation Valves (MSIV), equalizing headers, and Turbine Control and Stop Valves (TCV, TSV). Figures 8 and 9 are schematics of a typical main steam line routing from the RPV to the turbine. Main steam line systems also have smaller diameter branch lines connected to the main steam lines such as Safety and Relief Valve (S/RV) standpipes and extraction lines for HPCI, RCIC and feedwater pump turbines. These branch lines are not shown in Figures 8 and 9. The specific dimensions of the steam piping vary according to the plant power output and balance of plant layout. The nominal main steam line piping ranges between 16 and 28 inches in diameter.

The steam in the main steam lines and steam plenum of a BWR can generally be described by the following parameters:

Pressure:	1000-1050 psig
Temperature:	540 °F
Density:	2.24 lb/ft^3
Dynamic Viscosity:	0.0459 lb/(hr-ft)
Quality:	~ 99.9 %
Sound Speed:	1600 ft/s
Average Steam Velocity in MSL:	120 ft/s – 200 ft/s

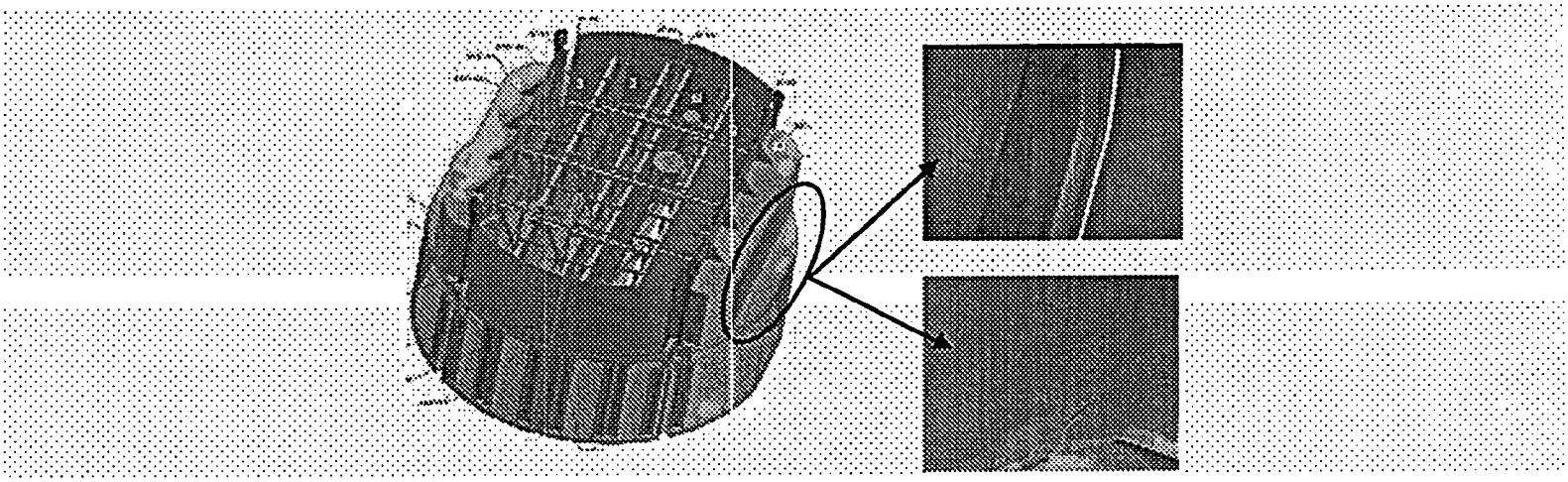

Figure 1: Photograph of cover plate failure

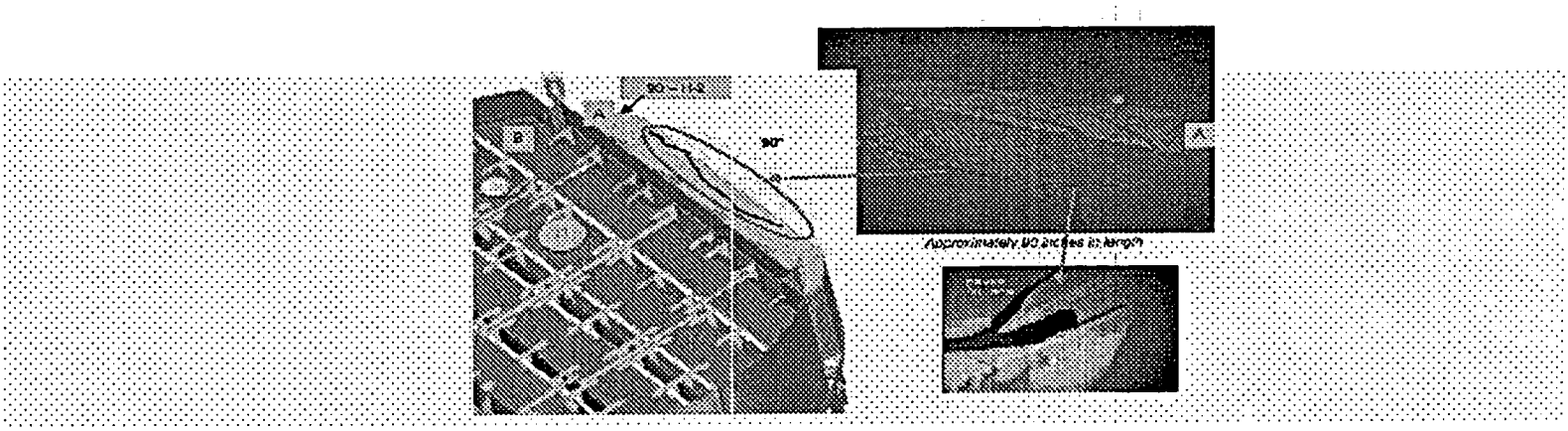

Figure 2: Photograph of vertical hood failure

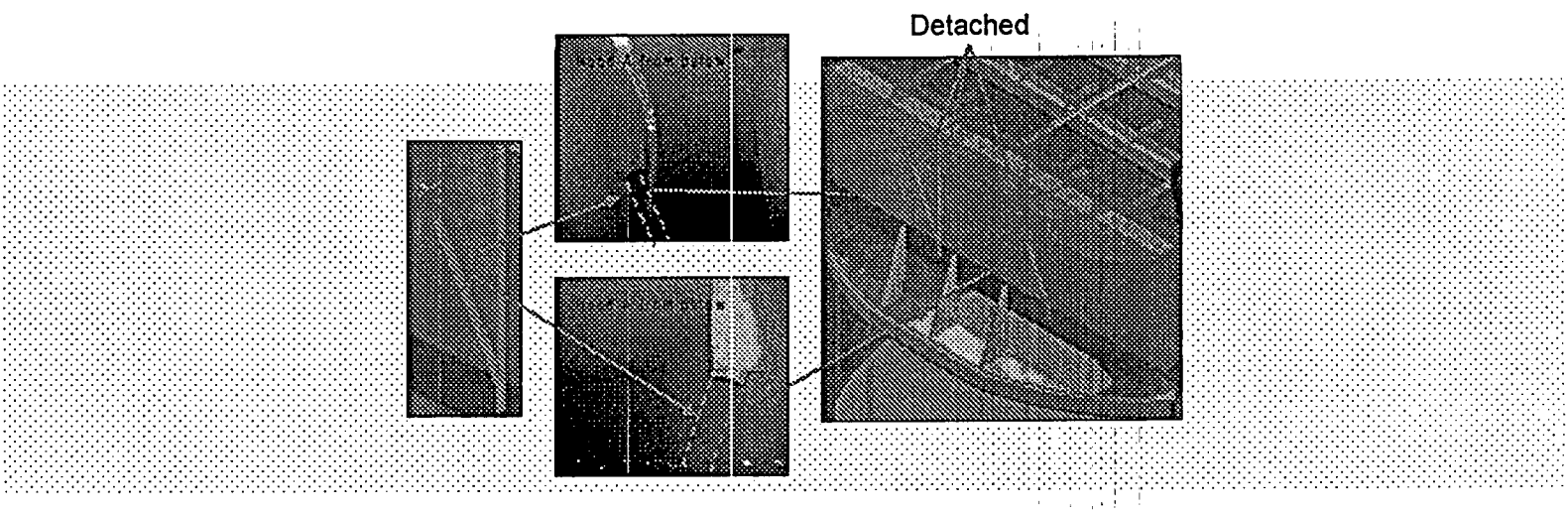

Figure 3: Photograph of diagonal brace failure

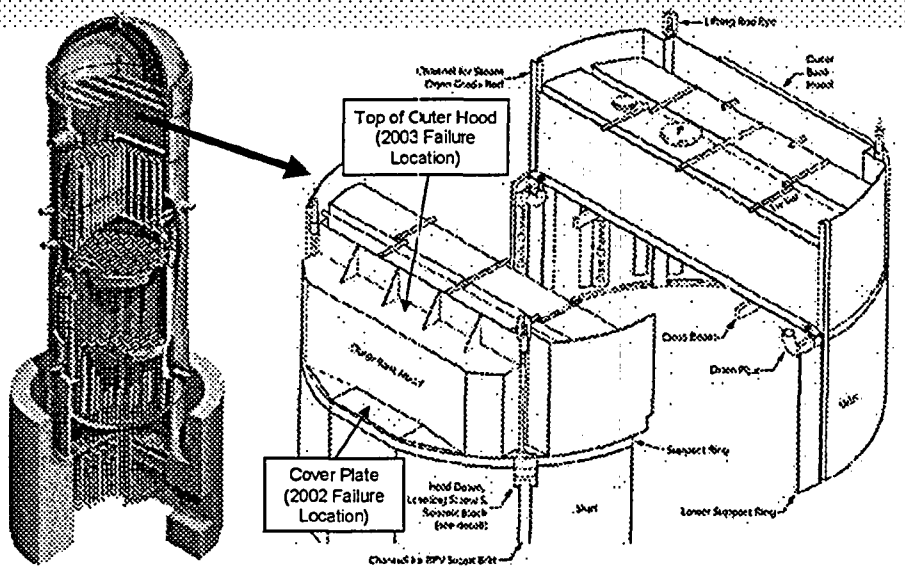

Figure 4: General schematic of the RPV and steam dryer

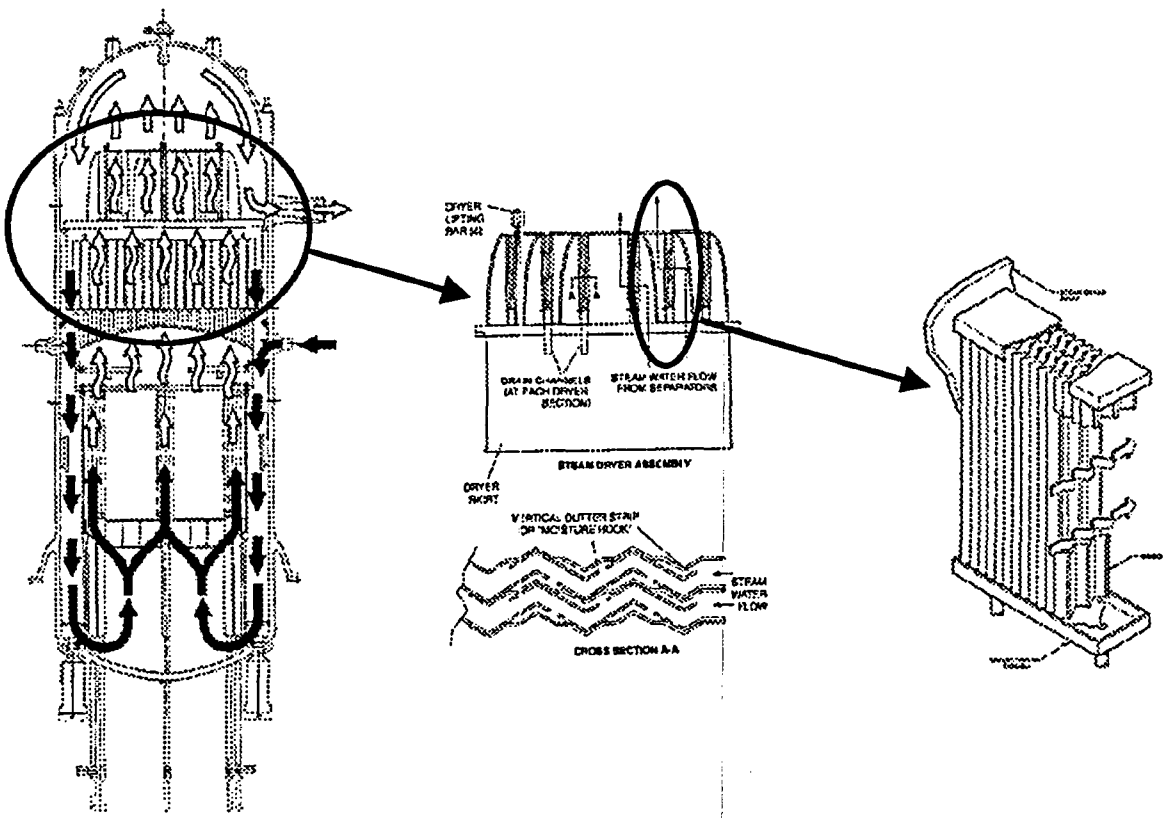

Figure 5: Coolant flow path through reactor pressure vessel

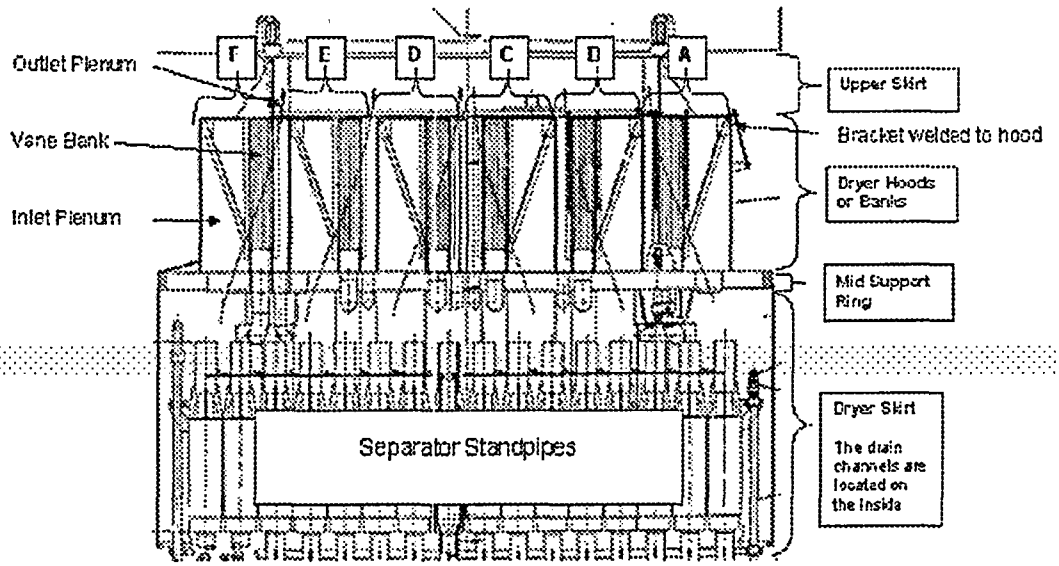

Figure 6: Section view of a BWR steam dryer and steam separator

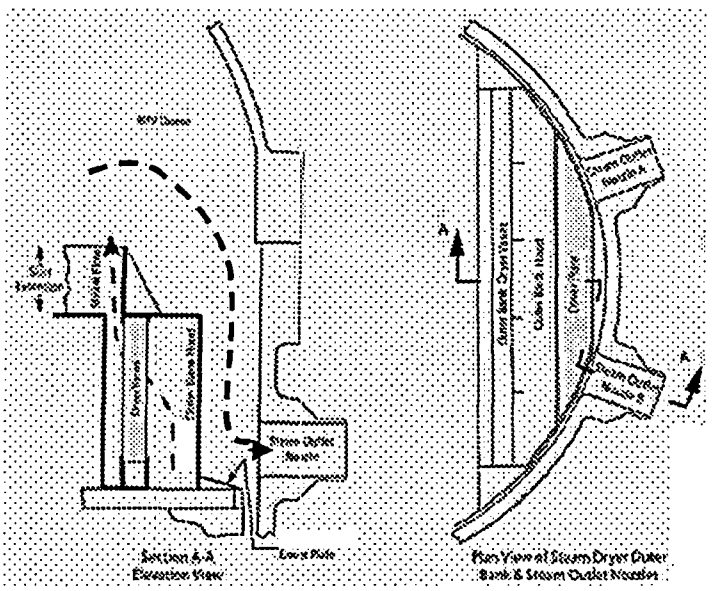

Figure 7: Orientation of main steam nozzles to steam dryer

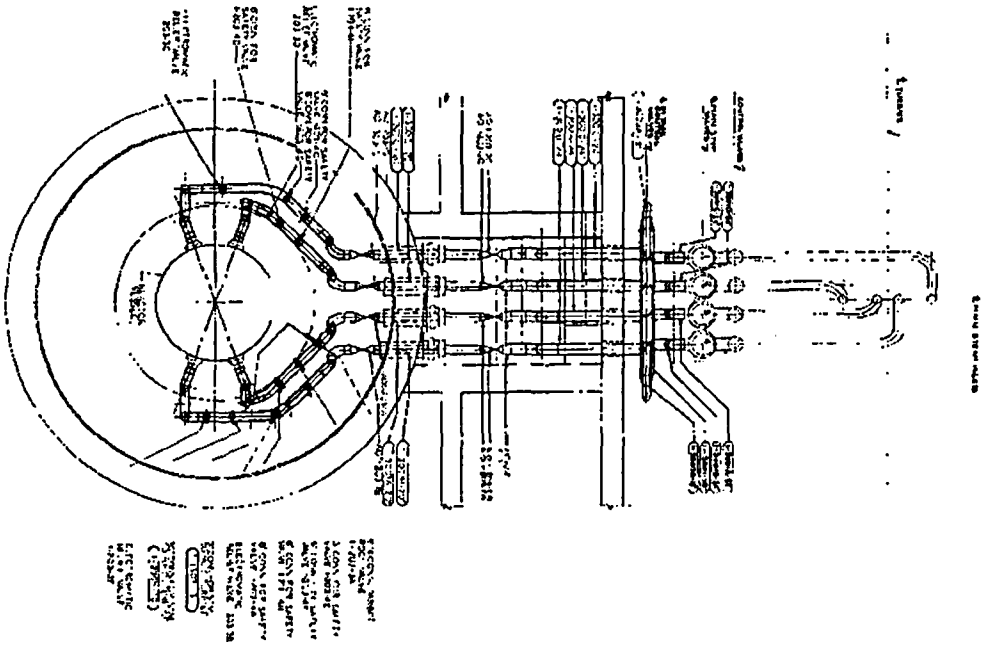

Figure 8: Plan view of a typical main steam line layout between RPV and turbine

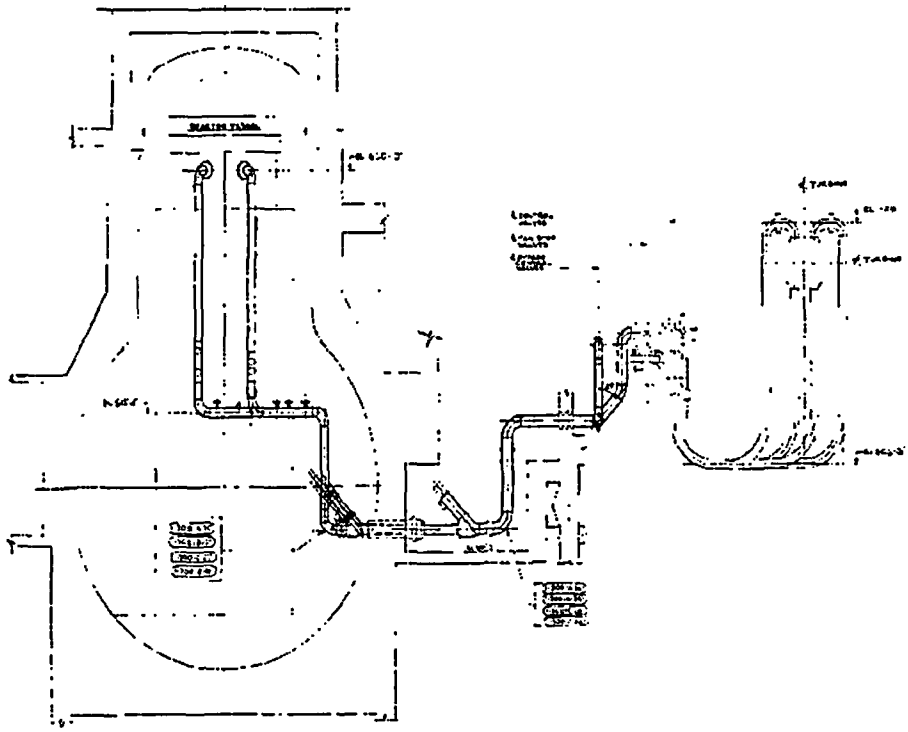

Figure 9: Elevation view of a typical main steam line layout between RPV and turbine

3.0 Fluctuating Pressure Loads on BWR Steam Dryers

This section summarizes and analyzes the existing data available from in-vessel steam dryer instrumentation programs performed during reactor startup power ascension test programs and dryer repair test programs. The results of the data characterizations are compared to identified theoretical and technical literature to characterize the important processes involved in dryer loading and vibration response. This data has been used for benchmarking of the GE scale model test program. The frequencies discussed in this section are reported at the plant scale; in Section 6 model data are presented in which the frequencies are in the model scale. The model data must be corrected to the plant scale using the frequency scaling relationships presented in Section 4.1 to be compared to the data presented in this section.

3.1 Sample Population

Although the steam dryer degradation from Quad Cities described above is the most significant in-service damage observed in BWR steam dryers, it is not the first time cracking has been observed in steam dryers. Various instances of cracking in tie bars, skirts, and hoods have been observed in reactors operating at original licensed power. This cracking has been attributed to either high cycle fatigue or IGSCC. Typically this cracking has been minor and could be addressed by stop drilling the crack or by repairing the cracked components. Although the source of the loading causing the fatigue cracks was never identified, successful repairs were installed and the components were returned to service without exhibiting any future problems. In a few cases, in-vessel instrumentation programs were conducted. The purpose of these instrumentation programs was either to monitor structural behavior for a new plant design or to demonstrate adequacy of the repair rather than to identify the nature of the loading; therefore, the instrumentation used typically consisted of strain gauges and accelerometers. In 2005 a replacement steam dryer for the Quad Cities nuclear power

station was instrumented and installed in Unit 2. This test program included more steam dryer instrumentation than any previous steam dryer power ascension test program.

Pressure transducers have been installed on the steam dryers of four of the approximately 60 operating BWRs in the commercial fleet. The data from each of these units have been reviewed for this survey. The data were obtained from two BWR/3s, one BWR/4, and an ABWR. These four plant types have substantially different RPV and MSL diameters; however, their overall geometry is similar. One BWR/3 has a square hood dryer, one BWR/3 has a slanted hood dryer, and both the BWR/4 and the ABWR have curved hood dryers.

From this sample population, data was available from 47 pressure transducers. Of these there exist 11 pairs (22 total) located on both the inside and outside of the steam dryer skirt and outer hoods, 3 in the steam plenum above the steam dryer, 2 on the cover plates adjacent to the main steam nozzles, 16 on outer hoods, 2 on inner hoods, and 2 on side end panels. The two gauges placed on the steam dryer cover plates were strain gauges mounted on a pressure drum; therefore, the applied pressure is determined from the strain induced in the drum.

Power ascension data is available from three of the four plants. These data were obtained from 20-100%, 34-100% and 50-100% power. Data is currently available from the fourth plant at 100% power only. Table 1 summarizes the vessel diameter, average steam line velocity, approximate Reynolds number based on MSL ID, plant vintage, and steam dryer hood design for each plant from which data is available.

Table 1: Summary of sample population

Plant	RPV Diameter, in (mm)	Average MSL velocity, ft/s (m/s)	Reynolds Number, Re_D	Vintage	Dryer Hood Design
A	188 (4775)	149 (45.4)	3.1E7	BWR/3	Square
B	251 (6375)	200 (60.9)	5.3E7	BWR/3	Slanted[1]
C	251 (6375)	129 (39.3)	4.6E7	BWR/4	Curved
D	280 (7112)	139 (42.4)	5.1E7	ABWR	Curved

1. This is the replacement dryer designed by GE for QC and Dresden

3.2 Data Analysis

The following items are presented in this section:

- Data Analysis Methods
- Fluid Loads
  - Frequency content vs. flow
  - Amplitude vs. flow
  - Frequency spectra
  - Spatial pressure distribution
- Structural Response
  - Strain gauge data

Although the primary focus of this section is the fluctuating loads observed in the BWR steam plenum, both the fluctuating pressure loads measured by the pressure transducers as well as the dynamic strain measured by the strain gauges mounted on the steam dryers are presented here. The latter is included to provide information regarding the bandwidth of the loading that should be considered to obtain a reliable steam dryer durability assessment.

3.2.1 Data Analysis Methods

Plant data was analyzed with both an HP3566 dynamic signal analyzer and a LMS SCADAS III dynamic signal analyzer. The sampling rate was determined using the Nyquist theorem to obtain accurate frequency content in excess of 300 Hz. Peak hold spectra as well as linear averaged RMS spectra were typically used to investigate the data. All data were digitized from the original analog media used to record and store the data during the original plant testing.

The individual spectra created from the data available at each power level were combined to form spectrograms and waterfalls to visualize trends in the pressure and strain data as the reactor power level increased. Frequency bands or sections were selected and cut from these plots to obtain RMS levels of specific frequency bands versus power level. These frequency bands were then compared to similar information from other plants and also curve-fit to observe characteristics of the data.

3.2.2 Summary of Fluid Loads

Figures 10 and 11 are spectrograms exhibiting the trend of fluctuating pressure amplitude with reactor power level. The horizontal axis displays frequency, the vertical axis corresponds to reactor power level and the color scale depicts pressure amplitude. Power ascension data is available for Plants A, B and D only. From these plants it is apparent that the frequency spectra can be separated into two regions exhibiting different behaviors:

- $f < 100$ Hz
- $f > 100$ Hz.

Based on the model testing described later in this document, the plant test data discussed in this section will be segregated further into the following four frequency bands:

- 0-10 Hz
- 10-30 Hz
- f >30 Hz.
- f >100 Hz. (sharp peaks apparent in data above 100 Hz)

Focusing on the first three bands, it is evident that there are multiple prominent frequency peaks observable in the data. For each of these peaks, the amplitude increases as the reactor power level is increased; however, the frequency remains constant. For reference, steam flow is approximately proportional to reactor power level. To better understand the trend of fluctuating pressure amplitude with flow rate at each frequency, the RMS pressure amplitudes for the first three frequency bands shown above are plotted against reactor power level in Figures 12 and 13. These data are cut from the spectrogram data shown in Figures 10 and 11. Also shown are power law curve fit equations for the fluctuating pressure trends. These trends are typical of the power ascension data obtained from Plants A, B and D. It is apparent that the pressure oscillations can be approximated by the following relationship:

$$P = A \cdot U^b \qquad (1)$$

Where: P is the fluctuating pressure amplitude
A is a reference pressure
U is the mean fluid velocity
b is the power law exponent,
[[ ]]

[[

]]

Figures 16 through 19 are peak hold autopower spectra at 100% power for Plants A, B, C, and D. These figures show similarities in frequency content, especially in the 10-30 Hz, 30-100 Hz and f > 100 Hz frequency bands. Figure 17 is shown with two different vertical scales because the amplitude of the frequency content in the f > 100 Hz frequency band is much greater than the other plants and hides the lower frequency content. To show the lower frequency content the vertical axis has been truncated in the bottom half of Figure 17.

3.2.3 Structural Response

Figures 14 and 15 are autopower spectra of the data obtained from strain gauges mounted on the outer hood at Plant A and the skirt at Plant B. These figures show that the structure is responding to both the low and high frequency pressure loads and a comparison with Figures 16 and 17, respectively, shows that the structural response is consistent with the frequency content of the pressure load. From these plots it can be inferred that the structure will respond to forcing frequencies throughout the frequency band monitored.

3.3 Evaluation of Plant Data

The process of evaluating possible explanations for the observed plant behavior will consist of:

1) Discussion of Flow Induced Vibration (FIV) mechanisms

2) Evaluation of each FIV mechanism considering the plant vessel and piping configuration

3.3.1 Flow Induced Vibration Mechanisms

Examples of structural vibration induced by fluid flow are found in many industries. The existence of this class of problem is so common that a unique term has been coined to describe it, Flow Induced Vibration (FIV). FIV has been the subject of substantial research for many decades; from this effort various FIV mechanisms have been identified and classified as separate phenomena. Au-Yang [1] and Blevins [2] have written informative monographs that provide a thorough introduction to the common types of flow induced vibration experienced in industrial systems. The following are the most common FIV mechanisms:

- Galloping/Flutter
- Fluid-Elastic Instability
- Turbulence Induced Vibration
- Vortex Induced Vibration
- Acoustic Vibration

3.3.1.1 Galloping/Flutter and other Fluid-Elastic Instabilities

From Reference 2 it is evident that Galloping and Flutter are typically of concern for lightweight flexible structures in which the span-wise dimension is much greater than the in-plane dimensions. Chimneys, airfoils, heat exchanger tubes and power lines are excellent examples of the types of structures for which these mechanisms should be a concern. Alternately internal or external axial flow can also cause fluid-elastic instabilities of thin walled piping. Here, again, the critical characteristic of the mechanical system is that it is long and flexible. [[

]]

3.3.1.2 Turbulence Induced Vibration

Turbulence induced vibration can be an excitation mechanism affecting structural components; however, review of discussion and sample data contained in both Au-Yang [1] and Blevins [2] show the frequency content created by turbulent loading on a structure tends to exhibit [[

]] This is discussed in Section 3.3.1.4 below.

3.3.1.3 Vortex Induced Vibration

Vortex shedding is also known to excite structures. Typically this is a problem for long slender structures subjected to cross-flow. As vortices are alternately shed from opposite sides of the structure, an oscillating force is imposed on the structure normal to the flow direction. [[

]]

This is discussed in Section 3.3.1.4 below.

3.3.1.4 Acoustic Induced Vibration

Power and process plant piping systems have long been known to be susceptible to acoustic resonance during operation. Pipe runs, cavities formed by valve bodies, closed end branch lines, and pressure vessels form resonating chambers that can be excited by a variety of excitation mechanisms. Acoustic resonances are typically observed as high amplitude narrow frequency peaks. The plant data shown in Figures 16 through 19 exhibit this characteristic which suggests that acoustic induced vibration is the primary load mechanism that should be considered. It is known that fluctuating pressure oscillations in fluid systems can be caused by the following factors:

- Mechanical
  - Periodic valve motion
  - Pump, compressor operation
- Internal Flow
  - Flow through an orifice or other abrupt geometric discontinuity
  - Flow through elbows
- External Flow
  - Turbulent flow
  - Vortex Shedding from flow across bluff bodies

Periodic valve motion can cause pressure pulses in a fluid system which can excite structural response or fluid acoustic modes. This valve motion may be the result of feedback from the fluid system or control logic that causes the valve position to oscillate about a set point.

Pumps and compressors are also known to introduce periodic acoustic pressure pulses to the working fluid. The frequencies expected from these components can be determined by considering the speed of the device (RPM) and the number of vanes on the rotor. The fundamental vane passing frequency as well as its higher harmonics can be transmitted to the fluid.

In some cases flow through valves has been shown to excite local valve body acoustic modes, standing waves in upstream or downstream piping, and emit broadband noise that can cause fatigue damage to adjacent piping [3,4]. Elbows have also been shown to cause turbulent flow that can emit broadband noise [5]. These studies also suggest that currently, the only way to reliably predict the existence of valve noise is through model testing programs.

Bluff bodies exposed to external flow will shed vortices with a certain periodicity [1, 2]. This periodic vortex shedding has been observed to excite acoustic resonances in ducts. In a similar manner shear layer instabilities have also been shown to excite acoustic oscillations in closed side branches [6].

There are many examples in the literature of aero-acoustic excitation of piping systems and the resultant degradation of components in these systems. Vibration caused by acoustic resonance in the standpipes of safety and relief valves has been a common problem in piping systems. Baldwin and Simmons [7] summarize operational experiences in which S/RV resonances were observed and provide guidelines that can be used to predict susceptibility of a S/RV to an aero-acoustic resonance. They also recommend potential mitigation techniques for problem valves. S/RV acoustic resonances can be grouped into a broader category in which a self-sustained acoustic oscillation is induced in a cavity by flow across the cavity mouth. Rockwell and Naudascher [8] have prepared an excellent review of literature related to this phenomenon. Although there are a large number of articles regarding piping acoustics in the literature, there appears to be little discussion regarding sonic fatigue of components inside large pressure vessels.

Although the focus of this section is the evaluation of available plant data, the results of some CFD analyses of the steam dryer will be briefly discussed considering their relevance to the topic considered here. [[

]]

The following sections evaluate the typical BWR plant piping and vessel configuration with respect to their potential to exhibit the various acoustic excitation mechanisms discussed above.

3.3.2 Plant Piping Configuration

The acoustic response of the steam system is controlled by the steam system arrangement and geometry. [[

]]

Other than the high pressure turbine and feedwater pump turbines, there are no pumps, compressors or other mechanical equipment that interact with the flow in the main steam piping system. [[

]]

A review of the fluid flow path in the BWR steam system (Figures 8 and 9) shows that the steam passes through multiple elbows. [[

]]

Also shown in Figures 8 and 9 is the presence of multiple valves in the main steam lines. No model testing of any of the typical BWR steam line valves has been performed; therefore, it can only be said that the MSIVs, TSVs, and TCVs may produce noise that can excite the steam line acoustic modes. Model testing is the only practical method to examine if the various MSL valves contribute to the sound observed in the RPV. The valves must be considered a possible excitation source.

[[

]]

[[

]]

[[

]]

Table 2: Expected [[ ]] frequencies for Plants A & B.

[[	

]]

Sound induced by flow over cavities has been observed to occur at specific shear wave modes [6,10] with peak amplitudes occurring at a St number of approximately 0.42 (first shear wave mode) and 0.85 (second shear wave mode). Baldwin & Simmons [7] report data in which the St ranges between 0.3 and 0.6. Table 3 summarizes St ranges over which S/RV resonances have been observed to occur in the literature. Recognizing that the flow rate at which resonance is created is affected by the entrance radius as well as upstream and downstream piping, the St numbers presented in Table 3 should only be considered as general values around which a deep cavity resonance may be expected to occur.

Table 3: Strouhal numbers associated with S/RV resonances.

Strouhal Range[1]	Peak Strouhal[2]	Source
0.3-0.6	0.42 0.85	Ziada [10]
< 0.6	None Reported	Baldwin & Simmons [7]

1. Ranges are shown for the first shear wave mode
2. Values are reported for the first and second shear wave modes, respectively

[[

]]

Table 4: Summary of St number for approximate peak resonances observed in data.

Plant	Frequency, Hz	Strouhal Number	Power Level
A	[[		
A			
A			
A			
A			
A			
B			
B			
B			
B			
B			
C			]]

[[

]]

[[

]]

Summarizing the above discussion:

[[

]]

3.3.3 Vessel Configuration

Similar to the discussion provided for the main steam lines, each of the excitation mechanisms introduced above will be evaluated here with respect to the RPV configuration.

The reactor pressure vessel can experience transient loads emanating from the main steam lines when a MSIV or a S/RV is closed/opened; however, these are off-normal conditions. The fatigue cracking observed in the steam dryers occurred during normal operation. There are no other valves connected to the RPV steam plenum which cycle during normal operation; [[

]]

The large pumps connected to the RPV are the recirculation pumps and the feedwater pumps. There have been examples of resonances in BWR internals being excited by recirculation pump Vane Passing Frequencies (VPF); however, these incidents have occurred in components that are either in the recirculation system or in the submerged

portion of the vessel. [[

]]

The steam flow path begins in the reactor core as water is boiled as it passes through the fuel bundles. This steam flows through a set of steam separators and dryer vanes. The average separator exit steam quality is typically greater than 95%, and the superficial steam velocity though the steam dryer banks is relatively low, on the order of a few feet per second. [[

]]

After the steam exits upward from the steam dryer it enters the steam plenum in the reactor top head. The steam is redirected by the top head and flows downward into a smaller cavity between the RPV and steam dryer before it exits the vessel through the MSL nozzles as shown in Figures 5, and 20 through 22. As the flow enters the smaller cavity close to the MSL nozzles it impinges on the top plate of the steam dryer. This flow configuration is similar to flow over a step and/or a shallow cavity. Equation (4) can be used to estimate the vortex shedding frequency for turbulent flow over a step [2]. [[

]]

Table 5: Possible vortex shedding frequencies from dryer top plate

N	Frequency, Hz
[[	
	]]

[[

]] Shallow cavity data suggest that multiple shear wave modes can exist simultaneously [8]. It should be recognized that these values are approximate and are intended only to illustrate the general range of expected vortex shedding frequencies in this region. The actual frequencies can be expected to vary about these numbers depending on specific dryer geometries, MSL diameters, and reactor power level. [[

]] A detailed acoustic finite element analysis of plants A, C, and D has not been performed; however, the [[

]] using the frequency scaling relationships derived for the GE scale testing methodology (See Section 4.1) [[

]] It must be noted that the steam dryer designs at plants A, C, and D are different than the steam dryer used in the QC scale model. Recognizing this difference the values presented in Table 6 are only approximate and are intended to "roughly" approximate the expected natural frequencies of the [[

]]

Table 6: Estimated RPV acoustic cavity modes.

[[				
				]]

[[

]]

Recognizing the limitations inherent in the approach used to approximate some of the lower acoustic cavity modes, it can be seen that much of the frequency content [[

]]

Acknowledging that hypotheses have been suggested for the 0-10 Hz frequency content, the f > 30 Hz content and the f > 100 Hz content, no discussion has been offered about the 10-30 Hz content observed in each plant. Additional work must be performed to develop and interrogate an explanation for the 10-30 Hz content.

3.3.4 Summary of FIV Discussion

The significant points from the Flow Induced Vibration discussion are summarized below:

1. The fluctuating pressure load spectra shown by the in-plant measurements from four separate BWRs and the inherent similarity in BWR steam system design suggests that all BWRs can be expected to contain similar sources and exhibit steady state fluctuating load frequency content in each of the four frequency bands discussed in this document (0-10 Hz, 10-30 Hz, f > 30 Hz and f > 100 Hz). The frequencies and amplitudes exhibited by a plant specific configuration will depend primarily on the plant specific configuration. In other words each BWR is expected to have the potential to possess frequency content in the four frequency bands listed above; however, the load amplitudes for each plant are not expected to be identical for all plants.

2. Acoustic pressure loading is considered to be the dominant excitation mechanism for steam dryer vibrations.

3. Flow turbulence and vortex shedding are both possible excitation mechanisms for the acoustics observed in the plant data.

[[

]]

5. As with all FIV mechanisms, the fluid velocity is an important factor for the resultant load. It must be understood that increased steam flow does not guarantee increased loads for every FIV mechanism. For turbulence induced acoustics increased steam flow correlates with increased load. For a deep cavity resonance the primary factor is the Strouhal number; therefore, there are ranges of flow where the resonance amplitude decreases as flow is increased.

3.4 Discussion of Possibility of Fluid-Structure Interaction

Fluid Structure Interaction (FSI) is a broad term used to describe a variety of mechanisms through which the dynamics of a structure couples to the dynamics of a fluid medium. A fluid/structure problem can be described as either "strongly" or "weakly" coupled where the adjective denotes the relative importance of FSI in determining the behavior of the system. In a rigorous evaluation the equations of fluid motion would be solved with the equations of structural motion [1].

Equations of Fluid Dynamics:

Continuity:
$$\frac{\partial \rho}{\partial t} + \nabla(\rho \vec{V}) = 0 \tag{5}$$

Momentum:
$$\frac{\partial \vec{V}}{\partial t} + \vec{V} \bullet \nabla \vec{V} + \frac{\nabla P}{\rho} - \vec{F} = 0 \tag{6}$$

Energy:
$$\frac{\partial E}{\partial t} + \nabla \bullet (E\vec{V} + P\vec{V}) - \rho \vec{F} \bullet \vec{V} = 0 \tag{7}$$

Where

$$E = \rho e + \rho \vec{V} \bullet \vec{V}/2$$

Equations of Structural Dynamics:

$$[m]\{y''\} + [c]\{y'\} + [k]\{y\} = \{F\} \tag{8}$$

The equation of structural motion is expressed in matrix notation above. The fluid equations are expressed in vector notation. These two systems are coupled by the requirement that the fluid velocity normal to the structure be equivalent to the normal component of the structural velocity at the surface. It is apparent that these equations do not lend themselves to a simple solution and it is because of this fact that system models are simplified for analysis when possible.

The interaction or coupling between the fluid and the structure can be observed in the following ways:

- Structural deflection changes the flow pattern
- Structural deflection changes the characteristic acoustic modes of the cavity
- Immersion of the structure in fluid affects the dynamic characteristics of the structure.
- Structural motion while immersed in fluid introduces an energy loss mechanism through which energy is radiated into the fluid.

3.4.1 Fluid Structure Coupling Resulting from Large Structural Displacements

The first two concepts introduced above require very large structural displacements to occur before the fluid flow patterns are substantially disturbed or the acoustic cavity created by the steam plenum is changed enough to affect the lower modes of interest (0-200 Hz). Obviously the response of each steam dryer will depend not only on the steam dryer structural design but also on the fluid loading applied to it; therefore, no single evaluation can be said to bound all configurations. Even so, it can be said that the BWR steam plenum configuration and the various steam dryer structures are not so dissimilar that the behavior of any one system will be expected to be drastically different than another. Considering the RPV and steam dryer geometry, it can be expected that the dryer panels would have to experience displacements on the order of 6-12 inches before the fluid path would either be substantially disturbed or the natural frequencies of the cavity would begin to change in the frequency range of interest.

Available plant data from instrumented dryers has been reviewed to determine the amplitude of displacements observed at four different plants. From accelerometer measurements, the structural displacement can be determined by integrating the acceleration signal twice. Assuming a harmonic acceleration, the structural displacement

can also be determined by dividing the amplitude of the acceleration by the square of the frequency of oscillation in radians/sec:

$$X = \frac{X''}{\omega^2} \qquad (9)$$

Consistent with the plant data observations described above, two frequency bands are considered here: [[ ]] The maximum acceleration observed in all of the available data from Plant A in these frequency ranges is used with the lowest observed frequency peak to estimate a bounding structural displacement.

[[ ]]

This value was obtained from the Plant B instrumented dryer test; the accelerometer signals were double integrated in the DAS to output a displacement. [15]

[[

]]

3.4.2 Hydrodynamic Mass and Acoustic Radiation Damping

Immersion of a structure in a fluid with a density similar to that of the structure can introduce additional phenomena which should be considered to obtain an accurate prediction of the structural behavior. Hydrodynamic mass and Radiation damping pertain only to the response of the structure and do not affect the fluid behavior; therefore, it is not necessary to consider them for the model testing program. The scale model is intended only to model the fluid behavior in the steam plenum; the model dryer is not intended to be dynamically similar to the plant structure.

3.4.3 Structural Resonance

An additional condition which must be considered is the effect of a simultaneous existence of a forcing function with a structural mode. This coincidence of forcing mode shape and frequency with structural mode shape and frequency is best described as the structure being driven at or near resonance. Because the response of the structure at resonance is not sufficient in and of itself to affect the fluid load acting on the structure, this is not, strictly speaking, FSI; however, it is an important consideration when the mechanical system contains structural modes with more than one degree of freedom. For a SDOF system it is only necessary to consider the excitation frequency when determining if resonance is a concern. For a MDOF system it becomes important to consider both the frequency and distribution of the load and the system response. The model test program is designed to acquire data that describes both the frequency content and spatial distribution of the fluid loading. In addition, the structural evaluation considers the dynamic response of the structure; therefore, the methods applied for this evaluation are adequate to address structural resonance.

3.5 Conclusions

The data presented herein suggest the following conclusions:

1. The fluctuating pressure load spectra shown by the in-plant measurements indicate that the characteristics of the pressure loading on the steam dryer is similar for all BWRs, regardless of vessel size or steam dryer hood design.

2. Acoustic induced vibration is the dominant excitation mechanism for the steam dryer

3. Flow turbulence and shear layer instabilities are each separately responsible for exciting portions of the frequency content observed in the steam plenums of four separate BWRs.

[[

]]

[[

]]

Figure 10: 0-Peak power ascension colormap of pressure transducer from Plant A.

[[

]]

Figure 11: 0-Peak power ascension colormap of pressure transducer from Plant B

[[

]]

Figure 12: Trend of RMS pressure amplitude vs. steam flow at Plant A.

[[

]]

Figure 13: Trend of RMS pressure amplitude vs. steam flow at Plant B.

[[

]]

Figure 14: Peak Hold RMS frequency spectra from strain gauge mounted on outer hood at Plant A.

[[

]]

Figure 15: Linear averaged 0-Peak Autopower spectrum from strain gauge mounted on skirt at Plant B.

[[

]]

Figure 16: Representative peak hold Autopower spectrum, 100% power, Plant A, skirt below cover plate.

[[

]]

Figure 17: Representative peak hold Autopower spectrum, 100% power, Plant B, skirt below cover plate.

[[

]]

Figure 18: Representative peak hold Autopower spectrum, 100% power, Plant C, cover plate.

[[

]]

Figure 19: Representative peak hold Autopower spectrum, 100% power, Plant D, dryer skirt below cover plate (exterior).

[[

]]

Figure 20: Velocity streamlines adjacent to the outer hood and MS nozzles in a QC1 style steam dryer, RANS analysis

[[

]]

Figure 21: Velocity streamlines adjacent to the outer hood and MS nozzles in a QC1 style steam dryer, LES analysis

[[

]]

Figure 22: In vessel visual examination data of steam dryer outer hood.

[[

]]

Figure 23: Plant C MSL layout illustrating S/RVs located in stagnant branch on two of four MSL.

[[

]]

Figure 24: QC2 model steam plenum Acoustic Mode #1, [[ ]]

[[

]]

Figure 25: QC2 model steam plenum Acoustic Mode #2, [[ ]]

[[

]]

Figure 26: QC2 model steam plenum Acoustic Modes #3 & #4, [[ ]]

[[

]]

Figure 27a: QC2 model steam plenum Acoustic Modes #5 & #6, [[ ]]

[[

]]

Figure 27b: QC2 model steam plenum Acoustic Modes #7 & #8, [[ ]]

[[

]]

Figure 28: QC2 model steam plenum Acoustic Mode #9, [[ ]]

4.0 Scale Model Test Methods and Apparatus

After review of the available instrumented dryer data, the most probable cause of steam dryer fluctuating loads is considered to be acoustic induced vibration. Furthermore, there is strong evidence that multiple excitation mechanisms and source locations exist in the BWR steam system. Each source separately contributes to the total fluctuating load experienced by the steam dryer structure. Two mechanisms considered likely to exist in the BWR steam system are flow turbulence and shear layer instabilities (vortex shedding). Although it is known that flow through valves and elbows can excite piping acoustics [2] and shear layer instabilities can occur when there is flow over a step, past the stem of a tee branch, or other geometry where shear layer interruption occurs [8], the locations of the dominant sources cannot be conclusively identified from review of the existing plant data alone.

Considering that,

1. The physical mechanisms responsible for the excitation of aero-acoustic resonances are not easily modeled using purely analytic methods,

2. It is often prohibitively expensive to instrument an operating reactor for operational testing, and

3. It is impractical if not impossible to perform parametric tests on an operating plant configuration,

GE decided to pursue model testing of the BWR plant configurations to investigate the possible existence of acoustic loads in the steam system and as a core component of a steam dryer fluctuating load definition process. Oftentimes model tests prove to be an effective and efficient method for investigating Flow Induced Vibration (FIV) problems in power plant systems. It is usually not practical to build a full scale model of the system of interest; therefore, small scale models are typically used as an alternative. Prior to designing a model, the important phenomena must be identified so that they may be preserved in the model through appropriate model and test design. This section summarizes the scaling laws used for the scale model testing.

4.1 Scale Model Relationships

Attachment A contains a detailed derivation of the scale model relationships and scaling laws used for this program. The reader is encouraged to review Attachment A to obtain a thorough understanding of the SMT scaling laws.

Review of the available instrumented dryer test data suggest that the following phenomena are probable excitation mechanisms in the steam system:

- Shear layer instabilities (vortex shedding)
- Turbulence

Non-dimensionalization of the governing system equations and estimating the relative order of magnitude of the resulting terms shows the following parameters to be significant for the phenomena considered:

- Mach Number
- Strouhal Number

Recognizing that the Strouhal number is primarily a function of geometry and that preservation of acoustics in the model requires preservation of the system geometry, the significant parameters that must be preserved in the model are:

Geometry, $$D_m = \frac{D_p}{X} \quad (10)$$

Mach Number, $$(V_0)_m = (V_0)_p \left(\frac{C_m}{C_p} \right) \quad (11)$$

Using reference values for time (frequency) and pressure, the following scaling relationships are derived to enable conversion of model data into plant frequency and fluctuating pressure predictions:

$$F_p = F_m \left(\frac{D_m}{D_p} \right) \left(\frac{C_p}{C_m} \right) \quad (12)$$

$$P_p = P_m \frac{(\rho C^2)_p}{(\rho C^2)_m} \quad (13)$$

Useful model testing can be performed if the full scale plant geometry is preserved at a consistent model scale and if the system flow rates for various plant power levels are determined by matching model and plant Mach numbers. Plant predictions can be obtained by scaling the model data to plant conditions using the scaling laws presented above.

4.2 Test Apparatus

This section provides a detailed description of the GE Scale Model test apparatus. Figure 29 is a schematic of the model BWR acoustic test apparatus designed for this test program. The BWR model extends from the steam/water interface inside the Reactor Pressure Vessel (RPV) out the steam lines to the turbine inlet. Ambient air is used as the test fluid. The test apparatus is composed of two primary components:

1. Test fixture
2. BWR model

The test fixture consists of the components necessary to provide the required air flow to the model. The model consists of the steam dryer, RPV, and steam lines. Both the test fixture and the model are described separately below.

The test fixture consists of the following components:

- Blowers
- Inlet Piping
- Flow Meter
- Muffler

The blower provides the air flow, which is routed through the inlet piping into the model. A venturi flow meter and muffler have been mounted between the blowers and the scale model. The venturi flow meter is used to measure the total system air flow and the muffler is used to isolate the model from the noise introduced into the system by the test fixture.

The BWR model consists of three components:

- RPV
- Steam Dryer
- Main Steam Lines

The model scale is determined by the flange diameter to which the BWR mockup is attached; therefore, plants with different RPV diameters would be modeled at different scales. The QC model is built to a 1:17.3 scale. The RPV is acrylic and the top head is stainless steel. The steam dryers are fabricated from a polymer using a rapid prototyping process and are then metal plated to prevent air flow through the porous structure of the dryer surfaces.

The steam lines are fabricated from standard stainless steel piping. All valves in the MSL were considered during design of the main steam line piping. Each valve location was determined using the same geometric scaling factor selected for the vessel and steam dryer. The main steam lines and all branch lines greater than 2" in outer diameter at the plant scale were replicated in the model. Figures 30 through 36 are images of the test apparatus and BWR models designed for these tests.

Most dimensions used to build the model were taken from GE design drawings. Where possible, as-built dimensions of the main steam lines provided by Exelon Generating Company, LLC were used for the MSL model.

4.3 Modeling Assumptions

It is recognized that no model is an exact replica of the system under investigation; simplifying assumptions must always be made. This section presents the assumptions and simplifications used to build the BWR scale model used in the tests, and provides the justification that these simplifications and assumptions are adequate

4.3.1 BWR Components Omitted

The following components are not present in the scale model of the QC steam system:

[[

]]

[[

]]

4.3.2 BWR Components Approximated

The following components are included; however, specific assumptions have been made which affect the manner in which they are modeled in the system.

[[

]]

[[

]]

4.3.3 Boundary Condition Approximations

The following approximations have been made for the boundary conditions:

[[

]]

4.3.4 Environmental differences

The following differences exist between the environmental parameters at the test scale and the full scale:

[[

]]

The environmental conditions during each test run are recorded and used as inputs into the pressure and frequency scaling when the SMT data are scaled to plant conditions.

4.3.5 System Configuration

The following differences exist between the system configuration used for the test program and the full scale system configuration:

[[

]]

4.4 Data Acquisition System

Acoustic pressures were measured using electret microphones located in both the MSL and the RPV. Total system flow was measured using a calibrated venturi and Rosemount pressure transducer. For some tests the air flows in the individual MSLs were measured using averaging pitot tubes in each line. Air temperatures in the system were measured using K-type thermocouples in the RPV on the steam dryer cover plate and at the turbine inlet in the MSL.

The analog time history data was sampled using a LMS SCADAS III dynamic signal analyzer. The SCADAS III performs the analog to digital conversion necessary so that the sampled data can be stored as a throughput file on the test computer. A Dell D600 Latitude with 1 Gigabyte of RAM or a Dell M70 Precision with 2 Gigabytes of RAM running the LMS Test.Lab 5A SL1 or SL2 software was used for the data acquisition and analysis.

4.5 Sensor Locations

Tests were performed with both the original and replacement QC steam dryer models installed in the test apparatus. Microphones were installed in the main steam lines as well as on the dryer surfaces. All microphones were mounted such that the sensor diaphragm was placed flush with the steam dryer outer surfaces or the MSL inner surface. Forty-one (41) microphone locations were defined on the main steam lines; however, not all locations were used for each test. Figure 37 identifies the microphone locations specified in the main steam lines. The following main steam line locations were instrumented:

[[

]]

Fifty-two (52) locations were defined on the original QC dryer and fifty-six (56) locations were defined on the replacement steam dryer. Figures 38 and 39 identify the microphone locations chosen for each dryer. The locations were chosen to be consistent with observed failures on the original dryer, the in-vessel instrumentation to be installed on the replacement dryer, and to obtain an understanding of the spatial pressure distribution around the dryer. Not all locations were used for each test. The following regions were instrumented on each dryer:

Original Dryer	Replacement Dryer
[[	]]

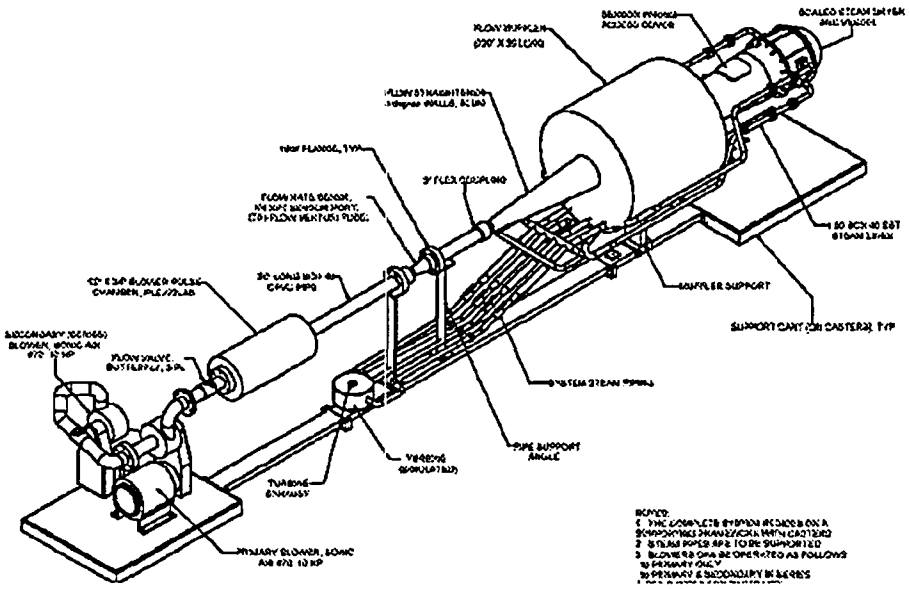

Figure 29: General schematic of GE scaled test apparatus

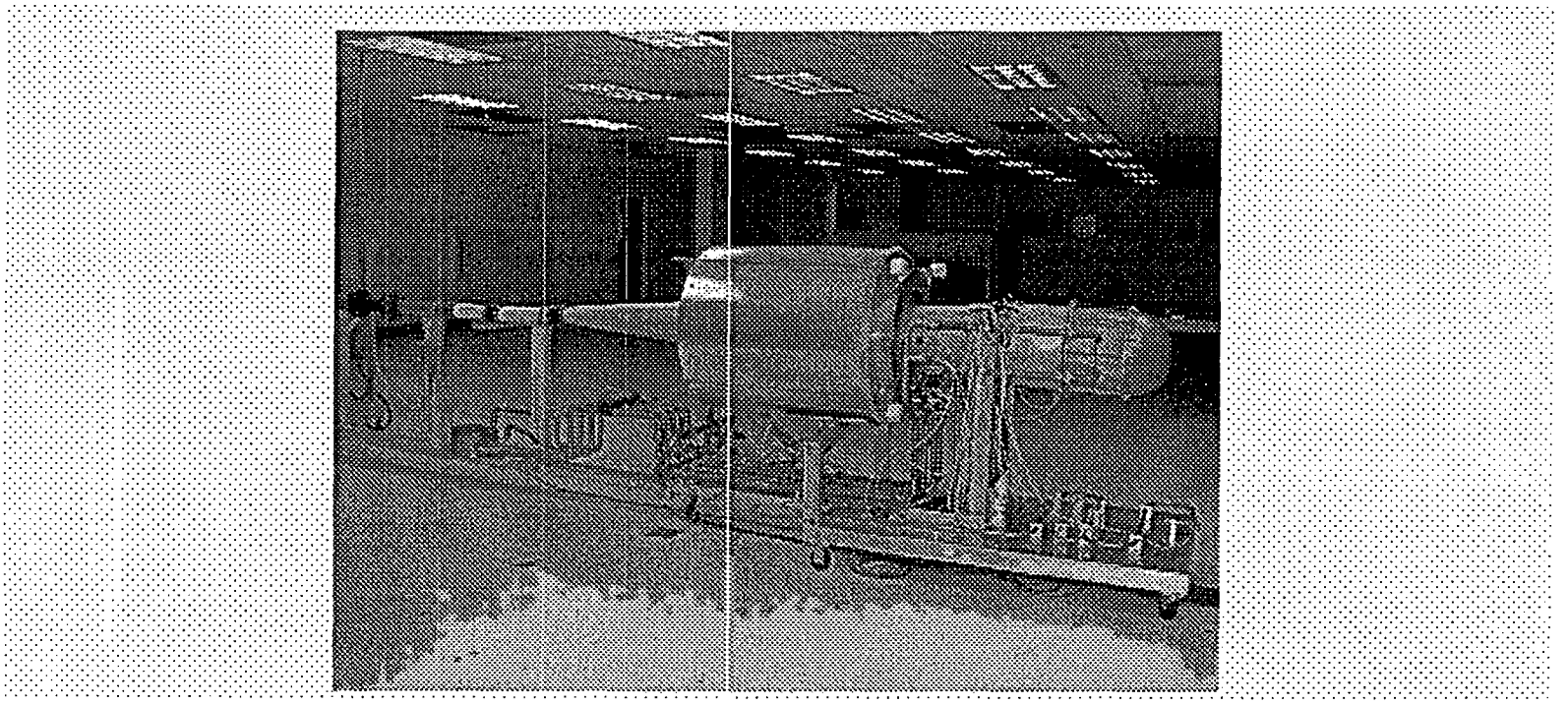

Figure 30: Test Apparatus

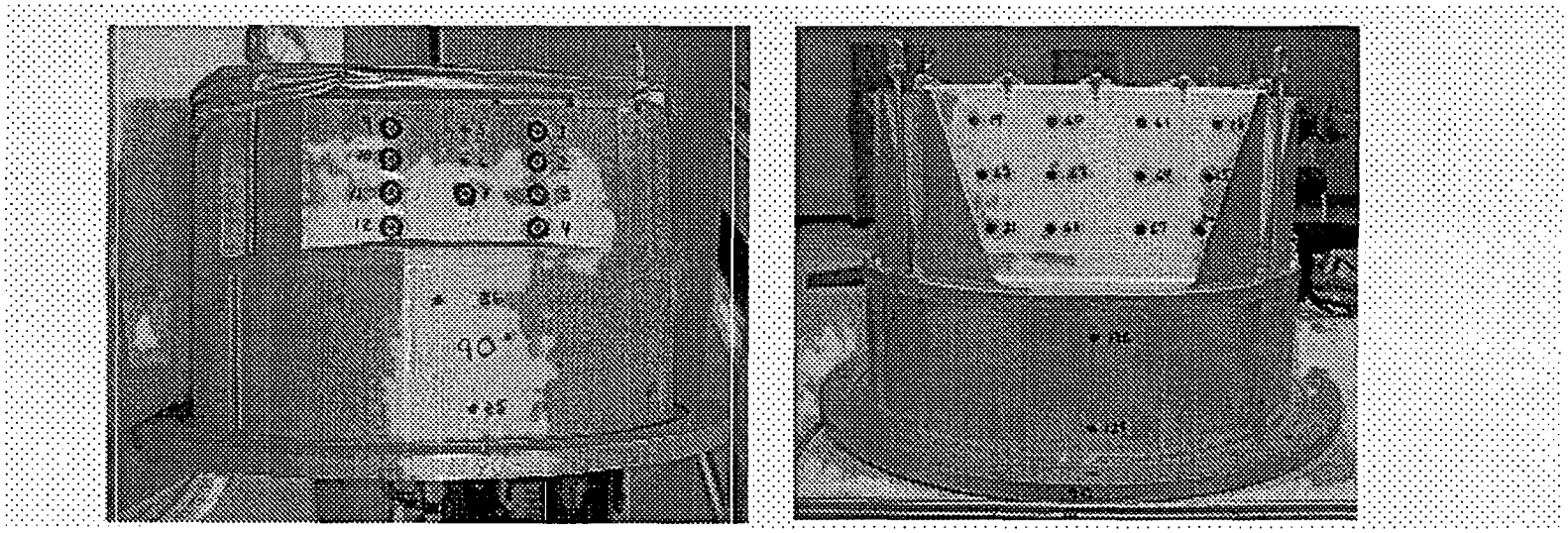

Figure 31: Steam dryer models, original (Left) & replacement (Right)

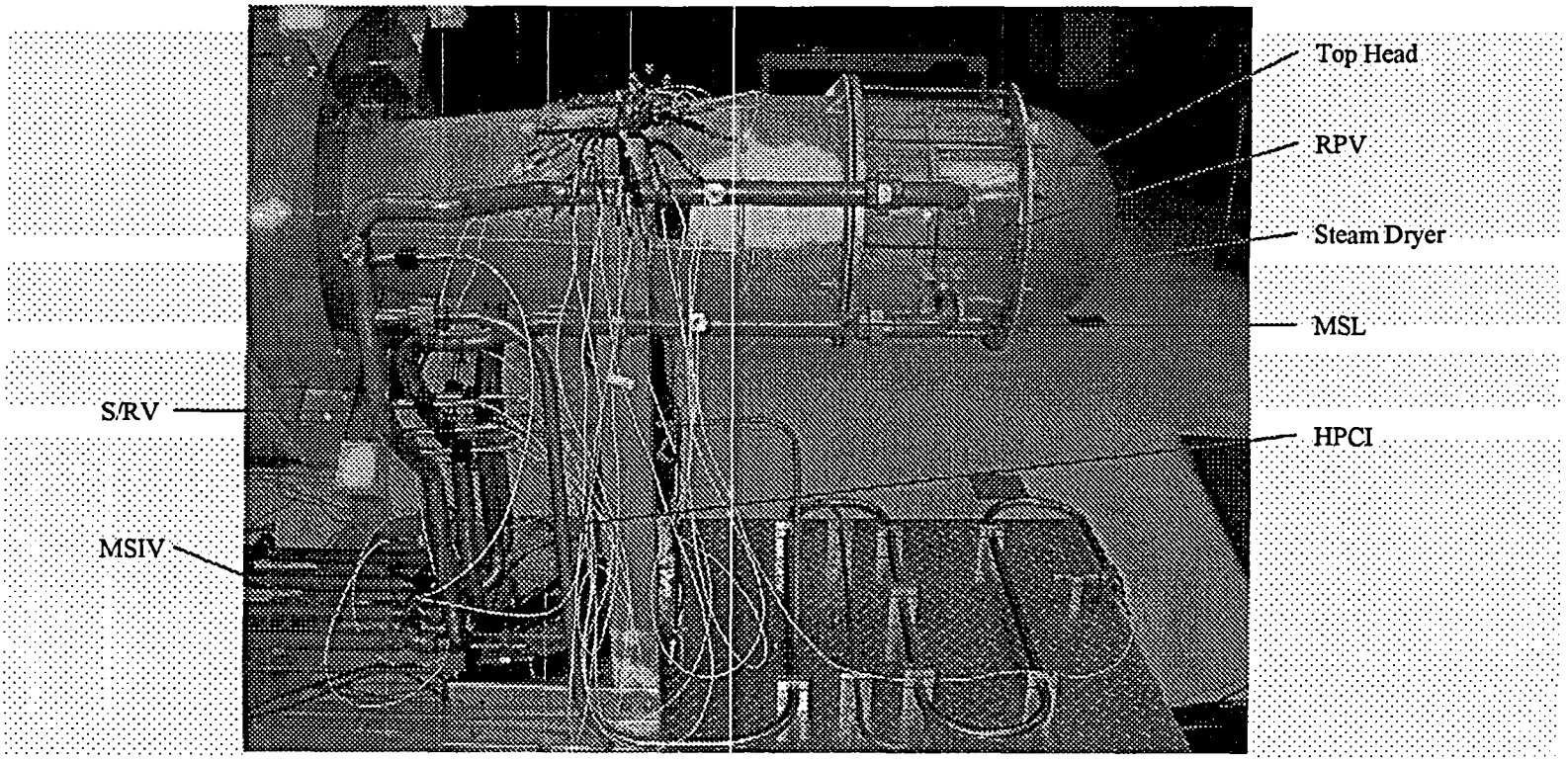

Figure 32: Close Up view of scale model identifying major components

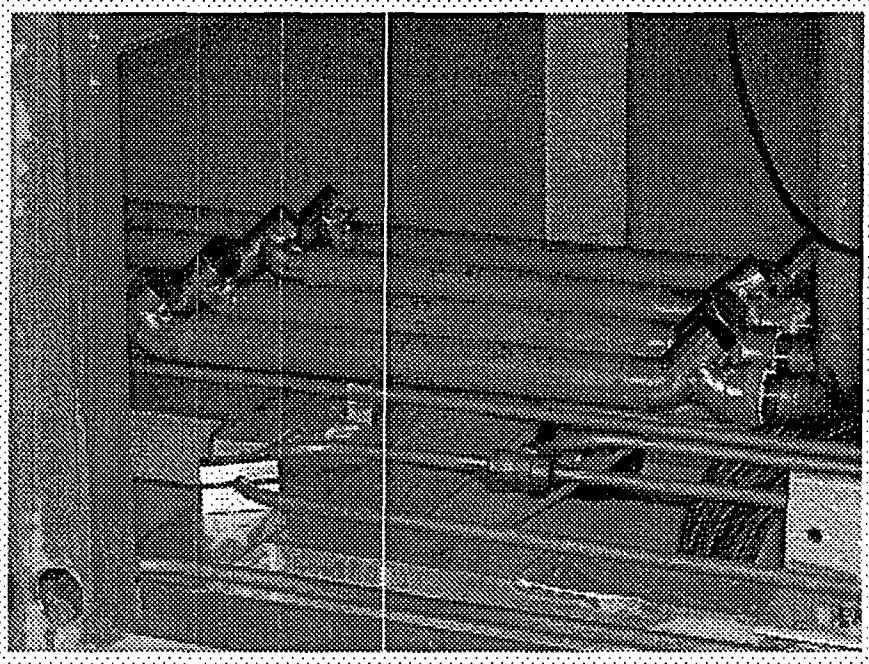

Figure 33: Main Steam Isolation Valves

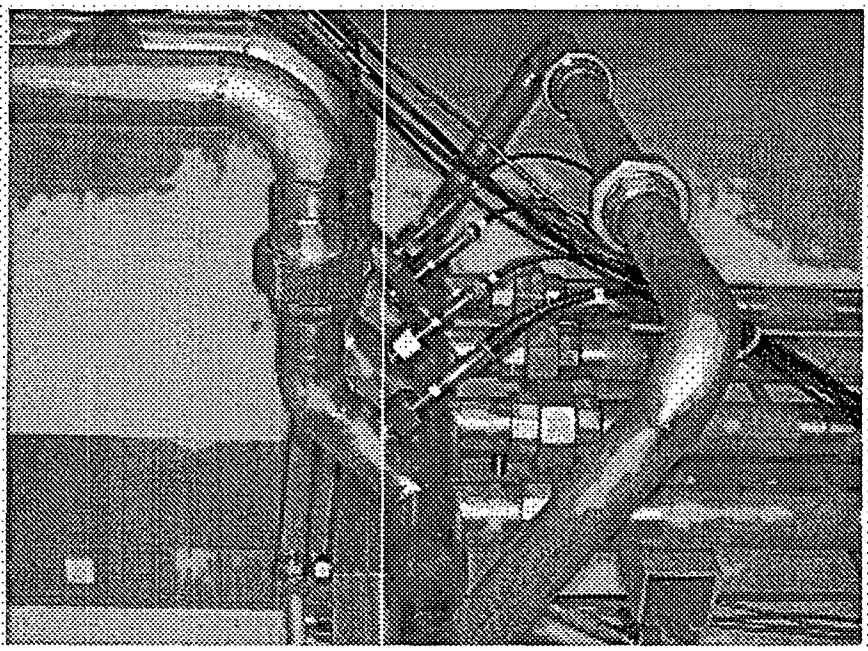

Figure 34: D-Ring Equalizing Header

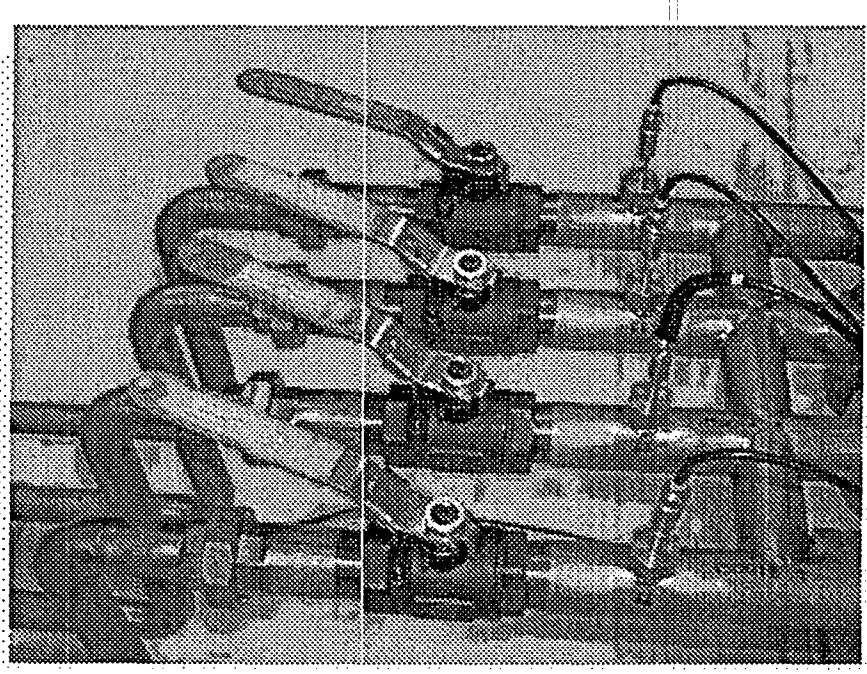

Figure 35: Turbine Stop and Control Valves

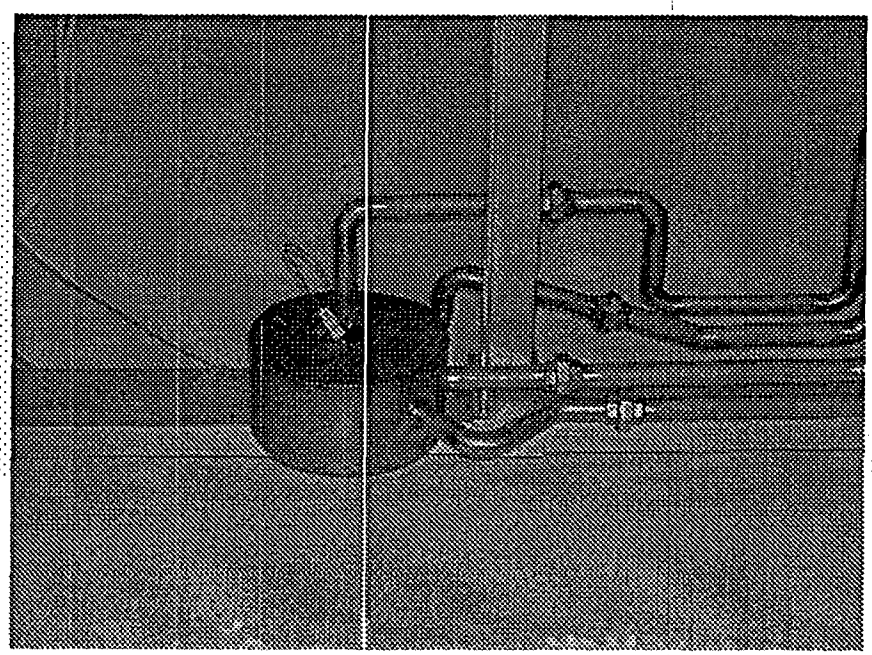

Figure 36: Turbine Inlet

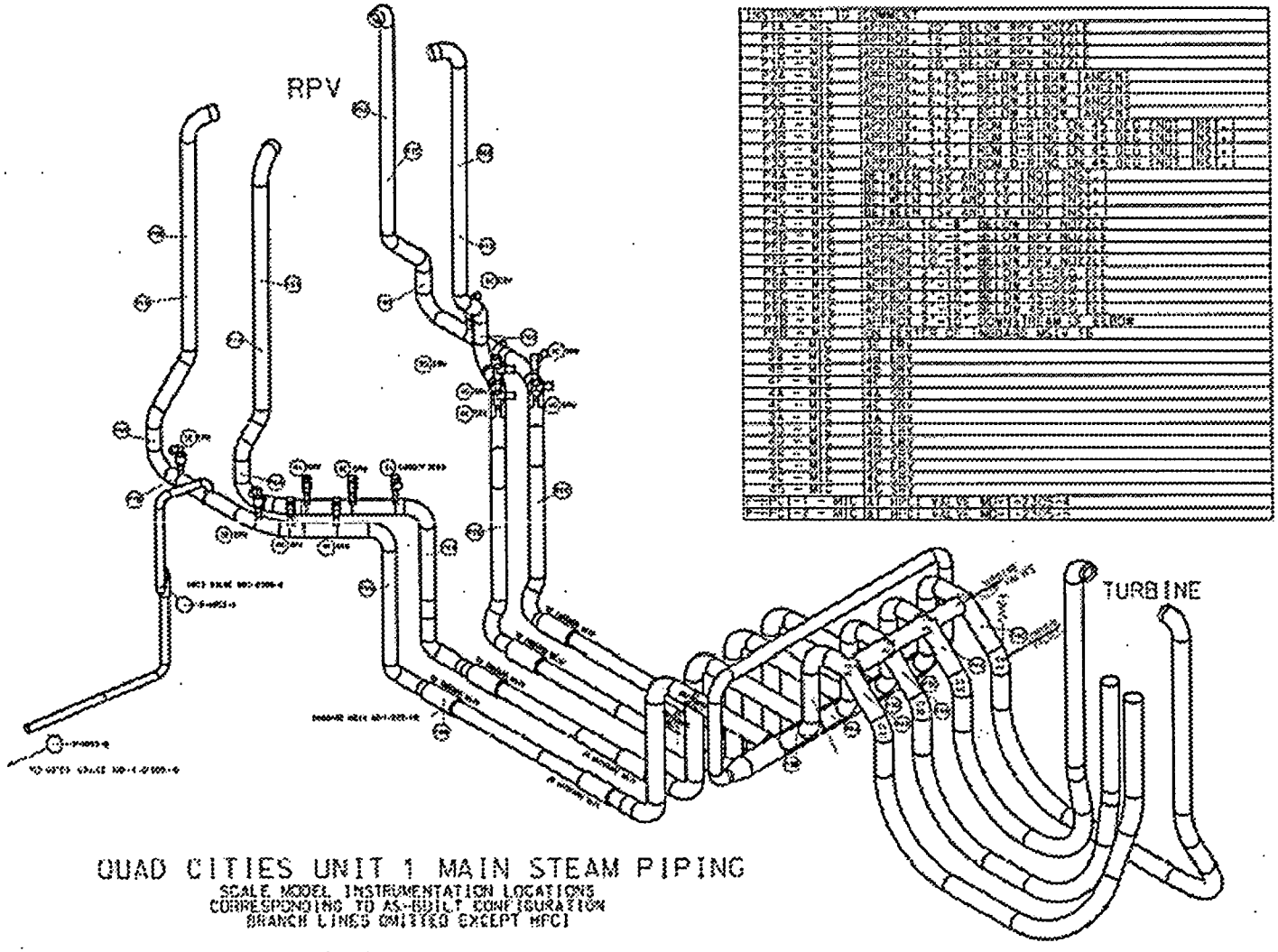

Note: The MSL figure shown here represents the plant MSL configuration not the SMT MSL configuration. This was done so that the reader could more easily relate the sensor locations to a typical plant configuration.

Figure 37: Scale model main steam line sensor locations.

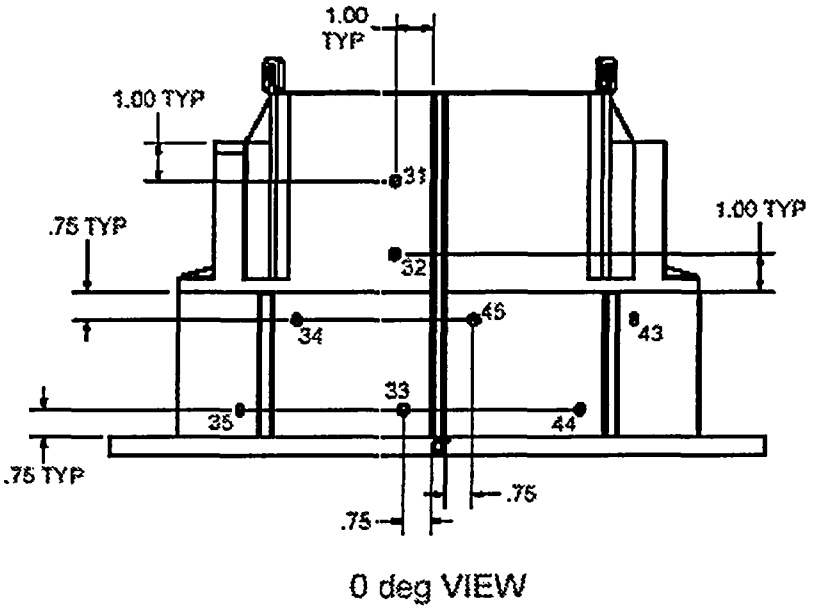

Figure 38a: Original dryer sensor locations

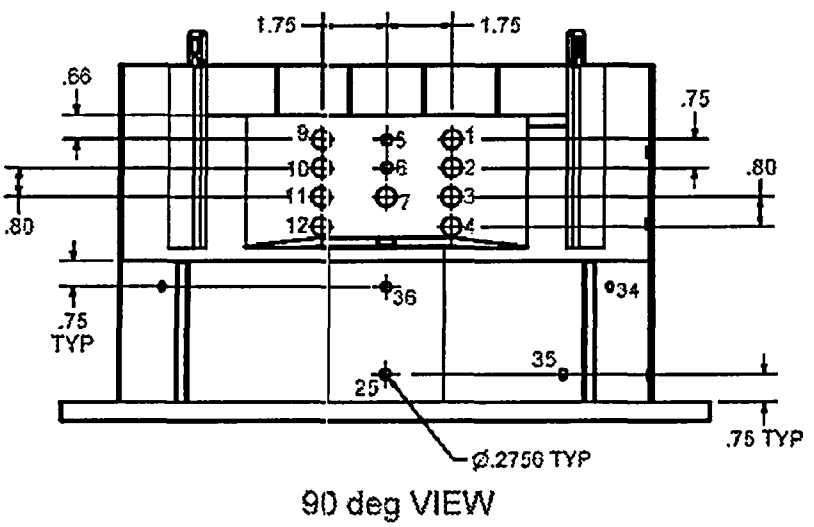

Figure 38b: Original dryer sensor locations

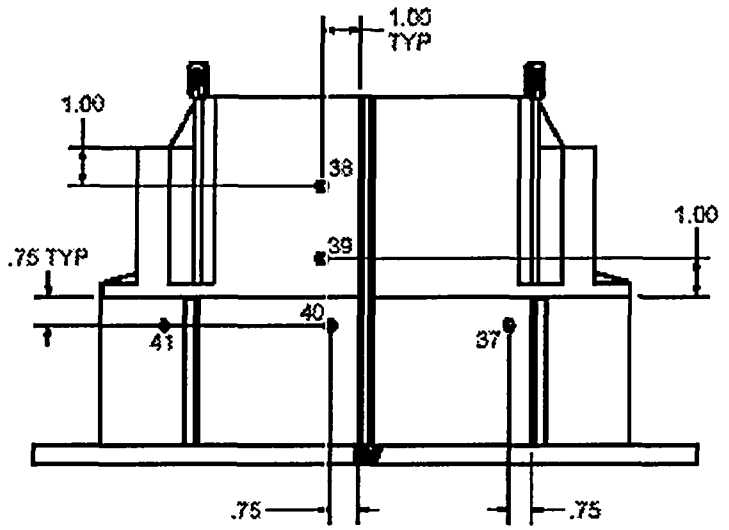

Figure 38c: Original dryer sensor locations

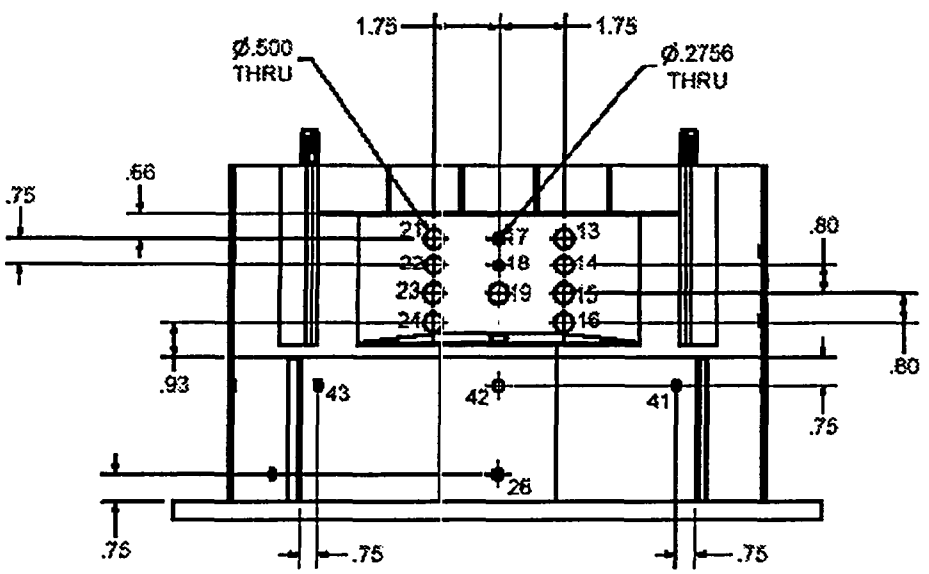

270 deg VIEW

Figure 38d: Original dryer sensor locations

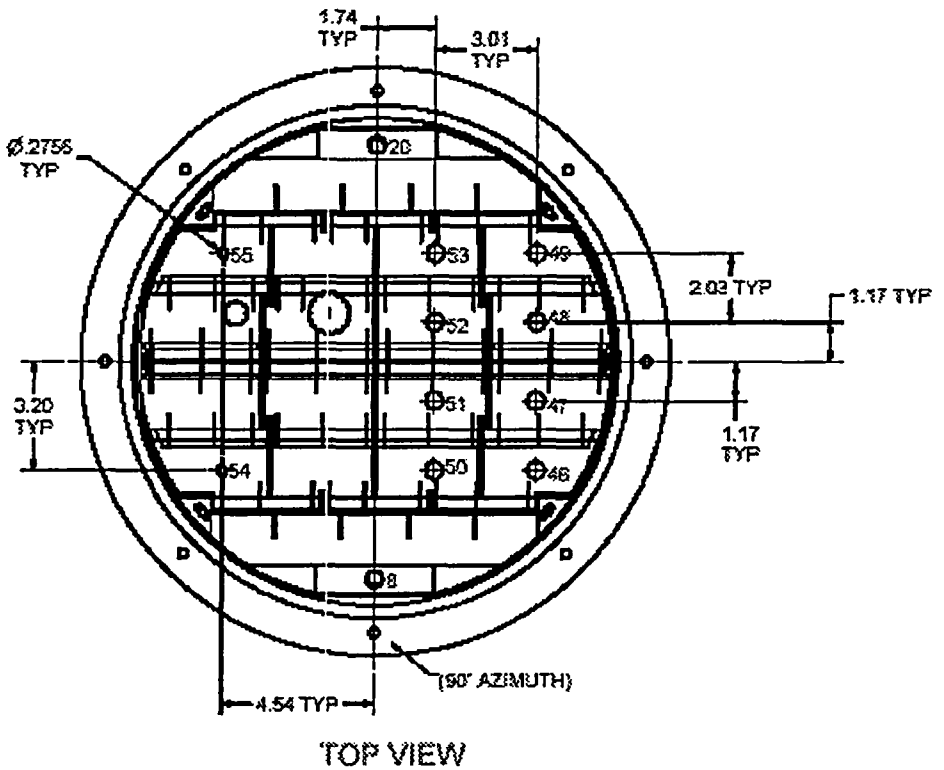

Figure 38e: Original dryer sensor locations

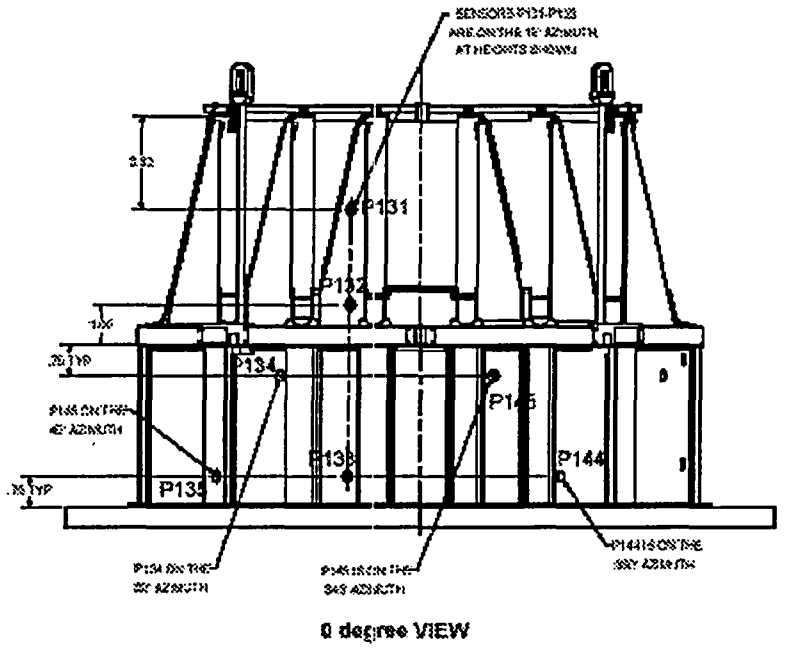

Figure 39a: Replacement dryer sensor locations

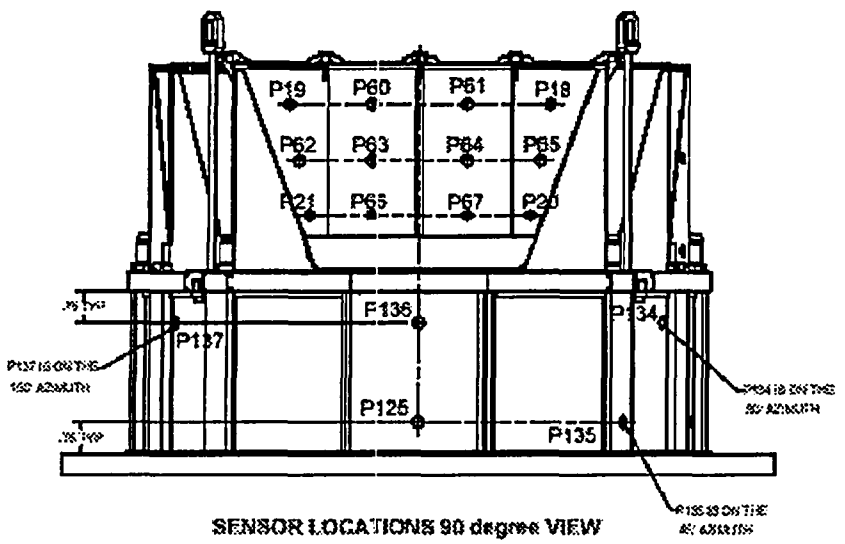

Figure 39b: Replacement dryer sensor locations

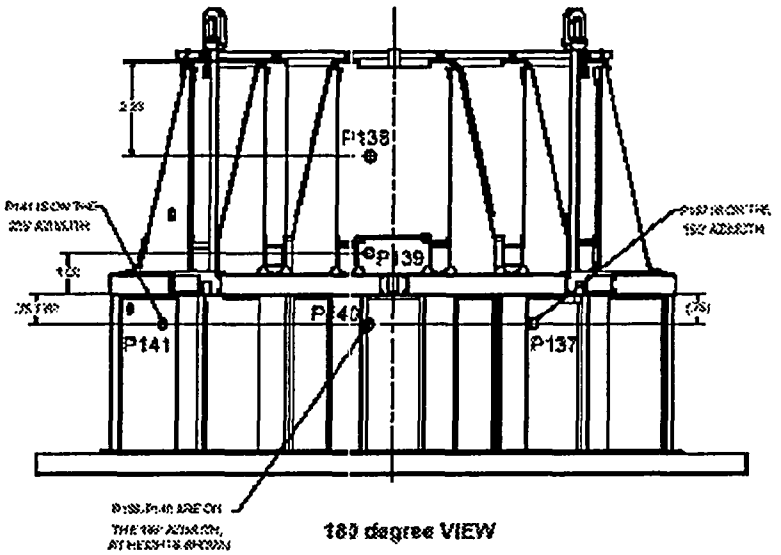

Figure 39c: Replacement dryer sensor locations

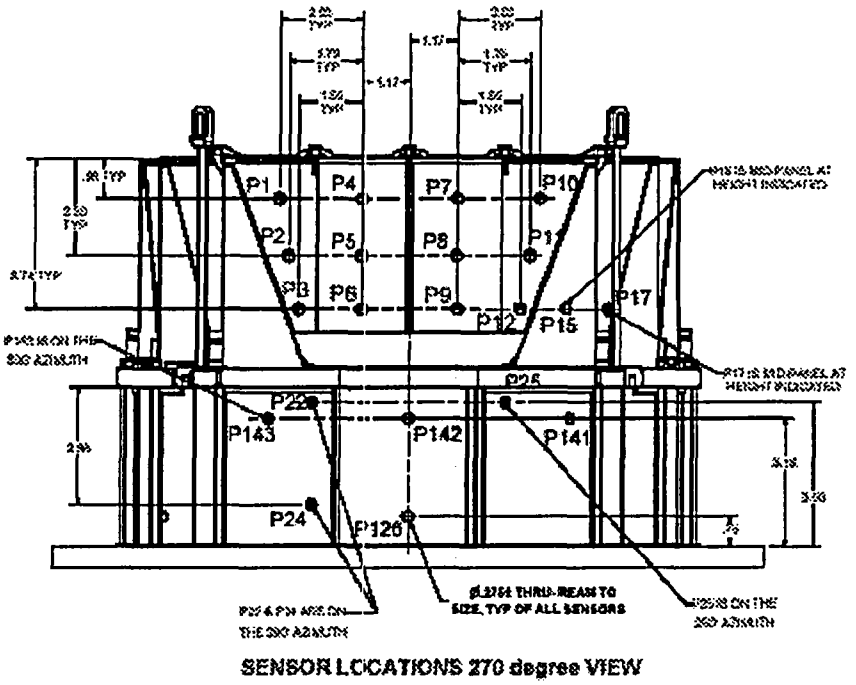

Figure 39d: Replacement dryer sensor locations

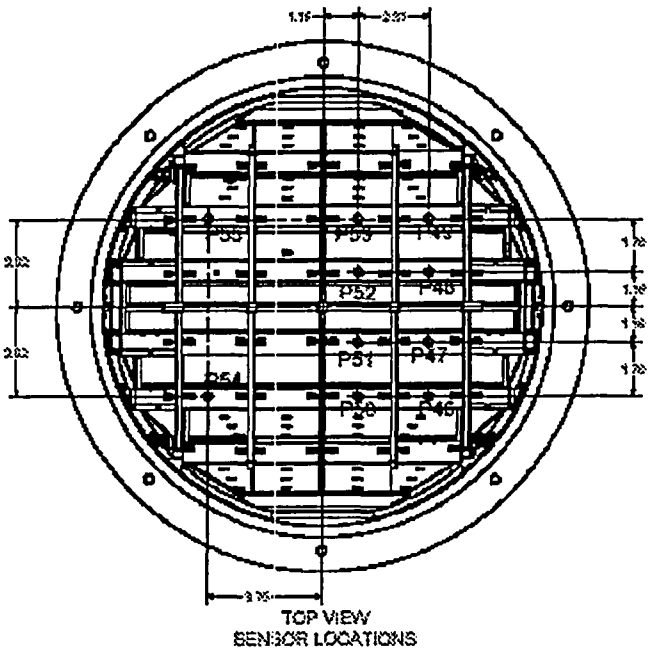

Figure 39e: Replacement dryer sensor locations

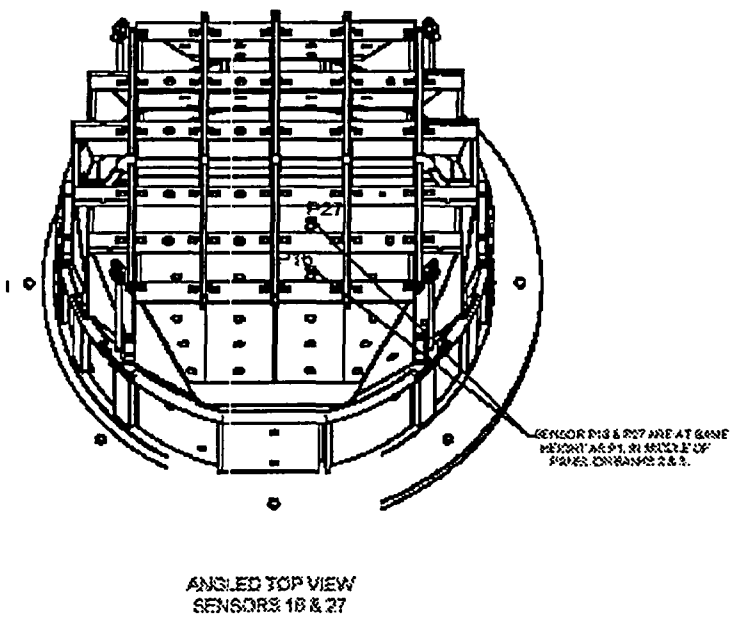

Figure 39f: Replacement dryer sensor locations

5.0 Data Analysis Methods

This section provides a description of the data acquisition, reduction and analysis performed for the Quad Cities tests.

5.1 Data Acquisition

Section 4 provides details of the sensor locations and types used for the testing. A LMS SCADAS III data acquisition front end controlled by a PC equipped with LMS Test.Lab software, revision 5A SL1 and SL2, received the transducer signals as analog voltages. The specific software module used during data acquisition was Signature Testing with the Time Recording During Signature Acquisition add-in. The front end performs an analog to digital conversion on the signal and transfers the signal to the PC where all of the signals from one run are stored in a throughput file, which is a LMS format of amplitude versus time. The initial digitization was performed with the following parameters:

- 16384 Hz sampling rate per channel
- AC coupling on dryer pressure transducer signals
- DC coupling on venturi and vessel pressure transducer signals and thermocouple signals
- Approximately 60 seconds of raw time data (throughput) recorded for dwells
- Approximately 500 to 600 seconds of raw time data (throughput) recorded for the 130 cfm to 250 cfm sweep (the whole sweep was captured – the time recording was stopped once the sweep had reached its upper flow limit)

All test equipment were calibrated prior to initiating the testing described in this document. In addition, an "end-to-end" calibration check was performed for each microphone before and immediately after all tests. This step ensured that the instrumentation remained functional and exhibited sensitivities consistent with their calibration values. This also ensured that any instrumentation that may have

malfunctioned during a test evolution were identified after the test so that the data could be treated accordingly.

5.2 Data Processing

The data processing involved the conversion of the raw time data for the dryer pressure sensors and the main steam line pressure sensors in the throughput files (or original raw time domain data files) to the following output formats:

- Peak Hold Autopower Spectra
- Linear Averaged Autopower Spectra
- Linear Averaged Autopower Spectra with amplitude and frequency scaled from subscale to full scale
- Phase Referenced Frequency Spectra/Operating Deflection Shape
- RMS Level of Frequency Band versus time and flow

The LMS software module used for processing was Throughput Validation and Processing Host with the following add-ins:

- Signature Throughput Processing
- Time Signal Calculator
- Geometry
- Operating Deflection Shape
- Signature Post-Processing

5.2.1 Peak Hold Autopower Spectra

The peak hold autopower spectra were processed from the throughput files with the following parameters:

- 0 Hz to 6400 Hz frequency range
- 1 Hz frequency resolution
- Hanning Window
- 0 to peak amplitude
- linear (square root of autopower) units
- linear or no weighting
- peak hold averaging
- 2 averages per second

5.2.2 Linear Averaged Autopower Spectra

Linear averaged autopower spectra were processed from the dwell throughput files using the following parameters:

- 0 Hz to 8192 Hz frequency range
- 2 Hz frequency resolution
- Hanning Window
- 0 to peak amplitude
- power units for the dwell condition, linear (square root of autopower) units for the sweep
- linear or no weighting
- linear averaging
- 2 averages per second for the dwell condition
- 1 spectrum every 5 seconds for the sweep condition

5.2.3 Linear Averaged Autopower Spectra Scaled to Full Scale

The linear averaged autopower spectra as processed above were exported to Excel. In Excel, the frequency resolution was reduced by the frequency scaling factor and the spectral amplitude was increased by the pressure scaling factor to correct the model data to plant conditions. These scaling factors were calculated using the scaling relationships shown in equations (12) and (13) described in Section 4.1. The scaling factors obtained for the EPU load case are:

[[

]]

5.2.4 Linear Averaged Crosspower Spectra

Linear averaged crosspower spectra were processed from the throughput files using the following parameters:

- 0 Hz to 6400 Hz frequency range
- 1 Hz frequency resolution
- Hanning Window
- 0 to peak amplitude
- power units
- linear or no weighting
- linear averaging
- 2 averages per second for the dwell condition
- Original Dryer Reference Sensor: M26
- Replacement Dryer Reference Sensor: M1

The linear averaged crosspower spectra were used to produce operating deflection shapes from the dwell condition.

5.2.5 Phase-referenced Frequency Spectra

Phase-referenced frequency spectra were processed from the throughput files using the following parameters:

- 0 Hz to 6400 Hz frequency range
- 1 Hz frequency resolution
- Hanning Window
- 0 to peak amplitude
- power units
- linear or no weighting
- linear averaging
- 1 measurement every 5 seconds for the sweep, and 1 measurement every 1 second for the dwell
- Original Dryer Reference Sensor: M26 pressure for the post-processed data, M25 pressure for the online-processed data
- Replacement Dryer Reference Sensor: M136 pressure

The result of phase referencing is that the frequency spectrum of the reference has 0° phase throughout the frequency range, and the phase of the other transducers is adjusted so that for each frequency line the phase is with respect to the reference instead of the start of the measurement time record. The phase-referenced frequency spectra from the sweep using M26 as the reference were used to produce operating deflection shapes from the sweep condition. The phase referenced-frequency spectra using M25 as the reference were only used for examining system trends.

5.2.6 RMS Level of Frequency Band versus time and flow

For the sweep, frequency bands were selected by visual review of the waterfall and using cursors to select borders of frequency bands that appeared significant. The RMS level of these bands was calculated and was plotted versus time and flow rate.

6.0 Scale Model Test Results of Pilot Plant Application

This section describes the tests performed on the Quad Cities scale model and summarizes the critical results and conclusions. The Quad Cities steam system was selected because the data obtained from the QC2 instrumented dryer in 2005 [15] was more comprehensive than any other instrumented dryer data available. Considering the number of sensor locations defined and the substantial number of tests performed, this document cannot present all data acquired from all tests. Data from all tests are archived at the GE San Jose site and are referenced in the DRF.

Because the plant data review described in Section 3 illustrated that the fluctuating pressures in the BWR steam system show substantial similarity from one plant to the next, the observations made from the QC scale model test data are a reasonable illustration of the general behaviors and sources expected in other BWRs. It is important to recognize that these data are not intended to represent the absolute frequency and amplitude expected for other BWRs; rather, the general observations made from these tests are applicable to other BWR configurations. In recognition of this, the SMT benchmark document presents a summary of the general knowledge gained from the QC SMT rather than simply a comparison of QC2 SMT load predictions and QC2 plant data. It is GE's intent to use the SMT to investigate the fundamental nature of the BWR steam dryer fluctuating loads in addition to providing the industry with a viable and predictive load definition process.

6.1 Test Purpose

The goals of the QC steam dryer tests were to:

1. Establish an understanding of the baseline behavior of system
2. Identify possible sources of the fluctuating pressures observed in the system
3. Develop an explanation of the observed frequency content
4. Obtain fluctuating pressure time history data that can be used to develop a dryer load definition

6.2 Summary of Testing Performed

To satisfy the goals described above, three distinct test evolutions were performed:

- Baseline Testing
  - Original Dryer Configuration
  - Replacement Dryer Configuration
- Source Screening Tests
  - Original Dryer Configuration
  - Replacement Dryer Configuration
- Characterization Testing
  - Replacement Dryer Configuration

All frequencies reported in this section are model frequencies. The equivalent plant frequency can be determined by applying the frequency scaling factor described in Section 4.1.

6.2.1 Baseline Tests

These tests were performed to acquire data throughout the range of expected plant operating conditions from which a general understanding of the system behavior could be obtained. These data were also used to benchmark the model against in-plant data. Sweep and dwell tests were performed with both dryer configurations. The model flow rates calculated for OLTP and EPU power conditions at the plant were determined using the scaling laws presented in Section 4.1.

The test fluid static pressure and temperature remained within the following range for all tests:

[[

]]

Because the system temperature and pressure increase as the blower output increases, the actual model flow rates which correspond to specific plant power levels (OLTP, EPU) are calculated during each test using the measured temperature to calculate the model sound speed.

6.2.2 Source Screening Tests

Recognizing the similarity of the BWR steam plenum acoustic loads described earlier in this document, GE decided to conduct source screening tests on the QC scale models. These tests would provide valuable insight into the behavior of BWR steam systems and identify the probable source locations and mechanisms for BWRs. The source screening tests were performed to identify which components controlled the observed frequency content of the fluctuating pressures in the steam plenum. The following components were investigated:

[[

]]

Each of the components identified above is shown in Figure 40.

[[

]]

The contribution from a specific component was identified by comparing the response in the steam plenum measured for each test configuration.

6.2.3 Characterization Tests

Characterization testing was performed to acquire data that could be used to correlate the acoustic Finite Element Model (FEM) of the physical model. The acoustic FEM was used to predict the normal modes of the steam system; these modes were then used to help interpret the frequency content and spatial pressure distribution of the data acquired in the steam plenum. The acoustic FEM is discussed in more detail in Section 6.3.4.2.

The characterization testing was performed by injecting a known noise source at various locations in the physical model and measuring the response at other locations. The noise source was a Mid-Frequency Volume Velocity Source (MFVVS), a device that provides a calibrated and controllable acoustic source and measures the volume acceleration that it imparts at its acoustic center or focal point. Volume acceleration is independent of boundary conditions so it is a consistent indicator of source strength. The volume velocity source is used as the reference, or input, and the microphones on the dryer and in the main steam lines are used as responses, or outputs, to calculate Frequency Response Functions (FRF). Several different types of input were evaluated:

- Periodic Chirp – a sine signal that, during the data acquisition period, is swept rapidly through the frequency range of interest. In this set of tests, it lasted for 70% of the acquisition time.
- Burst Random – a pure random signal in the frequency range of interest that is generated for only a portion of the time that is required to acquire a block of data and then drops to zero level for the remainder of the acquisition time. In this testing, it lasted for 70% of the acquisition time with a very brief ramp at the beginning of the acquisition.
- Random – a pure random signal that is continuous for the data acquisition period.

The different source types provided consistent results; however, in the frequency range of interest, the periodic chirp source generally provided the highest coherence value. The periodic results were used primarily for the analysis and comparisons with the acoustic FEM results.

The testing consisted of inserting the source at a known location and operating the source with the data acquisition system to obtain average results – FRFs, input autopower and response autopowers – that are the average of 100 individual measurements. Measurements were performed with the source at the MSL nozzles on the RPV and at locations along the MSL. Measurements were also performed with the MSLs removed and the nozzles plugged and with a rigid boundary at the steam-water interface. These tests were performed both with and without flow in the system in order to determine the effects of flow on the system.

The FRFs calculated from the test data were compared against FRFs calculated from the acoustic FEM to identify deficiencies in the acoustic FEM. The FRFs were also curve fit in an experimental acoustic modal analysis to obtain mode shapes of the acoustic space with associated frequency and damping values. The acoustic FEM was then modified, where appropriate, to improve the correlation – both to more closely match the frequencies of corresponding mode shapes from experiment to acoustic FEM and to increase the similarity between experimental and acoustic FRFs. This process is an acoustic analogy to a structural experimental modal analysis being performed to update a structural FEM. The volume velocity source is analogous to a shaker that provides an input force, and the microphones are analogous to accelerometers that provide an output acceleration. In the structural case, acceleration per force FRFs are obtained. In the acoustic case, pressure per volume acceleration FRFs are obtained. The RPV and MSL models were first correlated separately and then a final correlation was performed with both the RPV and MSL combined.

6.3 Summary of Model Data

The scale model data acquired from the tests described above are summarized in the following order:

- Baseline Test Data Characteristics
- Discussion of Source Screening Test Data
- Preliminary Source Identification and Explanation of Steam Plenum Frequency Content

The data presented in this section are reported in the model scale. These data must be corrected to the plant scale using the frequency and pressure scaling factors described in Section 4.1 to compare them with the plant data presented in Section 3.

6.3.1 Baseline Test Data Characteristics

This section provides data that describe the general trends observed in the original and replacement dryer tests.

6.3.1.1 System Trends versus Flow

Figure 42 is a spectrogram exhibiting the trend of fluctuating pressure amplitude with model flow rate. The horizontal axis displays frequency, the vertical axis corresponds to reactor power level and the color scale depicts fluctuating pressure amplitude. The data trends shown in Figure 42 are for the replacement dryer; these trends are also representative of the trends observed in the original dryer data. [[

]]

Although frequency spectra at various power levels are discussed in more detail in Section 6.3.1.3, some readers prefer to "calibrate" themselves by looking at a spectrum before reviewing waterfalls, spectrograms, or frequency cuts in detail. In recognition of this, Figure 52 shows three autopower spectra of QC2 replacement dryer data at EPU conditions obtained from sensors P1, P3, and P24. Figure 39 illustrates the sensor locations. These spectra will be discussed in additional detail later; however, they can be used to obtain a better understanding of the frequency content displayed in the spectrogram displayed as Figure 42.

From review of both the spectrogram and the autopower spectra it is evident that there are multiple frequencies observable in the data. To better understand the trend of fluctuating pressure amplitude with flow rate at each frequency, the RMS pressure amplitudes for the following frequency bands are displayed in Figures 43 through 46:

[[

]]

For convenience the model data amplitudes in these plots has been converted to the plant scale; however, the important information to observe is the trends exhibited by the data rather than the absolute amplitude. To illustrate that all sensors in the steam plenum exhibit the same general trend for a specific frequency band, frequency cuts from seven sensors on the outer hoods (P1, P3, P18, P20), inner hood (P27) and skirt (P24, P25) are shown in each plot. The trends shown in Figures 43 through 46 have also been fit with power law or exponential curve fit equations so that they can be compared to the plant data presented in Section 3.2.2. It is apparent that the pressure oscillations for the first three frequency bands can be approximated by the following relationship:

$$P = A \cdot U^b \qquad (1)$$

Where: P is the fluctuating pressure amplitude
A is a reference pressure
U is the mean fluid velocity
b is the power law exponent,
[[ ]]

[[

]]

[[

]]

6.3.1.2 Spatial Distribution of Fluctuating Pressures

This section describes the spatial distribution of the fluctuating pressures using Operational Deflection Shapes (ODS). For a first time viewer, these figures can be difficult to interpret; therefore, figure 48 has been provided to identify significant features of these figures. In this figure is provided a reference view from a 3-D CAD model of the dryer. Each of the four images in the figures corresponds to a different view angle of the steam dryer: side, front, top, isometric. The significant portions of the dryer have also been identified for you: top plates, skirt, outer hoods.

Figures 49 through 52 are static pictures of ODS animations. The nodes in the figure correspond to sensor locations. In these figures, displacement is proportional to a pressure applied normal to the surface shown. Eight of the prominent frequencies apparent in the model data are provided here. It should be observed that the spatial pressure distribution of the fluctuating loads becomes increasingly more complex as the frequency increases. This is expected and consistent with the hypothesis that the frequency content of the loading is controlled by the RPV steam plenum acoustic normal modes. The reader is encouraged to note the similarities between the model ODS and acoustic modes predicted using the FEM shown in Section 3.

6.3.1.3 OLTP & EPU Frequency Spectra

[[

]] Figure 52 contains autopower spectra of the data acquired at EPU operating conditions for the following locations: Outer Hood P1, Outer Hood P3, Skirt P24. Figure 39 identifies the microphone locations.

6.3.1.4 System Repeatability

To assess system repeatability, multiple tests were repeated throughout a day and on separate days. Figures 53 and 54 are autopower spectra of the model data obtained during the repeatability tests. Figure 53 displays data obtained from the outer hood (Original Dryer Microphone 14) during repeat runs at the same test conditions. Between each run reported in Figure 53, the test apparatus configuration had been changed to perform other tests and then returned to the repeatability test configuration. Figure 54 presents data obtained from a sensor placed on the steam dryer skirt (Original Dryer Microphone 26) for repeat runs performed at different times during the same day and on different days. The figure legends identify the sensor group (ga or gb) as well as the repeated run on each day (r2, r3). Group A and Group B tests were performed on different days. Observation of Figures 53 and 54 shows that the system exhibits the same frequency content and amplitude for test runs made with the same configuration. The data obtained from six repeat tests demonstrate that the scale test facility and the QC scale model produce consistent and repeatable results.

6.3.2 Discussion of Source Screening Test Data

The apparent effect of each component on the steam plenum fluctuating pressure loads was determined by a comparison of the autopower spectra obtained from the tests performed with and without the specific component. If a change in the frequency content or amplitude was observed in the steam plenum when the component was absent then the component was considered to be a possible source or important resonator. Using this simple criterion the following components were shown to have a strong effect on the dryer loads:

[[

]]

The remaining components discussed in Section 6.2.2 were not observed to have a significant affect on the dryer loads.

6.3.2.1 MSL Source Screening Test Observations

[[

]] Recognizing this, the amount of the observed effect contributed by individual components contained in the removed section is not immediately obvious. This limitation is not problematic because this test was only intended to obtain an initial assessment of the relative importance of the various components.

Figures 55 through 58 summarize the data discussed in this section. Figure 55 represents data acquired from Replacement Dryer sensor 136, which is located on the skirt. [[

]] Figure 56 shows the frequency spectra from 5-300 Hz in Figure 55 so that the lower frequency content can be clearly observed. Figures 57 and 58 show the frequency spectra from [[ ]], respectively. These three bands were chosen because they contain the most significant frequency content observed in the steam plenum for the configuration tested. The top half of each figure displays a linear average spectrum; whereas, the bottom half of the plot is a peak hold spectrum. The nomenclature used in the figure header to refer to the test performed at each cut line is explained in Table 7 below:

Table 7: Identification of MSL Source Screening Test header nomenclature

Legend Description	Cut Line[1]
[[	Nominal Condition
	1
	2
	3
	4
]]	5

1. Refer to Figure 41 for identification of the cut line locations.

The MSL screening test data suggest the following observations:

[[

]]

Figure 59 summarizes the percent of the baseline RMS pressures measured for each test condition. This figure provides a quantitative estimate of the signal content remaining in the steam plenum for each test. The five frequency bands shown in Figure 59 are slightly different than shown in Figures 55 through 58 and were chosen to highlight the significant frequency content observable in the steam plenum: [[ ]]

Review of Figures 55 through 58 shows that removal of the [[

]]

6.3.2.2 MSIV Source Screening Test Observations

[[

]]

Table 8: Percent change in steam plenum RMS pressure loads when MSIVs removed

[[			

]]

6.3.2.3 S/RV Source Screening Test Observations

[[

]]

6.3.2.4 Remaining MSL Components Considered in Source Screening Tests

[[

]]

6.3.3 Source Identification and Explanation of Frequency Content

The testing performed to date has shown that the frequency content observed in the model steam plenum can be segregated into three separate groups for discussion of source mechanisms and critical resonating chambers:

[[

]]

Figure 64 is an autopower spectra from sensors located on the outer hood and skirt region of the replacement QC steam dryer. [[

]] For each frequency observable in the model data at least two critical pieces of information must be known to offer an explanation of the content: excitation mechanism and resonator. These items will be addressed for each of the three groups introduced above.

6.3.3.1 Main Steam Line Acoustics

Review of Figures 56, 60, and 62 suggest the following observations:

[[

]]

[[

]]

6.3.3.2 Steam Plenum Acoustic Modes

[[

]]

6.3.3.2.1 QC Test Apparatus Acoustic Finite Element Model

An acoustic finite element model of the test apparatus was built to assist in the interpretation of the scale model test data. The LMS VL.Acoustics and Sysnoise Finite Element Analysis software was used for this analysis. Figures 65 and 66 show the finite element mesh used to model the steam plenum and main steam lines. [[

]]

The acoustic FEM was correlated to the test apparatus using the test data acquired during the characterization tests described above. Figure 67 shows an overlay of some of the experimental and analytical FRFs which indicate a generally good correlation between the model and the test apparatus. The correlated acoustic FEM is now useful for understanding the normal modes of the SMT as well as those in the plant.
Characterization tests were also performed at various flow rates to show that the acoustic FEM could adequately replicate the system normal modes at the flow rates of interest. It is recognized that the Mach number in the system is low; therefore, it was assumed that the normal modes would not be largely affected by the mean flow. To be thorough, some of the correlation testing was performed with flow in order to confirm this assumption.

Once the acoustic FEM was correlated then the normal modes predicted by an acoustic modal analysis were used to help interpret the data measured in the steam plenum. Figures 68 through 73 show the first nine steam plenum acoustic cavity modes for the test apparatus. These modes can be

scaled to plant conditions using the same frequency scaling factor discussed in Section 4.1 above.

[[

]]

6.3.3.2.2 Test Data Characteristics in Steam Plenum

[[

]]

6.3.3.2.3 Possible Source Mechanisms for Steam Plenum Acoustic Modes

[[

]]

6.3.3.3 SRV/ Steam Plenum Coupled Acoustic Modes

[[

]]

6.3.3.4 Summary of Frequency Content

The discussion of the observed frequency content and postulated excitation mechanisms discussed above are summarized:

1. [[

]]

[[

]]

Figure 40: MSL Components considered in the source screening tests.

[[

]]

Figure 41: Locations at which the MSL was removed for the MSL source screening test.

[[

]]

Figure 42: Spectrogram of Replacement Dryer test data, Microphone 1, ~80-120% power.

[[

]]

Figure 43: Frequency cuts for the model data equivalent to the plant [[ ]] frequency band.

[[

]]

Figure 44: Frequency cuts for the model data equivalent to the plant [[ ]] frequency band.
[[

]]

Figure 45: Frequency cuts for the model data equivalent to the plant [[ ]] frequency band.

[[

]]

Figure 46: Frequency cuts for the model data equivalent to the plant [[ ]] frequency band.

[[

]]

Figure 47: Comparison of fluctuating pressure trends with reactor power level for four frequency bands, sensor P1.

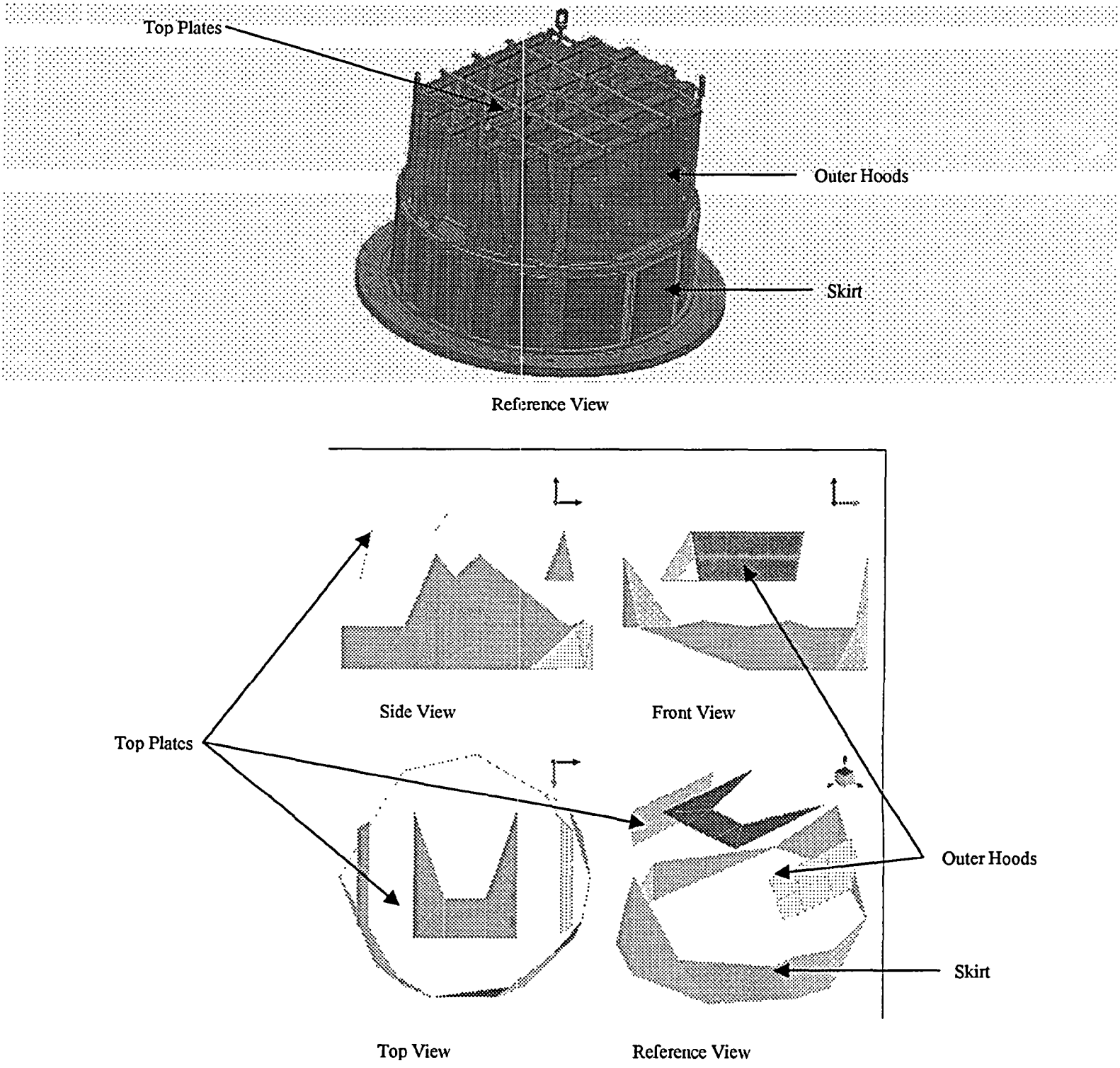

Figure 48: Reference images for interpretation of ODS figures.

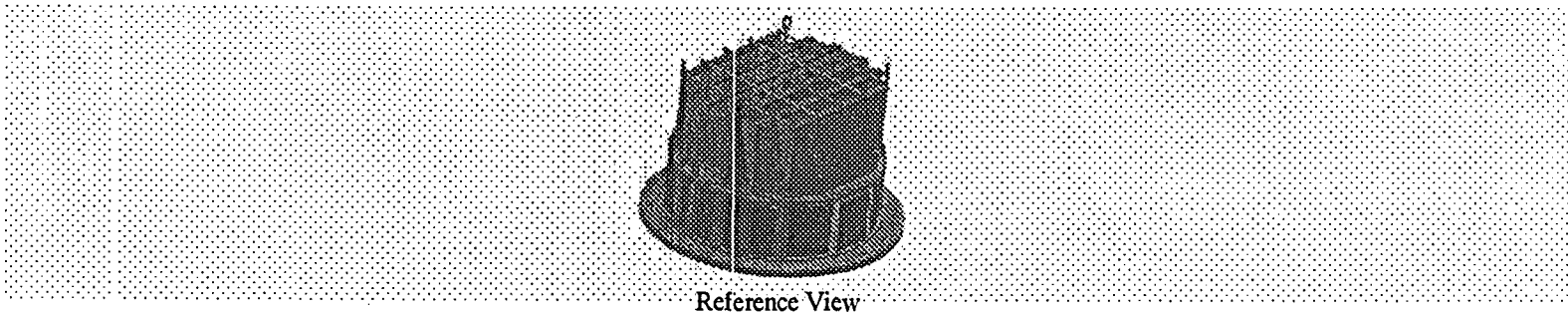

Reference View

[[

]]

Figure 49: ODS for prominent QC2 SMT frequencies.

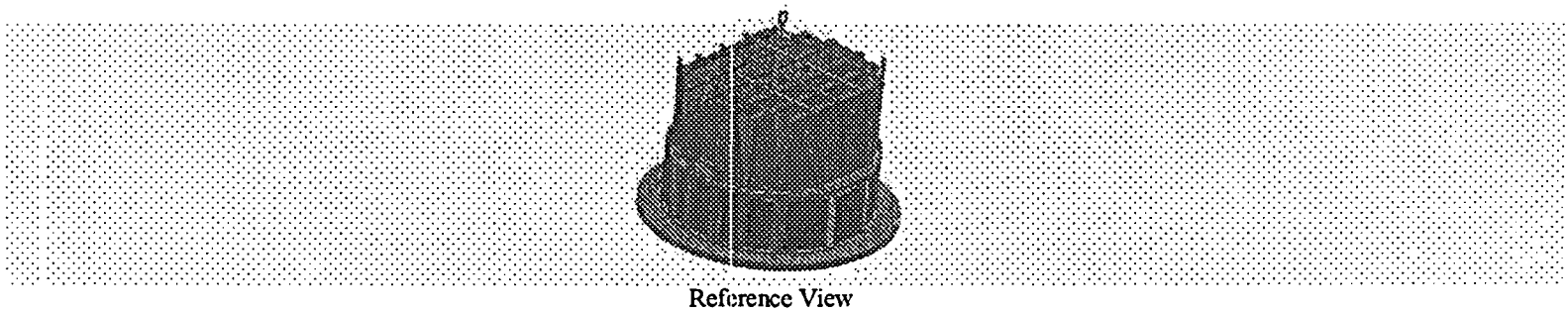

Reference View

[[

]]

Figure 50: ODS for prominent QC2 SMT frequencies.

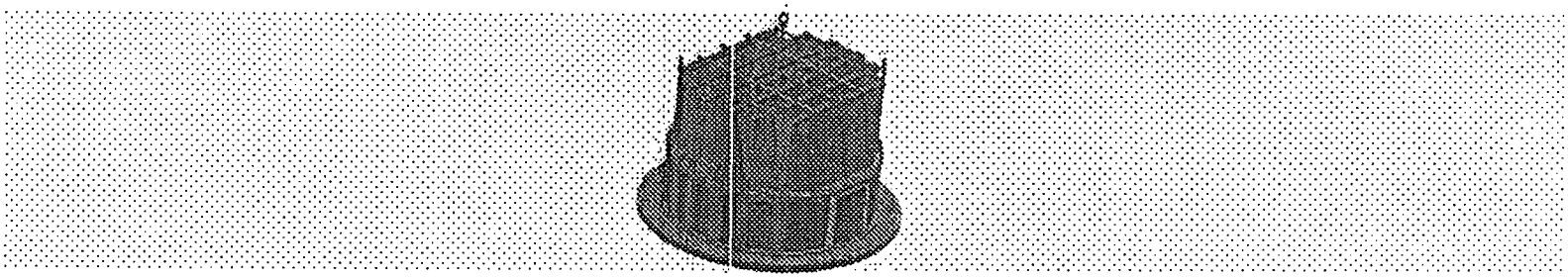

Reference View

[[

]]

Figure 51: ODS for prominent QC2 SMT frequencies.

[[

]]

Figure 52: QC2 SMT, EPU Power, Autopower spectra, P1, P3, P24.

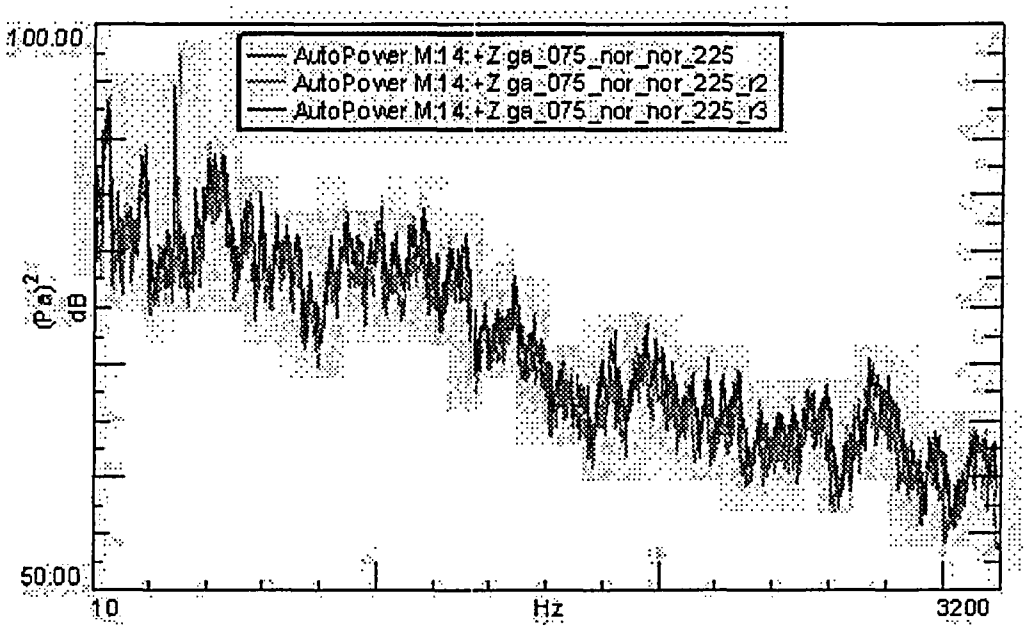

Figure 53: Original Dryer Sensor 14 Repeatability test data

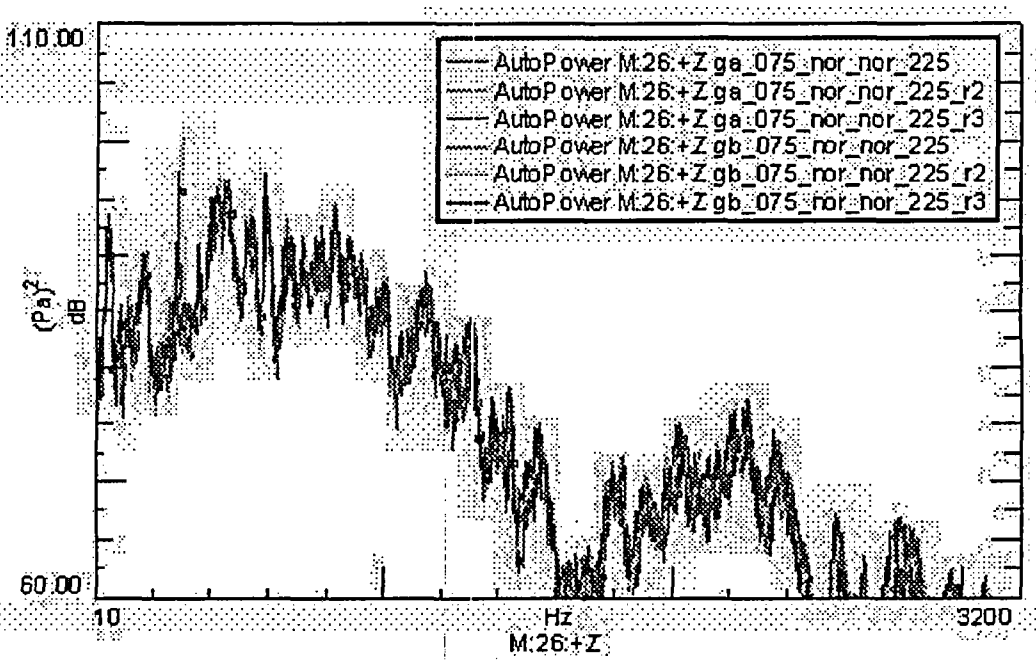

Figure 54: Original Dryer Sensor 26 Repeatability test data

[[

]]

Figure 55: Frequency spectra for MSL source screening tests, [[ ]]

[[

]]

Figure 56: Frequency spectra for MSL source screening tests, [[ ]]

[[

]]

Figure 57: Frequency spectra for MSL source screening tests, [[ ]]

[[

]]

Figure 58: Frequency spectra for MSL source screening tests, [[ ]]

[[

]]

Figure 59: Percent of baseline RMS pressure measured in steam plenum for MSL source screening test.

[[

]]

Figure 60: Frequency spectra from MSIV source screening test, Original Dryer, Top Plates.

[[

]]

Figure 61: Frequency spectra from MSIV source screening test, Original Dryer, Outer Hoods.

[[

]]

Figure 62: Frequency spectra from MSIV source screening test, Original Dryer, Skirt.

[[

]]

Figure 63: S/RV source screening test data from dryer outer hood, 4 SRV plugged

[[

]]

Figure 64: Identification of separate frequency bands in model data.

[[

]]

Figure 65: Acoustic FEM cavity mesh and skin mesh of QC1 steam plenum and dryer surfaces.

[[

]]

Figure 66: Acoustic FEM mesh of the entire QC1 model steam system.

[[

]]

Figure 67: Subset of Acoustic FEM correlation results to characterization test data.

[[

]]

Figure 68: QC1 model steam plenum Acoustic Mode #1, [[ ]]

[[

]]

Figure 69: QC1 model steam plenum Acoustic Mode #2, [[ ]].

[[

]]

Figure 70: QC1 model steam plenum Acoustic Modes #3 & #4, [[ ]]

[[

]]

Figure 71: QC1 model steam plenum Acoustic Modes #5 & #6, [[ ]].

[[

]]

Figure 72: QC1 model steam plenum Acoustic Modes #7 & #8, [[ ]]

[[

]]

Figure 73: QC1 model steam plenum Acoustic Mode #9, [[ ]]

[[

]]

Figure 74: QC steam plenum Acoustic Mode believed to be coupled to S/RV resonance, [[ ]]

7.0 Benchmark of SMT Process

This section compares the QC2 scale model load predictions with the QC2 plant data acquired during the 2005 power ascension test program conducted by GE [15]. The benchmark is performed to assess the quality of the GE SMT methodology. To obtain a valid assessment of a methodology's ability to make accurate load predictions the following items must be reviewed:

1. Similarity of frequency content and amplitude between the plant measurement and model prediction
2. Trends apparent in plant data and model prediction
3. Spatial pressure distribution of plant loads and model prediction
4. Process uncertainty (See Attachment B)

To satisfy the first three items above, the following comparisons shall be presented here:

1. PSDs at EPU conditions
2. Spectrograms
3. Frequency cuts
4. Operational Deflection Shapes

The PSD is an appropriate tool to determine if the model predictions at a specific power level exhibit similar frequency content and amplitude as observed in the plant data. This is necessary but not sufficient for an acceptable load definition or prediction process. In addition to showing the same frequency content, the SMT must demonstrate that it can adequately preserve the trends apparent in the plant data. If the SMT preserves the trends then it can be inferred that the SMT has preserved the important excitation mechanisms that exist in the plant. Finally, it must still be demonstrated that the model loads exhibit the same spatial pressure distributions as observed in the plant data. The ODS displays the distribution of loads around the steam dryer. This tool is very useful for visualizing the spatial distribution of the load.

For the benchmark included in this document, all SMT data have been converted to the plant scale using the scaling method described in Section 4.1.

7.1 Comparison of PSD

Figures 75 through 98 show overlaid PSDs of the plant data and model predictions at the highest power level obtained during the 2005 power ascension testing [15]. It can be seen from the 1-100 Hz band that the SMT predictions preserve the frequency content observed in the plant data and that the loads predicted by the SMT are generally conservative. Table 9 compares the RMS fluctuating pressure amplitudes from the SMT prediction and the plant measurement. [[

]] Figure 99 is a histogram of the ratio between SMT predictions and plant measurements shown in Table 9. [[

]]

[[

]]

Table 10 summarizes the RMS and Peak pressures for the SMT prediction and the plant measurement in the [[

]] For this signal content the Peak comparison is considered to be more appropriate considering that we are [[

]] It is more important that the model predicts the existence of resonances in the correct frequency range rather than the absolute number of resonances. The number of resonances is determined by variations in the as-built configuration of the plant which cannot be known by the utility up front. If the SMT correctly predicts a resonance in the proper frequency band then the structural effect of these resonances will be investigated with the structural analysis. Figure 100 is a histogram of the ratio between SMT peak amplitude predictions and plant peak amplitude measurements shown in Table 10. This histogram illustrates the distribution of the data. [[

]] One possible explanation for this behavior is offered later in this section. The results contained in Table 10 illustrate that the SMT prediction for the [[ ]]

Table 11 summarizes the RMS and Peak pressures for the SMT prediction and the plant measurement in the [[

]]. For this signal content the Peak comparison is considered to be more appropriate considering that we are [[

]] Figure 101 is a histogram of the ratio between SMT peak amplitude predictions and plant peak amplitude measurements shown in Table 11. This histogram illustrates the distribution of the data. [[

]] One possible explanation for this behavior is offered later in this section. [[

]]

The results shown in the provided PSDs and tables warrant additional discussion before moving on to the spectrograms, frequency cuts and ODS comparisons. [[

]]

[[

]]

7.2 Comparison of Spectrograms

Figures 102 through 105 are side-by-side comparisons of model (Left) and plant (Right) spectrograms from 80-120% power. The frequency scale of these plots has been set to equivalent model and plant frequency ranges. The purpose of these plots is to demonstrate that the model accurately predicts [[ ]] at the same range of power levels as observed in the plant data. The spectrograms shown here are from sensor locations P1, P10, P18, P20. These data are representative of the remaining instrument locations.

7.3 Comparison of Frequency Cuts

Figures 106 through 121 are trends of fluctuating pressure versus reactor power level for the four frequency bands introduced above. Trends from four sensors are shown here; these trends are representative of the remaining sensor locations. It can be seen here that the SMT exhibits conservative trends in the 0-10 Hz, 10-30 Hz, and 30-100 Hz frequency bands. This is consistent with the PSDs shown above. The model exhibits the same functional relationship as the plant data in the [[ ]] This illustrates that the model has preserved the excitation mechanism for this content.

Table 9: Summary of plant and model RMS values for 1-100 Hz frequency band.

Sensor Location	SMT RMS, Pa	Plant RMS, Pa	Error, %	Ratio
[[				
				]]

[[ ]]

Table 10: Summary of plant and model RMS & peak values for [[ ]]

Sensor Location	SMT RMS, Pa	Plant RMS, Pa	Error, %	Ratio	SMT Peak, Pa^2/Hz	Plant Peak, Pa^2/Hz	Error, %	Ratio
[[								
								]]

Table 11: Summary of plant and model RMS & peak values for [[ ]]

Sensor Location	SMT RMS, Pa	Plant RMS, Pa	Error, %	Ratio	SMT Peak, Pa^2/Hz	Plant Peak, Pa^2/Hz	Error, %	Ratio
[[								
								]]

7.4 Comparison of Operational Deflection Shapes

Figures 123 through 130 are static pictures of ODS animations. Each figure contains a side-by-side comparison of the spatial pressure distribution exhibited in the model data (Left) and plant data (Right) at a specific frequency. The nodes in the figure correspond to sensor locations. In these figures, displacement is proportional to a pressure applied normal to the surface shown. Eight of the prominent frequencies apparent in the model and plant data are provided here. These figures are included to illustrate the ability of the SMT to preserve the spatial distribution of the fluctuating pressure loads on the steam dryer. An accurate stress analysis cannot be performed if the load distribution applied to the structural FEM is not shown to be accurate.

For a first time viewer, these figures can be difficult to interpret; therefore, figure 122 has been provided to identify significant features of these figures. A reference view is provided in this figure from a 3-D CAD model of the dryer. Each of the four images in the left and right portions of the figures corresponds to a different view angle of the steam dryer: side, front, top, isometric. The significant portions of the dryer have also been identified for you: top plates, skirt, outer hoods.

The plant data has less resolution than the model data because the plant instrumentation program could not use as many instruments as the SMT. This is one obvious benefit of the SMT; in the laboratory, a significant amount of instrumentation can be used to obtain a more detailed understanding of the system behavior than can be obtained from a plant test program. The provided ODSs demonstrate that the SMT predictions and plant data show good agreement. These data demonstrate that the SMT can provide load predictions that accurately represent the spatial pressure distributions of the loads expected in the plant steam system.

7.5 Discussion of Benchmark

It has been shown in the benchmark comparisons provided here that the current SMT method:

1. Adequately predicts the expected frequency content of the BWR steam dryer fluctuating loads

2. Provides conservative amplitude predictions (on the order of a factor of 1 to 4) in the frequency band not influenced by the [[ ]]

3. Adequately predicts the existence of the significant [[ ]]

4. Preserves the excitation mechanism responsible for exciting [[ ]]

5. Adequately predicts the power levels at which [[ ]] will occur in a plant

6. Adequately predicts the spatial pressure distribution of the applied loading

Although the SMT methodology, in its current state, has been shown to provide adequate and useful input to load definitions, it is desirable to continue to improve the technology to remove the variability in the predicted [[ ]].

[[

]]

Figure 75: Overlaid PSD: QC2 SMT Prediction & QC2 Plant Data, Plant TC 41, Sensor P1

[[

]]

Figure 76: Overlaid PSD: QC2 SMT Prediction & QC2 Plant Data, Plant TC 41, Sensor P2

[[

]]

Figure 77: Overlaid PSD: QC2 SMT Prediction & QC2 Plant Data, Plant TC 41, Sensor P3

[[

]]

Figure 78: Overlaid PSD: QC2 SMT Prediction & QC2 Plant Data, Plant TC 41, Sensor P4

[[

]]

Figure 79: Overlaid PSD: QC2 SMT Prediction & QC2 Plant Data, Plant TC 41, Sensor P5

[[

]]

Figure 80: Overlaid PSD: QC2 SMT Prediction & QC2 Plant Data, Plant TC 41, Sensor P6

[[

]]

Figure 81: Overlaid PSD: QC2 SMT Prediction & QC2 Plant Data, Plant TC 41, Sensor P7

[[

]]

Figure 82: Overlaid PSD: QC2 SMT Prediction & QC2 Plant Data, Plant TC 41, Sensor P8

[[

]]

Figure 83: Overlaid PSD: QC2 SMT Prediction & QC2 Plant Data, Plant TC 41, Sensor P9

[[

]]

Figure 84: Overlaid PSD: QC2 SMT Prediction & QC2 Plant Data, Plant TC 41, Sensor P10

[[

]]

Figure 85: Overlaid PSD: QC2 SMT Prediction & QC2 Plant Data, Plant TC 41, Sensor P11

[[

]]

Figure 86: Overlaid PSD: QC2 SMT Prediction & QC2 Plant Data, Plant TC 41, Sensor P12

[[

]]

Figure 87: Overlaid PSD: QC2 SMT Prediction & QC2 Plant Data, Plant TC 41, Sensor P15

[[

]]

Figure 88: Overlaid PSD: QC2 SMT Prediction & QC2 Plant Data, Plant TC 41, Sensor P16

[[

]]

Figure 89: Overlaid PSD: QC2 SMT Prediction & QC2 Plant Data, Plant TC 41, Sensor P17

[[

]]

Figure 90: Overlaid PSD: QC2 SMT Prediction & QC2 Plant Data, Plant TC 41, Sensor P18

[[

]]

Figure 91: Overlaid PSD: QC2 SMT Prediction & QC2 Plant Data, Plant TC 41, Sensor P19

[[

]]

Figure 92: Overlaid PSD: QC2 SMT Prediction & QC2 Plant Data, Plant TC 41, Sensor P20

[[

]]

Figure 93: Overlaid PSD: QC2 SMT Prediction & QC2 Plant Data, Plant TC 41, Sensor P21

[[

]]

Figure 94: Overlaid PSD: QC2 SMT Prediction & QC2 Plant Data, Plant TC 41, Sensor P22

[[

]]

Figure 95: Overlaid PSD: QC2 SMT Prediction & QC2 Plant Data, Plant TC 41, Sensor P23

[[

]]

Figure 96: Overlaid PSD: QC2 SMT Prediction & QC2 Plant Data, Plant TC 41, Sensor P24

[[

]]

Figure 97: Overlaid PSD: QC2 SMT Prediction & QC2 Plant Data, Plant TC 41, Sensor P25

[[

]]

Figure 98: Overlaid PSD: QC2 SMT Prediction & QC2 Plant Data, Plant TC 41, Sensor P27

[[

]]

Figure 99: Histogram of [[ ]]prediction ratio

[[

]]

Figure 100: Histogram of [[ ]] prediction ratio

[[

]]

Figure 101: Histogram of [[ ]]prediction ratio

[[

]]

Figure 102: Spectrograms of QC2 S/RV resonances for SMT Prediction (Left) and Plant data (Right), P1

[[

]]

Figure 103: Spectrograms of QC2 S/RV resonances for SMT Prediction (Left) and Plant data (Right), P10

[[

]]

Figure 104: Spectrograms of QC2 S/RV resonances for SMT Prediction (Left) and Plant data (Right), P18

]]

Figure 105: Spectrograms of QC2 S/RV resonances for SMT Prediction (Left) and Plant data (Right), P20

[[

]]

Figure 106: Comparison of QC2 model prediction and plant data frequency cut, [[ ]], P1

[[

]]

Figure 107: Comparison of QC2 model prediction and plant data frequency cut, [[ ]], P1

[[

]]

Figure 108: Comparison of QC2 model prediction and plant data frequency cut, [[ ]], P1

[[

]]

Figure 109: Comparison of QC2 model prediction and plant data frequency cut, [[ ]], P1

[[

]]

Figure 110: Comparison of QC2 model prediction and plant data frequency cut, [[ ]], P12

[[

]]

Figure 111: Comparison of QC2 model prediction and plant data frequency cut, [[ ]], P12

[[

]]

Figure 112: Comparison of QC2 model prediction and plant data frequency cut, [[ ]], P12

[[

]]

Figure 113: Comparison of QC2 model prediction and plant data frequency cut, [[ ]], P12

[[

]]

Figure 114: Comparison of QC2 model prediction and plant data frequency cut, [[ ]], P18

[[

]]

Figure 115: Comparison of QC2 model prediction and plant data frequency cut, [[ ]], P18

[[

]]

Figure 116: Comparison of QC2 model prediction and plant data frequency cut, [[ ]], P18

[[

]]

Figure 117: Comparison of QC2 model prediction and plant data frequency cut, [[ ]], P18

[[

]]

Figure 118: Comparison of QC2 model prediction and plant data frequency cut, [[ ]], P21

[[

]]

Figure 119: Comparison of QC2 model prediction and plant data frequency cut, [[ ]], P21

[[

]]

Figure 120: Comparison of QC2 model prediction and plant data frequency cut, [[ ]], P21

[[

]]

Figure 121: Comparison of QC2 model prediction and plant data frequency cut, [[ ]], P21

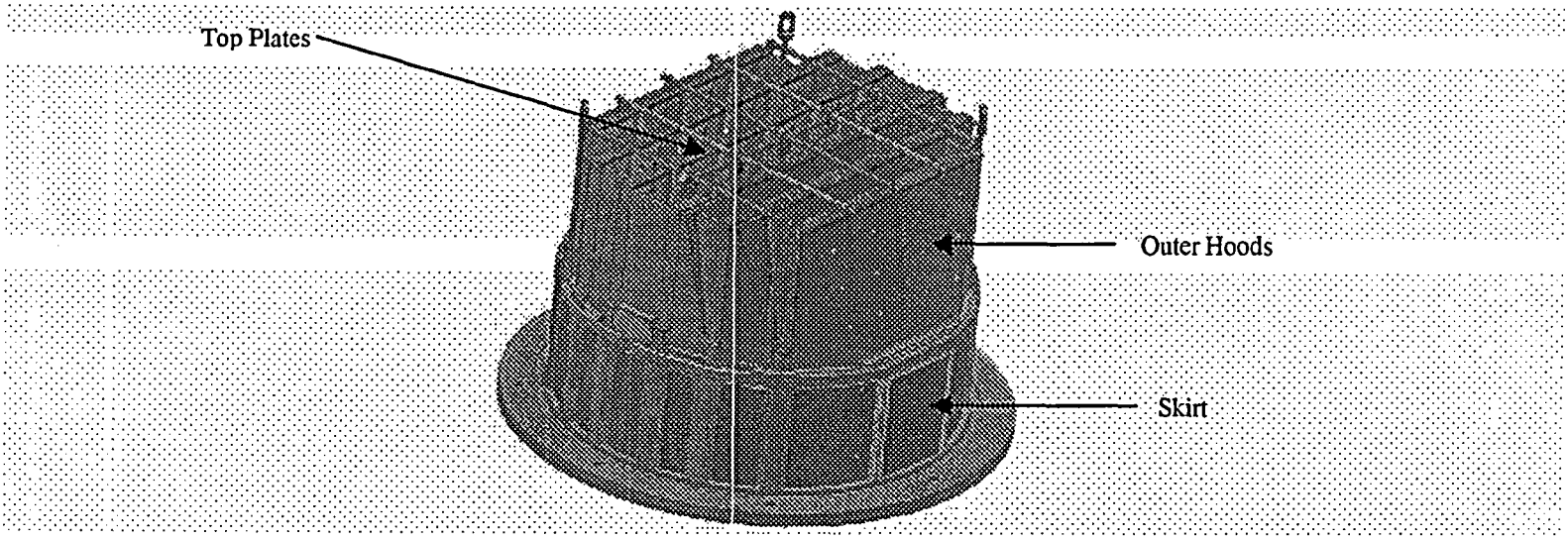

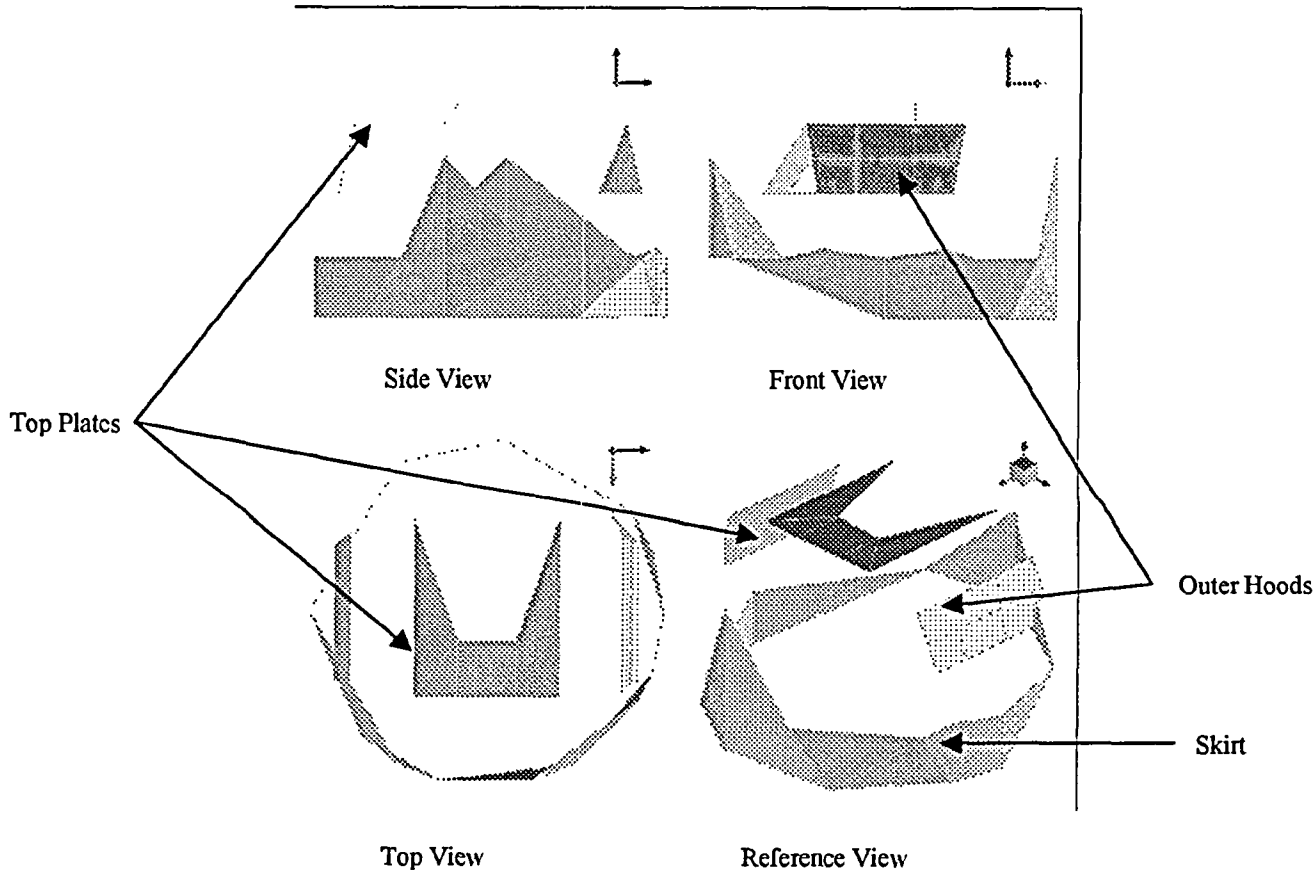

Figure 122: Reference images for interpretation of ODS figures.

[[

]]

Figure 123: QC2 Spatial Pressure Distribution comparison, SMT (Left) & Plant (Right), [[ ]]

[[

]]

Figure 124: QC2 Spatial Pressure Distribution comparison, SMT (Left) & Plant (Right), [[ ]]

[[

]]

Figure 125: QC2 Spatial Pressure Distribution comparison, SMT (Left) & Plant (Right), [[ ]]

[[

]]

Figure 126: QC2 Spatial Pressure Distribution comparison, SMT (Left) & Plant (Right), [[ ]]

[[

]]

Figure 127: QC2 Spatial Pressure Distribution comparison, SMT (Left) & Plant (Right), [[ ]]

[[

]]

Figure 128: QC2 Spatial Pressure Distribution comparison, SMT (Left) & Plant (Right), [[ ]]

[[

]]

Figure 129: QC2 Spatial Pressure Distribution comparison, SMT (Left) & Plant (Right), [[ ]]

[[

]]

Figure 130: QC2 Spatial Pressure Distribution comparison, SMT (Left) & Plant (Right), [[ ]]

8.0 Development and Validation of Plant Specific Load Definitions

This section describes the process for creating the structural finite element model load definition and introduces the GE recommended approach for performing power ascension testing to validate a plant specific steam dryer load definition. This scope of this document does not include detailed discussions of the load interpolation algorithm or the plant power ascension testing; therefore, this section is provided only to provide the reader with an understanding of the overall process. Detailed descriptions of the load interpolation algorithm and power ascension testing will be provided in separate documents.

8.1 Load Definition Process

The final load definition process used to develop the load input to the structural analysis of the steam dryer is illustrated in Figure 131. As shown in this figure, there are two inputs to the Load Interpolation Algorithm:

[[

]]

8.2 Plant Power Ascension Testing for Validation of SMT Load Definition

Recognizing that the SMT S/RV amplitude predictions exhibited greater error than the remaining frequency content, GE is continuing to do work to refine the quality of the S/RV amplitude predictions. Until the error for this load component is reduced, GE is recommending power ascension monitoring of a plant as it ascends to EPU power levels. This monitoring is performed to confirm the adequacy of the SMT load definition in the S/RV frequency range.

[[

]]

Many utilities are currently using main steam line strain gauging techniques in order to measure the dynamic pressures in the steam system and infer the pressure loading on the steam dryer. These techniques and the strain gauge locations being used on the MSL are suitable for the power ascension monitoring recommended here. Future plant specific applications should include plans to instrument their MSL close to the RPV steam plenum; the SMT will be instrumented at equivalent locations so that comparison data sets can be acquired.

[[

]]

Figure 131: Flow-chart for load definition development from SMT data.

9.0 Summary and Conclusions

The following conclusions are made from the information presented above:

1. Using the available plant data, acoustic induced vibration is considered to be the most significant load on the steam dryer.

2. The scale model test data matches well with the available in-plant data; therefore,

    a. The scale model test apparatus and methodology are viable tools to predict fluctuating pressure loads on the steam dryer.

    b. The conclusion that acoustic loads are the primary contribution to the fluctuating loads on the BWR steam dryer is validated.

    c. The model predictions are consistently conservative in the 1-100 Hz frequency band at the plant scale.

    d. The model can adequately predict the existence of [[ ]].

4. The sources for the fluctuating pressures acting on the dryer can be explained by the following:

    [[

]]

Additional work is on-going to improve the understanding of the excitation mechanisms and source locations as well as [[

]]

10.0 References

1. Au-Yang, M. K., "Flow-Induced Vibration of Power and Process Plant Components", Professional Engineering Publishing Limited, 2001.

2. Blevins, R. D., "Flow Induced Vibration", 2nd Edition. Krieger Publishing Company. 2001.

3. Ziada, S., Buhlmann, E.T., Bolleter, U., "Flow Impingement as an Excitation Source in Control Valves", Journal of Fluids and Structures, 3, 529-549.

4. Graf, H.R., Ziada, S., Rohner, R., Kalin, R., "Verification of Scaling Rules for Control Valve Noise by Means of Model Tests", AD-Vol. 53-2, Fluid-Structure Interaction, Aero elasticity, Flow-Induced Vibration and Noise, Volume II, ASME 1997.

5. Ziada, S., Sperling, H., Fisker, H., "Flow-Induced Vibration of a Spherical Elbow Conveying Steam at High Pressure", PVP-Vol 389, Flow-Induced Vibration. 1989.

6. Ziada, S., "A Flow Visualization Study of the Flow-Acoustic Coupling at the Mouth of a Resonant Side-Branch". ASME Pressure Vessel and Piping Journal. Vol 258. pp. 35-59. 1993.

7. Baldwin, R. M., Simmons, H. R., "Flow-Induced Vibration in Safety Relief Valves", Journal of Pressure Vessel Technology, Vol. 108, Aug. 1986, pp. 267-272.

8. Rockwell, D., Naudascher, E., "Review – Self-Sustaining Oscillations of Flow Past Cavities", Journal of Fluids Engineering, Vol. 100, June 1978, pp. 152-165.

9. Elmore, W.C., Heald, M. A., "Physics of Waves". Dover Publications. 1969.

10. Journal of Fluids and Structures (1999) 13, 127 – 142. Article No.: jfls. 1998.0189. Ziada, S. & Shine, S. (1999). Strouhal Numbers of Flow-Excited Acoustic Resonance of Closed Side Branches.

11. Not Used

12. Malone, Bobby. "Computational Fluid Dynamics Flow Visualization of Quad Cities Sub-Scale Original Dryer Model as a Function of Reynolds Number". GE-NE-0000-0038-3018-01. April 2005. GENE. Wilmington, NC. GE Proprietary Information.

13. Not Used

14. Morse, Philip M., Ingard, K. Uno., "Theoretical Acoustics". Princeton University Press. 1986.

15. Ramani, Venkat, "Quad Cities Unit 2 Replacement Steam Dryer Vibration Instrumentation Program Plant Startup Test Report", GE-NE-0000-0044-2240-01. GENE, San Jose, CA. August 2005. GE Proprietary Information.

Attachment A

SCALING LAWS FOR BWR SCALE MODEL TEST LOAD DEFINITION PROCESS

Scaling Laws for Model Test Based BWR Steam Dryer Fluctuating Load Definitions

D.V. Sommerville

November 2, 2005

ABSTRACT

In recent years some Boiling Water Reactors have experienced significant steam dryer cracking. In some cases this cracking has necessitated unplanned outages to implement steam dryer repairs and has also resulted in de-rated operation of the affected units. In response to these recent steam dryer failures, GE has initiated a research program focused on identifying the nature of the fluctuating loads experienced by the steam dryer and developing predictive methods that can be used to develop load definitions for steam dryers. The physical mechanisms responsible for excitation of aero-acoustic resonances are not easily modeled using purely analytic methods; therefore, GE has decided to perform model tests to investigate the nature of the expected steam dryer loading. The objectives of the study documented in this paper are to: 1) Provide guidance regarding how to preserve, in the model, the significant fluid phenomena occurring in the plant, and 2) Derive scaling laws to convert model data to plant load predictions.

NOMENCLATURE

Acronyms

BWR	Boiling Water Reactor
FIV	Flow Induced Vibration
GE	General Electric Company
MSIV	Main Steam Isolation Valves
MSL	Main Steam Line
RPV	Reactor Pressure Vessel
S/RV	Safety and Relief Valves
TCV	Turbine Control Valves
TSV	Turbine Stop Valves

Symbols		*Units*
A	Area	ft^2
α	Thermal diffusivity	ft^2/s
b	Body force exerted on fluid	ft/s^2
β	Coefficient of volumetric expansion	$1/^\circ R$
C	Speed of sound	ft/s
c_p	Specific heat of fluid	$BTU/(lbm-^\circ R)$
D	Diameter	ft
d	Branch line diameter	ft
δ	Boundary layer thickness	ft
F	Frequency	Hz
$\Im$	Frictional heating power	$(lbf)/(ft^2-s)$
f	Friction factor	-
g	Gravitational acceleration	ft/s^2
g_0	Newton's constant	$(lbm-ft)/(lbf-s^2)$
K	Flow resistance coefficient	-

k	Ratio of specific heats	-
κ	Fluid thermal conductivity	$BTU/(ft-°R)$
L	Length	ft
l	MSL length upstream of component of concern	ft
M	Mach Number	-
μ	Fluid dynamic viscosity	$lbm/(ft-s)$
ν	Kinematic viscosity	ft^2/s
P	Total fluid pressure	lbf/ft^2
θ	Angle of reference frame	*Radians*
R	Gas constant	$(lbf-ft)/(lbm-°R)$
r	Radius of MSL	ft
Re	Reynolds Number	-
ρ	Fluid density	lbm/ft^3
St	Strouhal Number	-
t	Time	s
T	Fluid temperature	R
τ	Shear stress in fluid	lbf/ft^2
V	Total fluid velocity	ft/s
X	Geometric scale factor used to design model	-

Subscripts

p	Constant pressure
i	Initial
r	Reference
RPV	Reactor Pressure Vessel
h	hydraulic
s	Constant entropy
0	Mean value
MSL	Main Steam Line
n	Nozzle

e	Effective
Total	Total effective pipe length
Nozzle	Main steam line entrance nozzle
Elbow	Pipe elbow
m	Model
p	Plant
Superscripts	
0	Mean value

INTRODUCTION

Steam dryer cracking has been observed in Boiling Water Reactor (BWR) steam dryer components for many years. In most cases the cracking has been minor and continued operation could be justified with minor repairs. In some cases in-vessel instrumentation and testing programs were performed to demonstrate adequacy of the repair. In recent years the Quad Cities power plants have experienced significant steam dryer cracking. These dryer failures have resulted in unplanned outages required to implement repairs and have also resulted in de-rated operation of these units. Subsequent to the indications observed at Quad Cities additional cracking has been observed in Dresden units 2 and 3. After observing indications in repaired dryers it became evident that additional work was necessary to understand the cause of the loads responsible for the Quad Cities and Dresden cracking. In response to these recent steam dryer failures, GE has initiated a research program with the following goals:

1. Identify the nature of the fluctuating loads acting on BWR steam dryers.

2. Identify the significant excitation mechanisms and source locations.

3. Develop engineering methods capable of providing accurate steam dryer fluctuating load predictions.

After review of the available instrumented dryer data the most probable cause of steam dryer fluctuating loads is considered to be acoustic induced vibration [1]. Furthermore, there is strong evidence that multiple excitation mechanisms and source locations exist in the BWR steam system. Each source separately contributes to the total fluctuating load experienced by the steam dryer structure [1]. Two mechanisms considered likely to exist in the BWR steam system are flow turbulence and shear layer instabilities (vortex shedding). Although it is known that flow through valves and elbows can excite piping acoustics [2] and shear layer instabilities can occur when there is flow over a step, past the stem of a tee branch, or other geometry where shear layer interruption occurs [3], the locations of the dominant sources cannot be conclusively identified from review of the existing plant data alone.

Considering that,

1. The physical mechanisms responsible for the excitation of aero-acoustic resonances are not easily modeled using purely analytic methods,

2. It is often prohibitively expensive to instrument an operating reactor for operational testing, and

3. It is impractical if not impossible to perform parametric tests on an operating plant configuration,

GE decided to pursue model testing of the Quad Cities plant configurations to investigate the possible existence of acoustic loads in the steam system. Oftentimes model tests prove to be an effective and efficient method for investigating Flow Induced Vibration (FIV) problems in power plant systems. It is usually not practical to build a full scale model of the system of interest; therefore, small scale models are typically used as an alternative. Prior to designing a model, the important phenomena must be identified so that they may be preserved in the model through appropriate model and test design.

The objective of the study documented in this paper is to:

1. Identify the non-dimensional parameters that are expected to govern the system behavior at the plant scale
2. Derive model laws necessary to conduct useful model tests
3. Derive scaling laws required to convert model data to plant conditions

The important phenomena for this problem are highlighted as they appear in basic principle formulations of mass conservation and momentum. Non-dimensional variables are defined so that they have orders of magnitude equal to 1.0; that is, their magnitudes are labeled *O(1)* . When the non-dimensional variables are incorporated into the formulations, non-dimensional groups appear, whose relative magnitudes show which effects play the largest role in governing the excitation and acoustic response of the BWR steam system. The largest non-dimensional groups must be identical in the full size and in the small scale systems in order to preserve the dominant phenomena. The non-dimensional variables provide scaled and full size ratios for the independent length and time scales as well as the dependent properties like pressure and velocity. Scale model laws extracted from the non-dimensional formulations show how to design and interpret measurements from a small scale test in order to predict full size behavior.

Substantial work has been done during the course of the GE research program. This document draws heavily on earlier work performed for this project [4,5,6,7,8]. Without the insights provided by these previous contributors the progress enjoyed by the current researchers would not have been possible.

BASIC PRINCIPLES GOVERNING THE SYSTEM RESPONSE

The primary objectives of the model tests are to identify source mechanisms and locations and to measure model loads that can be scaled to plant conditions to provide empirical load definitions for BWR steam dryers. The BWR steam system from the steam/water interface inside the Reactor Pressure Vessel (RPV) to the high pressure turbine inlet in the Main Steam Lines (MSL) is simulated in a geometrically similar scale model facility. The dome is characterized in this study by multidimensional flow, and the steam lines by one-dimensional flow.

Since temperature and heat transfer are not of primary interest, only the mass conservation and momentum laws are considered since they govern the pressure response. Mass conservation and momentum for multidimensional and one dimensional flow are summarized here [9]:

Multidimensional Mass Conservation

$$\frac{\partial P}{\partial t}+\mathbf{V}\cdot\nabla P+\frac{\rho C^2}{g_0}\nabla\cdot\mathbf{V}=\frac{\beta C^2}{g_0 c_p}\left[\nabla\cdot(\kappa\nabla T)+\boldsymbol{\Gamma}\cdot\nabla\cdot\mathbf{V}\right] \tag{1}$$

Multidimensional Momentum

$$\frac{\partial \mathbf{V}}{\partial t}+\mathbf{V}\cdot\nabla\mathbf{V}+\frac{g_0}{\rho}\nabla P+\mathbf{b}=\frac{g_0}{\rho}\nabla\cdot\boldsymbol{\Gamma} \tag{2}$$

where

$$\beta=-\frac{1}{\rho}\left(\frac{\partial\rho}{\partial T}\right)_p \qquad \text{(coefficient of volume expansion)} \tag{3}$$

$$\boldsymbol{\Gamma}=\sum_j\sum_i \mathbf{n}_i\tau_{ij}\mathbf{n}_j \quad ; \quad i,j=x,y,z \qquad \text{(shear stress dyadic)} \tag{4}$$

with

$$\tau_{xx,yy,zz} = \mu\left[\left(2+\frac{\varsigma}{\mu}\right)\frac{\partial u,v,w}{\partial x,y,z} - \frac{2}{3}\nabla \bullet \mathbf{V}\right] \tag{5}$$

and

$$\tau_{xy,yz,zx} = \tau_{yx,zy,xz} = (\mu+\varsigma)\left(\frac{\partial u,v,w}{\partial y,z,x} + \frac{\partial v,w,u}{\partial x,y,z}\right) \tag{6}$$

The body force acceleration vector, which is gravity in this case, is designated by ***b***.

One-Dimensional Mass Conservation

$$\frac{\partial P}{\partial t} + V\frac{\partial P}{\partial x} + \frac{\rho C^2}{g_0}\frac{\partial V}{\partial x} + \frac{\rho C^2}{g_0}\frac{1}{A}\frac{\partial A}{\partial t} + \frac{\rho C^2}{g_0}\frac{1}{A}V\frac{\partial A}{\partial x} = \frac{\beta C^2}{g_0 c_p}\Im \tag{7}$$

The function $\Im$ involves heat transfer and frictional heating power [9], which have negligible importance in the case being considered.

One-Dimensional Momentum

$$\frac{\partial V}{\partial t} + V\frac{\partial V}{\partial x} + \frac{g_0}{\rho}\frac{\partial P}{\partial x} + \frac{f}{4}\frac{P_w}{A}\frac{|V|}{2}V + g\sin\theta = 0 \tag{8}$$

Before the governing equations can be written in non-dimensional form, normalized variables and properties are defined so that their numerical magnitude lies between zero and 1.0. That is, if φ is a variable with an initial value φ_i and a maximum anticipated change of $\Delta\varphi$, then the non-dimensional form,

$$\varphi^* = \frac{\varphi - \phi_i}{\Delta\varphi} \tag{9}$$

has a range between 0.0 and 1.0, noted as *O(1)*, or an "order of magnitude of 1.0." Some properties are non-dimensionalized more simply as $\varphi^* = \varphi/\varphi_r$ where φ_r is a reference value. The following non-dimensional variables are used:

$$P^* = \frac{P - P_i}{\Delta P} \quad t^* = \frac{t}{\Delta t} \quad V^* = \frac{V - V_i}{\Delta V} \quad T^* = \frac{T - T_i}{\Delta T} \quad b^* = \frac{b}{b_i}$$

$$\rho^* = \frac{\rho - \rho_i}{\Delta \rho} \quad C^* = \frac{C}{C_i} \quad \beta^* = \frac{\beta}{\beta_i} \quad x^*, y^*, z^* = \frac{x}{\Delta L}, \frac{y}{\Delta L}, \frac{z}{\Delta L} \tag{10}$$

$$c_p{}^* = \frac{c_p}{c_{p,i}} \quad \kappa^* = \frac{\kappa}{\kappa_i} \quad \nu^* = \frac{\nu}{\nu_i} \quad \nabla^* = \Delta L \nabla \quad \Gamma^* = \frac{\Gamma \Delta L g_0}{\mu_i \Delta V}$$

$$A^* = \frac{A}{A_i} \quad D_h{}^* = \frac{D_h}{D_{h,i}} \quad \Im^* = \frac{\Im}{\Im_i} = \Im \frac{\beta_i \Delta t}{c_{p,i} \rho_i}$$

Substituting the non-dimensional variables and properties into the governing equations leads to the following:

Normalized Multidimensional Mass Conservation

$$\pi_1 \frac{\partial P^*}{\partial t^*} + \pi_1 (\pi_2 \mathbf{V}^* + \pi_2{}^0) \bullet \nabla^* P^* + \pi_2 C^{*2} (\pi_3 \rho^* + 1) \nabla^* \bullet \mathbf{V}^* = \frac{\beta^* C^{*2}}{c_p{}^*} [\pi_4 \nabla^* \bullet (\kappa^* \nabla^* T^*) + \pi_5 \Gamma^* \bullet \nabla^* \bullet \mathbf{V}] \tag{11}$$

Normalized Multidimensional Momentum

$$\pi_2 (\pi_3 \rho^* + 1) \left(\frac{\partial \mathbf{V}^*}{\partial t^*} + (\pi_2 \mathbf{V}^* + \pi_2{}^0) \bullet \nabla^* \mathbf{V}^* \right) + \pi_6 \nabla^* P^* + \pi_7 (\pi_3 \rho^* + 1) \mathbf{b}^* = \pi_8 \nabla^* \bullet \Gamma^* \tag{12}$$

Normalized One-Dimensional Mass Conservation

$$\pi_1 \left(\frac{\partial P^*}{\partial t^*} + (\pi_2 V^* + \pi_2{}^0) \frac{\partial P^*}{\partial x^*} \right) + C^{*2} (\pi_3 \rho^* + 1) \left(\pi_2 \frac{\partial V^*}{\partial x^*} + \frac{1}{A^*} \left[\frac{\partial A^*}{\partial t^*} + (\pi_2 V^* + \pi_2{}^0) \frac{\partial A^*}{\partial x^*} \right] \right) = \frac{\beta^* C^{*2}}{c_p{}^*} \Im^* \tag{13}$$

Normalized One-Dimensional Momentum

$$\pi_2(\pi_3\rho^*+1)\left(\frac{\partial V^*}{\partial t^*}+(\pi_2 V^*+\pi_2{}^0)\frac{\partial V^*}{\partial x^*}\right)$$
$$+\pi_6\frac{\partial P^*}{\partial x^*}+(\pi_3\rho^*+1)\left(\frac{1}{2D_h^*}(\pi_2 V^*+\pi_2{}^0)^2\pi_9+\pi_{10}\right)=0 \quad (14)$$

Where the non-dimensional groups or coefficients are,

$$\pi_1=\frac{g_0\Delta P}{\rho_r C_r{}^2} \qquad \pi_6=\frac{g_0\Delta P(\Delta t)^2}{\rho_r(\Delta L)^2}$$

$$\pi_2=\frac{\Delta t\Delta V}{\Delta L} \qquad \pi_7=\frac{b(\Delta t)^2}{\Delta L}$$

$$\pi_2{}^0=\frac{V_i\Delta t}{\Delta L} \qquad \pi_8=\frac{\nu\Delta V(\Delta t)^2}{(\Delta L)^3} \quad (15)$$

$$\pi_3=\frac{\Delta\rho}{\rho_r} \qquad \pi_9=\frac{f_r\Delta L}{D_r}$$

$$\pi_4=\frac{\kappa\beta\Delta T\Delta t}{\rho_r c_{p,r}(\Delta L)^2} \qquad \pi_{10}=\frac{g(\Delta t)^2}{\Delta L}\sin\theta$$

$$\pi_5=\frac{\nu\beta\Delta t(\Delta V)^2}{g_0 c_{p,r}(\Delta L)^2}$$

When it is decided to study a particular phenomenon, the reference response time, Δt, is determined, and combined with appropriate changes in flow or other behavior properties. The relative magnitude of the non-dimensional π values shows which groups need to be preserved in model tests. Magnitude ratios of dependent and independent quantities are obtained from the normalized time, space, and property variables. Acoustics, flow turbulence and shear layer instabilities are considered in the next sections.

NONDIMENSIONAL GROUPS FOR STUDYING ACOUSTIC EFFECTS

If acoustic effects are to be preserved in a scale model, basic acoustic relationships need to be employed in determining the model coefficients of Equations 15. The reference values for time, distance, and velocity are:

$$\Delta t = \frac{\Delta L}{C_r} \tag{16}$$

$$\Delta L = D_{RPV} \tag{17}$$

$$\Delta V = V_0 \tag{18}$$

Also, the acoustic relationship between small pressure and velocity disturbances is given by

$$\Delta P = \frac{\rho_r C_r \Delta V}{g_0} \tag{19}$$

The expression for sound speed in a simple compressible fluid,

$$C = \sqrt{g_0 \left(\frac{\partial P}{\partial \rho}\right)_s} \qquad \text{(useful for all thermal-hydraulic phenomena)} \tag{20}$$

can be used to express the density change for most thermal-hydraulic phenomena as

$$\Delta \rho \approx g_0 \frac{\Delta P}{C^2} \qquad \text{(useful for all thermal-hydraulic phenomena)} \tag{21}$$

If the steam is idealized as a perfect gas with the state equation,

$$P = \rho R T \tag{22}$$

then the temperature change for most processes can be written as

$$\Delta T \approx T\left(\frac{\Delta P}{P} - \frac{\Delta \rho}{\rho}\right) \qquad \text{(perfect gas)} \qquad (23)$$

The non-dimensional groups of Eqs. (15), which are associated with acoustic responses in steam, become

$$\pi_1 = \frac{\Delta V}{C} = M \qquad \pi_6 = \frac{\Delta V}{C} = M$$

$$\pi_2 = \frac{\Delta V}{C} = M \qquad \pi_7 = \frac{gD_{RPV}}{C^2}$$

$$\pi_2{}^0 = \frac{\Delta V}{C} = M \qquad \pi_8 = \left(\frac{\nu}{CD_{RPV}}\right)M \qquad (24)$$

$$\pi_3 = \frac{\Delta V}{C} = M \qquad \pi_9 = \frac{f_r D_{RPV}}{D_{MSL}}$$

$$\pi_4 = (k-1)\left(\frac{\alpha}{CD_{RPV}}\right)M \qquad \pi_{10} = \frac{gD_{RPV}}{C^2}\sin\theta$$

$$\pi_5 = \left(\frac{\nu(k-1)}{CD_{RPV}}\right)M^2$$

The Mach number, $\Delta V/C$, appears in several of the non-dimensional groups, which is expected for similarity in acoustic phenomena. However, the numerical magnitudes of each group need to be calculated and compared before it can be seen if Mach number indeed needs to be preserved; these calculations are performed later in this document.

NONDIMENSIONAL GROUPS FOR STUDYING SHEAR LAYER INSTABILITY OR VORTEX SHEDDING EFFECTS

The reference time for a cyclic instability for flow at velocity V_0 past an object, cavity, or other geometric discontinuity of length dimension d, may have a period approximated by the time for the instability to traverse its length. The available plant data suggest that a shear layer instability induced cavity resonance exists in the Safety and Relief Valve inlets (S/RVs). A substantial body of literature exists regarding the subject of cavity resonances. For the "order of magnitude" investigation being performed here the convection time for a vortex to cross the mouth of a cavity, the convection velocity, and the reference length will be assumed to be:

$$\Delta t \approx \frac{d}{0.4V_0} = \frac{1}{F} \tag{25}$$

Where, F is a characteristic vortex shedding frequency

$$\Delta V \leq 0.4V_0 \tag{26}$$

$$\Delta L = d \tag{27}$$

The empirical value for the vortex convection velocity used above, $0.4V_0$, is obtained from the literature [10,11]. It should be noted that the absolute value of the convection velocity is not important for the work at hand. For this work only an order of magnitude estimate is necessary.

Provided that $V_0 << C$, the corresponding pressure disturbance would correspond to the Bernoulli pressure, noting that the vortex convection velocity is used here rather than the bulk flow velocity,

$$\Delta P = \rho\frac{(\Delta V)^2}{2g_0} = 0.08\rho\frac{V_0^2}{g_0} \tag{28}$$

The density and temperature differences of Equations (21) and (23), which simply relate state properties, can be used for the instability, as well as the acoustic response. It is reasonable to consider this instability as a multidimensional effect. It follows that the resulting non-dimensional groups of Equation 15, expressing the reference time as a function of time domain parameters rather than a vortex shedding frequency, become:

$$\pi_1 = 0.08M^2 \qquad \pi_6 = \frac{1}{2}$$

$$\pi_2 = 1 \qquad \pi_7 = 6.25\frac{gd}{V_0^2}$$

$$\pi_2{}^0 = 2.5 \qquad \pi_8 = \frac{2.5}{\mathrm{Re}} \qquad (29)$$

$$\pi_3 = 0.08M^2 \qquad \pi_9 = f\frac{d}{D}$$

$$\pi_4 = 0.2\left(\frac{\alpha(k-1)}{V_0 d}\right)M^2 \qquad \pi_{10} = 6.25\frac{gd}{V_0^2}\sin\theta$$

$$\pi_5 = 0.4(k-1)\frac{M^2}{\mathrm{Re}}$$

The non-dimensional groups obtained above include the Mach and Reynolds numbers; however, it is also seen that after simplification three of the π groups do not appear to contain any reference parameters. It is known that vortex shedding phenomena exhibit a periodicity that is proportional to flow velocity; therefore, if the reference time is expressed as the inverse of a reference frequency (a characteristic vortex shedding frequency) then non-dimensional groups shown above become:

$$\pi_1 = 0.08M^2 \qquad \pi_6 = \frac{0.08}{St^2}$$

$$\pi_2 = \frac{0.4}{St} \qquad \pi_7 = \frac{g}{F^2 d}$$

$$\pi_2{}^0 = \frac{1}{St} \qquad \pi_8 = \frac{1}{\mathrm{Re}St} \qquad (30)$$

$$\pi_3 = 0.08M^2 \qquad \pi_9 = f\frac{d}{D}$$

$$\pi_4 = 0.08\left(\frac{\alpha(k-1)}{Fd^2}\right)M^2 \qquad \pi_{10} = \frac{g}{F^2 d}\sin\theta$$

$$\pi_5 = 0.16\frac{\nu(k-1)}{Fd^2}M^2$$

Here it can be seen that the Mach and Reynolds numbers are still evident; however, the Strouhal number has also become appeared in the some of the parameters above. This is expected and is consistent with the literature regarding vortex shedding and vortex induced acoustics.

After considering the most probable location of a shear layer instability induced acoustic resonance in the BWR steam system it can be seen that the non-dimensional groups obtained for shear layer instability effects show apparent dependence on Mach, Strouhal and Reynolds numbers. Significant research has been performed on deep cavity resonances which indicate that the most significant non-dimensional parameter affecting the periodicity of the vortex shedding phenomenon is the Strouhal number. Although some research has been done to investigate the effect of Reynolds number on shallow cavity resonances with laminar shear layers [13] there appears to be little work in the literature which directly considers the effect of Reynolds number on turbulent shear

layers over deep cavities. There has been some work which investigated the effect of displacement thickness on the amplitude of and existence of cavity resonances [14,15]; however, the available information is not extensive enough to be conclusive. Most of the data available suggest that the non-dimensionalized vortex shedding frequency for geometries with well defined separation points is weakly affected by Re [2]; in other words, St is not a function of Re. From the information available in the literature it can be said that Mach Number is important for acoustic effects and St Number is important for vortex shedding; however, the possible importance of Re Number on vortex induced acoustics has not been extensively investigated. Evaluating the relative size of the non-dimensional parameters shown above will give some insight into the expected significance of the various parameters.

NONDIMENSIONAL GROUPS FOR STUDYING FLOW TURBULENCE EFFECTS

Flow turbulence is a well known excitation mechanism for piping acoustics. There are many examples of piping acoustics excited by flow through valves and around elbows in the literature. The typical BWR steam system has four main steam lines, each which contain multiple valves and elbows. It is believed that these components rather than the vessel internals will provide the strongest source of turbulence induced acoustics. Before reference parameters are chosen the nature of the problem will be investigated further.

Aero-acoustic phenomena associated with either internal or external flows can be classified as either noise dissipating or noise generating. Friction can attenuate acoustics through viscous losses and rapid area changes can attenuate sound by reflecting an oncoming pressure fluctuation. Rapid area changes can also generate sound associated with turbulent mixing and turbulent jets when flow separates from a surface. Many references show that common factors associated with steady and unsteady flow behavior such as friction factors, f, loss coefficients, K, and vortex shedding, St, are independent of Reynolds Number once the flow is fully turbulent [2,8,9,12,16]. If the plant flow has become fully turbulent once it has reached the location of the aero-acoustic sources then Reynolds Number is not expected to be significant.

The locations of the most probable sources of turbulence induced acoustics in the BWR steam system are the Main Steam Isolation Valves (MSIV), Turbine Control Valves (TCV), and Turbine Stop Valves (TSV). These components are shown in Figure 1. The MSIVs are typically 80-100 feet downstream from the vessel and the TSV/TCV assembly is further downstream than the MSIVs. There are also typically an entrance nozzle, one or two 90° elbows and one or two 45° elbows between the RPV and the MSIV. Considering the steam flow velocity typical for the BWR and the steam system geometry, both the boundary layer thickness and Reynolds Number will be assessed for the plant and proposed model conditions below. Reference values for the plant and model conditions are obtained from Table 1.

Plant Conditions

$$\mathrm{Re} = \frac{200\frac{ft}{s}1.5ft}{5.6E-6\frac{ft^2}{s}} = 5.36E7 \quad \leftarrow \text{The flow is turbulent}$$

If the size of the turbulent boundary layer is assumed to grow according to equation 31, then:

$$\Delta L = \delta = (0.37)\left(\frac{\nu}{V_0}\right)^{1/5} l^{4/5} \tag{31}$$

where l is the distance between the RPV and the first MSIV, $l \geq 60ft$

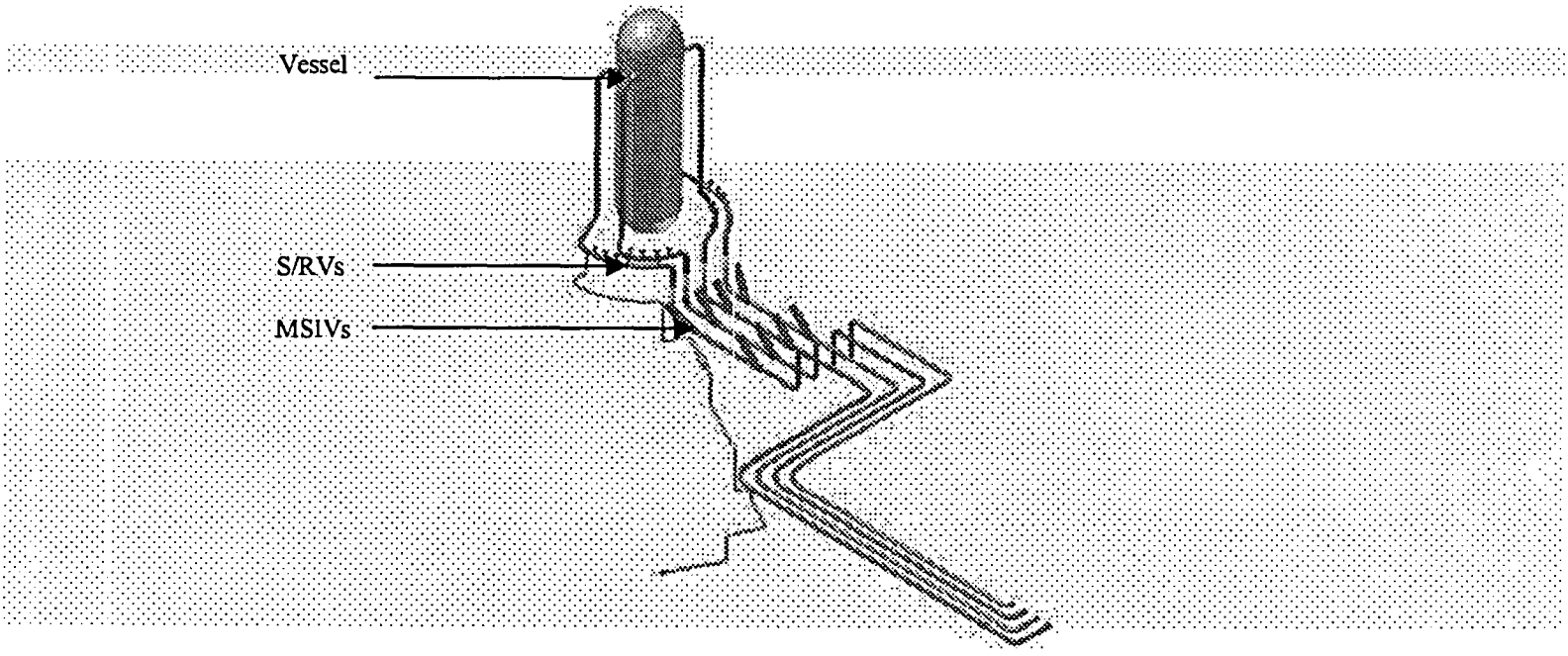

Figure 1: Typical BWR main steam line layout.

If the effect that the nozzle and elbows upstream of the MSIVs have on accelerating development of the boundary layer thickness can be considered as an additional pipe length similar to that assumed for bulk flow pressure drop calculations then the total effective length of MSL including the main steam nozzles and elbows upstream of the MSIVs is given as:

$$L_{Total} = L_{nozzle} + L_{elbow} + L_{elbow} + L_{MSL} \tag{32}$$

From Reference 12, representative vales of K and L_e/D can be obtained for the entrance nozzle and the elbows:

K_n=0.3 (Nozzle), where $K = f\frac{L_e}{D}$

L_e/D=16 (45° elbow)

L_e/D=30 (90° elbow)

This gives a total effective main steam line length, in the plant, of:

$$L_{Total} = L_{nozzle} + L_{elbow} + L_{elbow} + L_{MSL} \approx 212 ft$$

Using this length to calculate the boundary layer thickness yields:

δ=0.83 feet

For fully developed flow, the boundary layer thickness can be assumed to be the pipe radius, r=0.75 feet; therefore, the flow is fully developed.

Model Conditions

Using the same approach as shown above for the plant conditions the following results are obtained:

$$\delta = \frac{D_{MSL}}{2}$$ at MSIVs and further downstream

$$\mathrm{Re} = \frac{145 \frac{ft}{s} 0.083 ft}{1.3E-4 \frac{ft^2}{s}} = 9.26E4$$ ← The flow is turbulent

Note: The boundary layer thickness here is given as the pipe radius because the calculated thickness is greater than the pipe radius.

It can be seen above that the flow in both the model and the plant is fully developed turbulent flow by the time it reaches the components expected to be significant sources. Recognizing this and recalling that many flow parameters such as loss coefficients are insensitive to Reynolds Number once the flow is turbulent, the following reference values are selected for turbulence effects in the BWR steam system:

$$\Delta t \approx \frac{D_{MSL}}{V_0} \tag{33}$$

$$\Delta L = D_{MSL} \tag{34}$$

$$\Delta V = \frac{\Delta L}{\Delta t} = V_0 \tag{35}$$

$$\Delta P = \rho \frac{(\Delta V)^2}{2g_0} = \rho \frac{V_0^2}{2g_0} \tag{36}$$

Inserting these reference values into the non-dimensional groups defined in Equations 15 above, the following non-dimensional groups are obtained for turbulence effects:

$$\pi_1 = 0.5M^2 \qquad \pi_6 = \frac{1}{2}$$

$$\pi_2 = 1 \qquad \pi_7 = \frac{gD_{MSL}}{V_0^2}$$

$$\pi_2^{\,0} = 1 \qquad \pi_8 = \frac{1}{\mathrm{Re}} \tag{37}$$

$$\pi_3 = 0.5M^2 \qquad \pi_9 = f$$

$$\pi_4 = 0.5\left(\frac{\alpha(k-1)}{D_{MSL}V_0}\right)M^2 \qquad \pi_{10} = \frac{gD_{MSL}}{V_0^2}\sin\theta$$

$$\pi_5 = \frac{\nu(k-1)}{CD_{MSL}}M$$

RELATIVE IMPORTANCE OF NON-DIMENSIONAL GROUPS AT MODEL AND PLANT SCALES

To assess the relative importance of the various non-dimensional groups obtained for each phenomenon considered, representative values must be used at the plant and model scales. Both scales are considered here to determine if a parameter which is unimportant at one scale becomes important at the other scale; observing this trend would be problematic. Although many of the non-dimensional groups obtained above contain common parameters such as Mach Number, Reynolds Number, and Strouhal Number, the relative importance of the non-dimensional groups can be assessed by inserting numerical values for the reference parameters. Table 1 summarizes the values used for each reference parameter. Table 2 lists the numerical value for each non-dimensional group obtained for the phenomena considered. Finally, Table 3 summarizes the significant non-dimensional groups. It is the groups shown in Table 3 that will control the system behavior for the problem at hand and consequently must be preserved in a model test to obtain meaningful test data.

Table 1: Reference values for assessing non-dimensional parameters, Plant and Model Scale.

Parameter	Description	Reference Values	
		Plant Scale	Model Scale (1)
α	Thermal diffusivity	2.73E-6 ft^2/s	2.09E-4 ft^2/s (2)
C	Speed of sound	1620 ft/s	1180 ft/s
d	Branch line diameter	6 in	0.3 in
D_{MSL}	Main Steam Line diameter	18 in	1 in
D_{RPV}	Reactor Pressure Vessel diameter	251 in	14.5 in
F	Vortex shedding frequency	160 Hz	2320 Hz
f	Friction factor	0.012	0.025
g	Acceleration of gravity	32.2 ft/s^2	32.2 ft/s^2
k	Isotropic coefficient	1.25	1.4
ν	Kinematic viscosity	5.6E-6 ft^2/s	1.3E-4 ft^2/s
T	Temperature of fluid	540 °F	140 °F
V_0	Free stream steam velocity in main steam line	200 ft/s	145 ft/s

1. *The proposed model system is to be built at ~ 1:17 scale*
2. *http://www.hukseflux.com/thermal%20conductivity/thermal.htm*

Table 2: Numerical values for non-dimensional parameters obtained for each phenomenon considered.

Non-Dimensional Group	Acoustics		Shear Layer Instabilities		Turbulence	
	Plant	Model	Plant	Model	Plant	Model
π_1	**0.123**	**0.123**	1.21E-3	1.21E-3	7.56E-3	7.56E-3
π_2	**0.123**	**0.123**	**1**	**1**	**1**	**1**
π_2^0	**0.123**	**0.123**	**2.5**	**2.5**	**1**	**1**
π_3	**0.123**	**0.123**	1.21E-3	1.21E-3	7.56E-3	7.56E-3
π_4	2.49E-12	7.21E-9	2.06E-11	7.00E-8	1.72E-11	5.23E-8
π_5	6.30E-13	5.51E-10	8.47E-11	8.67E-8	7.09E-11	6.50E-8
π_6	**0.123**	**0.123**	**0.5**	**0.5**	**0.5**	**0.5**
π_7	2.57E-4	2.79E-5	2.52E-3	2.38E-4	3.35E-3	3.55E-4
π_8	2.04E-11	1.12E-8	1.40E-7	8.97E-5	1.87E-8	1.08E-5
π_9	0.167 (1)	0.363 (1)	4.0E-3	7.5E-3	0.012	0.025
π_{10}	2.57E-4	2.79E-5	2.52E-3	2.39E-4	1.21E-3	3.83E-5

1. π_9 appears to be significant for acoustics; however, when the non-dimensional equations 11-14 are observed in detail it becomes apparent that π_9 never occurs by itself. π_9 always occurs as a product with other terms. The largest product containing π_9 is $\pi_2^2\pi_9$ which becomes:

Plant Scale = 2.53E-3
Model Scale = 5.49E-3

Table 3: Summary of significant non-dimensional groups.

Non-Dimensional Group	Acoustics	Shear Layer Instabilities	Turbulence
π_1	M	-	-
π_2	M	$\frac{0.4}{St}$	1
π_2^0	M	$\frac{1}{St}$	1
π_3	M	-	-
π_6	M	$\frac{0.08}{St^2}$	0.5

From Table 3 it is apparent that the non-dimensional parameters of importance for the problem considered here are:

1. Mach Number (Necessary to preserve acoustical characteristics of system)
2. Strouhal Number (Necessary to preserve vortex shedding in system)

It should be noted that the turbulence effects in the system are preserved in the model without the need for Reynolds number similarity. It is thought that this results from the assumptions for source locations in the system. Recall that the significant source locations for vortex shedding and turbulence induced acoustics are considered to be in the MSL remote from the RPV. Because of this assumption the flow is fully developed turbulent flow at the model and plant scales by the time it reaches the components of interest.

SELECTION OF MODEL LAWS FOR TEST PROGRAM

It was shown above that the phenomena considered to be most important will be preserved in the model if the Mach and Strouhal Numbers are preserved between the model and plant scales. There is significant data [2] that indicates Strouhal number is sensitive to geometry and insensitive to Re; therefore, the St number is expected to be preserved in the model scale if the geometry is maintained at a consistent scale. Using the results obtained above, it is considered necessary to preserve the following parameters when constructing and performing model tests of the BWR steam system with the intention of predicting steam dryer fluctuating loads:

1. Geometry, $$D_m = \frac{D_p}{X} \tag{38}$$

2. Mach Number, $$(V_0)_m = (V_0)_p \left(\frac{C_m}{C_p} \right) \tag{39}$$

The discussion above provides guidance to ensure performance of successful model tests; however, it does not provide the reader with model scaling laws that will allow a plant prediction to be made using model data. To scale the model data to plant conditions the ratios of the time and pressure parameters at the plant and model scales must be determined:

The ratio of time scales is:

$$\frac{t_m}{t_p} = \frac{F_p}{F_m} = \frac{\left(\frac{D}{C} \right)_m}{\left(\frac{D}{C} \right)_p} = \frac{D_m}{D_p} \frac{C_p}{C_m}$$

Then, plant frequencies can be determined from model data using the following expression:

$$F_p = F_m\left(\frac{D_m}{D_p}\right)\left(\frac{C_p}{C_m}\right) \tag{40}$$

Because the model is built to a consistent geometric scale, D in the above expression can be any reference dimension in both the plant and model.

The ratio of pressure scales is:

$$\frac{P_p}{P_m} = \frac{\left(\frac{\rho C \Delta V}{g_0}\right)_p}{\left(\frac{\rho C \Delta V}{g_0}\right)_m} = \frac{(\rho C \Delta V)_p}{(\rho C \Delta V)_m}$$

Recall that the reference velocity is considered to be proportional to the mean velocity in the system and that Mach Number must be preserved in the model tests, then the expression above simplifies to:

$$\frac{P_p}{P_m} = \frac{(\rho C V_0)_p}{(\rho C V_0)_m}\left(\frac{M_m}{M_p}\right) = \frac{(\rho C V_0)_p}{(\rho C V_0)_m}\left(\frac{V_0}{C}\right)_m\left(\frac{C}{V_0}\right)_p = \frac{(\rho C^2)_p}{(\rho C^2)_m}$$

Then, plant pressure fluctuations can be determined from model data using the following expression:

$$P_p = P_m\frac{(\rho C^2)_p}{(\rho C^2)_m} \tag{41}$$

Although the scaling relationships shown above were obtained by starting from the reference parameters defined for acoustics it can be shown that the same relationships can be obtained by starting with the reference parameters for Shear Layer instabilities or Turbulence effects.

CONCLUSIONS

In response to the BWR steam dryer failures observed in recent years GE has initiated a research program focused on identifying the physical nature of the significant steam dryer loading and developing predictive methods that can be used to provide conservative steam dryer fluctuating load definitions. A significant aspect of the load prediction technology is model testing. This document describes the identification of non-dimensional parameters observed to control the system response for phenomena considered to be significant. Successful model testing can be achieved if these significant parameters are preserved in the model scale. The phenomena believed to control the fluctuating loads on the BWR steam dryer were identified from existing instrumented dryer data [1] and are:

1. Turbulence induced acoustics
2. Deep cavity aero-acoustic resonances excited by shear layer instabilities

Non-dimensionalizing the governing system equations and estimating their relative order of magnitude shows the following parameters to be significant for the phenomena considered:

- Mach Number
- Strouhal Number

Recognizing that the Strouhal number is primarily a function of geometry and that preservation of acoustics in the model requires preservation of the system geometry, the significant parameters that must be preserved in the model are:

1. Geometry, $$D_m = \frac{D_p}{X} \tag{38}$$

2. Mach Number, $$(V_0)_m = (V_0)_p \left(\frac{C_m}{C_p} \right) \tag{39}$$

Using the reference values for time (frequency) and pressure, the following scaling relationships are derived to enable conversion of model data into plant frequency and fluctuating pressure predictions:

$$F_p = F_m\left(\frac{D_m}{D_p}\right)\left(\frac{C_p}{C_m}\right) \tag{40}$$

$$P_p = P_m\frac{\left(\rho C^2\right)_p}{\left(\rho C^2\right)_m} \tag{41}$$

It is shown here that useful model testing can be performed if the full scale plant geometry is preserved at a consistent model scale and if the system flow rates for various plant power levels are determined by matching model and plant Mach numbers. Plant predictions can be obtained by scaling the model data to plant conditions using the scaling laws presented above.

REFERENCES

1. Sommerville, Daniel., "Engineering Report for Quad Cities Unit 1 Scale Model Testing". GENE-0000-0032-2219-01. GENE. San Jose, CA. April 2005. GE Proprietary Information.

2. Blevins, R. D., "Flow Induced Vibration", 2nd Edition. Krieger Publishing Company. 2001.

3. Rockwell, D., Naudascher, E., "Review – Self-Sustaining Oscillations of Flow Past Cavities", Journal of Fluids Engineering, Vol. 100, June 1978, pp. 152-165.

4. Moody, F.J., "Root Cause Scaling Rationale for the Quad Cities Dryer Incident". September 9, 2002. GE Proprietary Information.

5. Moody, F.J., "GE Scale Model of Steamline Acoustic Excitation", August 23, 2004. GE Proprietary Information.

6. Lynch, John, "Scaling of the Miniature Steam Dome", Revision 1. December 2, 2002. GE Proprietary Information.

7. Galbally, D., "Model for Analyzing the Effect of Mean Flow and Viscous Losses on the Acoustic Behavior of BWR Small Scale Steam System", November 18, 2004. GE Proprietary Information.

8. R. Blevins, Personal transmittal, August, 2004.

9. Moody, F. J., *Introduction to Unsteady Thermofluid Mechanics*, Wiley, 1990.

10. C. Shieh, Personal transmittal, September 2004

11. East, L.F., "Aerodynamically Induced Resonance in Rectangular Cavities", Journal of Sound and Vibration, Vol. 3, March 1966, pp. 277-287.

12. McDonald, A.T., Fox, R.W., "Introduction to Fluid Mechanics", 4th Ed., Wiley. C. 1992.

13. Sarohia, V., "Experimental Investigation of Oscillations in Flows Over Shallow Cavities", AIAA Journal. Vol. 15, No. 7. July 1977

14. Amandolese, X., Hemon, P., Regardin, C.,"An Experimental Study of the Acoustic Oscillations by Flows Over Cavities", Journal of Vibration and Acoustics. Vol. 126. April 2004.

15. DeMetz, F.C., and T.M. Farabee (1977) "Laminar and Turbulent Shear Flow Induced Cavity Resonances," AIAA Paper 77-1293, AIAA, New York.

16. Idelchik, I.E., "Handbook of Hydraulic Resistance", 3rd Ed., Begell House. c. 1996.

Attachment B

UNCERTAINTY ANALYSIS OF BWR STEAM DRYER SCALE MODEL TEST LOAD DEFINITION METHODOLOGY

UNCERTAINTY ANALYSIS OF SCALE MODEL TEST PREDICTIONS

D. Galbally and D. V. Sommerville

ABSTRACT

This document provides a method for calculating the experimental uncertainties associated with the steam dryer loads predicted using Scale Model Test (SMT) data. It is worth noting that this document only contains the uncertainties associated with the measuring processes and test equipment used in the scale model.

It has been determined that the uncertainty associated with the plant pressure prediction is approximately 13% for frequencies between 0 and 100 Hz and up to 35% for fluctuating pressures associated with S/RV resonances. Frequency uncertainties are on the order of 3% - 4% depending on the frequency range of interest.

NOMENCLATURE

C	sound speed
C_D	venturi discharge coefficient
c_p	specific isobaric heat capacity
c_v	specific isochoric heat capacity
d	throat diameter of venturi at flowing conditions
D_{MSL}	main steam line diameter
F	SCADAS scaling factor
g_0	Newton's constant in $F = Ma/g_0$
G	preamplifier gain
G_i	ideal specific gravity
h_w	differential pressure in venturi
k	ratio of specific heats $k = c_p/c_v$
L	characteristic length
P	pressure
Q	mass flow rate
R	universal gas constant
S	microphone sensitivity
T	temperature
$u(x)$	absolute uncertainty associated with variable x
$u_{\%}(x)$	percentage uncertainty associated with variable x
Y_1	adiabatic expansion factor

Z	compressibility factor
β	ratio of venturi diameters
ρ	density
$(\,)_0$	average value
$(\,)_m$	scale model variable
$(\,)_p$	plant variable

BACKGROUND THEORY

Although this document is not intended to act as a text on uncertainty analysis, it is important to introduce the fundamental theory applicable for this evaluation. The following text is adapted from References [1] and [2].

Assume that the true value of the quantity being measured can be expressed as a function of N other quantities,

$$Y = f(X_1, X_2, X_3, ..., X_N) \tag{1}$$

The process considered here is used to obtain an estimate of the true value; this estimate is expressed as:

$$y = f(x_1, x_2, x_3, ..., x_N) \tag{2}$$

Where, y represents an estimate of Y, and x represents and estimate of X. Estimating the "accuracy" of a process estimate will be defined here to consist of two components:

1. Bias error, ϕ_B
2. Process uncertainty, ϕ_u

$$Y - y = \phi_B \pm \phi_u$$

Figure 1 illustrates the concept introduced above. The bias error is a constant difference between the true value, Y, and the mean of the estimated value, y. This error term can be removed by adjusting the process estimate by the bias error term as shown below:

$$y_{corr} = y - \phi_B$$

The process estimate cannot be corrected for the process uncertainty. This quantity is typically accommodated by reporting an uncertainty associated with a process estimate.

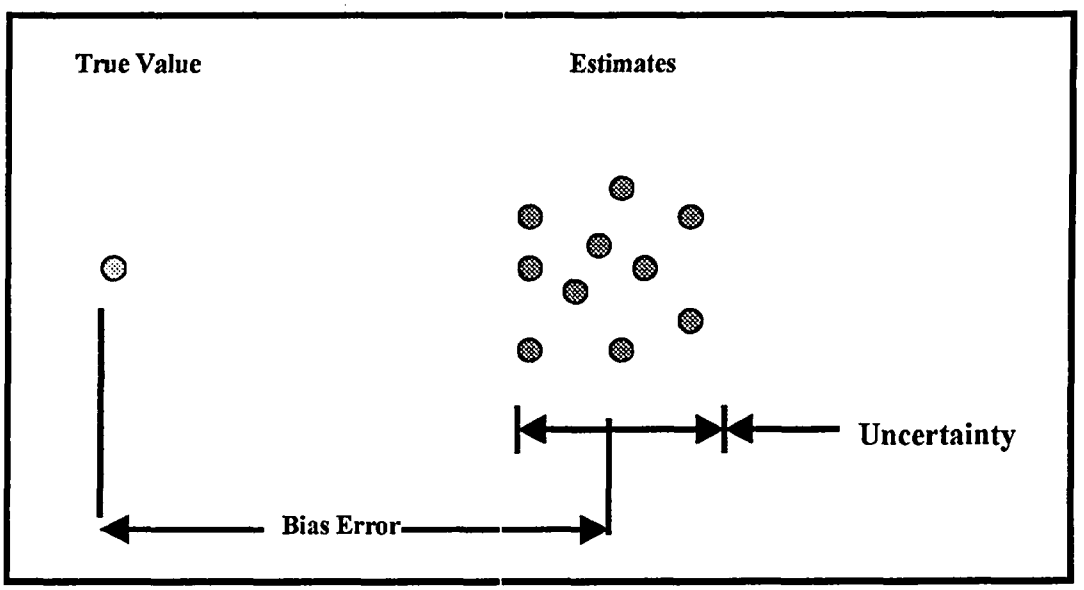

Figure 1: Schematic illustrating Bias Error and Uncertainty in a process estimate.

The true value of a quantity is that value to which one approaches closer and closer as increasing numbers of measurements are made with increasing care. If the processes used to obtain the estimates x_i are subject to many small random errors but negligible systematic errors, their distribution will be a normal distribution centered on the true value X. Taken together, all estimates can be evaluated to determine a sample mean (measure of central tendency) and standard deviation (measure of distribution about the mean). For convenience, equations for the sample mean and standard deviation are given below:

$$\bar{x}_i = \frac{1}{N}\sum_{k=1}^{N} x_{i,k} \tag{3}$$

$$u(x_i) = \left[\frac{1}{N-1}\sum_{k=1}^{N}(x_{i,k} - \bar{x}_{i,k})^2\right]^{0.5} \tag{4}$$

The uncertainty associated with the process estimate, y, can be wholly expressed as a function of the uncertainties associated with each of the quantities, x_n, as shown below:

$$u^2(y) = \sum_{i=1}^{N}\left(\frac{\partial f}{\partial x_i}\right)^2 u^2(x_i) + 2\sum_{i=1}^{N-1}\sum_{j=i+1}^{N}\frac{\partial f}{\partial x_i}\frac{\partial f}{\partial x_j}u(x_i, x_j) \tag{5}$$

Where Eq. (5) is a first order Taylor series approximation of the measurement equation, Eq. (1) and is commonly referred to as the Law of Propagation of Uncertainty. If the

input parameters are uncorrelated then the covariance term in Eq. (5) will be zero and the expression for the combined uncertainty of the process estimate can be expressed as:

$$u^2(y) = \sum_{i=1}^{N} \left(\frac{\partial f}{\partial x_i} \right)^2 u^2(x_i) \tag{6}$$

ANALYSIS

Uncertainty Expression for Plant Pressure Prediction:

The plant pressure estimate based on SMT data is given in [3] as:

$$P_p = P_m \frac{\rho_p}{\rho_m} \left(\frac{C_p}{C_m} \right)^2 \tag{7}$$

If the fluids in the plant and scale model, steam and air respectively, are treated as perfect gases with $C^2 = kg_0P_0/\rho$, the plant pressure estimate is obtained from Eq. (7) as

$$P_p = P_m \frac{\rho_p}{\rho_m} \frac{k_p g_0 P_{0,p} \rho_m}{k_m g_0 P_{0,m} \rho_p} = P_m \frac{k_p}{k_m} \frac{P_{0,p}}{P_{0,m}} \tag{8}$$

Since $k_p \approx k_m$, Eq. (8) reduces to

$$P_p = P_m \frac{P_{0,p}}{P_{0,m}} \tag{9}$$

So, the plant pressure prediction is a function of the following parameters

$$P_P = f\left(P_m, P_{0,p}, P_{0,m}\right) \tag{10}$$

Using the Law of Propagation of Uncertainty (Eq. 6), the uncertainty associated with the plant pressure measurement is given as:

$$u^2(P_p) = \left[\left(\frac{\partial P_p}{\partial P_m} \right)^2 u^2(P_m) + \left(\frac{\partial P_p}{\partial P_{0,p}} \right)^2 u^2(P_{0,p}) + \left(\frac{\partial P_p}{\partial P_{0,m}} \right)^2 u^2(P_{0,m}) \right] \tag{11}$$

where:

$$\frac{\partial P_p}{\partial P_m} = \frac{P_{0,p}}{P_{0,m}} \tag{12}$$

$$\frac{\partial P_p}{\partial P_{0,p}} = \frac{P_m}{P_{0,m}} \tag{13}$$

$$\frac{\partial P_p}{\partial P_{0,m}} = -P_m \frac{P_{0,p}}{P_{0,m}^2} \tag{14}$$

Substituting Eqs. (12) through (14) into Eq. (11) yields

$$u^2(P_p) = \left(\frac{P_{0,p}}{P_{0,m}}\right)^2 u^2(P_m) + \left(\frac{P_m}{P_{0,m}}\right)^2 u^2(P_{0,p}) + \left(P_m \frac{P_{0,p}}{P_{0,m}^2}\right)^2 u^2(P_{0,m}) \tag{15}$$

Therefore, the uncertainty expression for the plant pressure prediction is given by

$$u(P_p) = \sqrt{\left(\frac{P_{0,p}}{P_{0,m}}\right)^2 u^2(P_m) + \left(\frac{P_m}{P_{0,m}}\right)^2 u^2(P_{0,p}) + \left(P_m \frac{P_{0,p}}{P_{0,m}^2}\right)^2 u^2(P_{0,m})} \tag{16}$$

and the fractional uncertainty in P_p is the quadratic sum of the fractional uncertainties in P_m, $P_{0,p}$ and $P_{0,m}$:

$$\frac{u(P_p)}{P_p} = \sqrt{\frac{u^2(P_m)}{P_m^2} + \frac{u^2(P_{0,p})}{P_{0,p}^2} + \frac{u^2(P_{0,m})}{P_{0,m}^2}} \tag{17}$$

The following sections provide values for the uncertainties that appear in Eq. (17).

Uncertainty Expression for Scale Model Static Pressure.

The transducer used for measuring the static pressure inside the scale model, $P_{0,m}$, is a Rosemount 3051CD 2A22A1A. According to Reference [4], the total accuracy of this pressure transducer is ±0.15% of the calibrated span. According to GENE calibration records, this transducer is calibrated between 4.7 psia and 21.7 psia, for a total span of 17 psi. Therefore, the absolute uncertainty in the model static pressure measurement is ±0.026 psi.

Uncertainty Expression for Plant Static Pressure.

The typical absolute uncertainty associated with plant pressure sensors is ± 15 psi, which corresponds to a percentage uncertainty of 1.5% for a typical plant operating point of 1000 psi. This data was taken from Reference [5], page 17.

Uncertainty Expression for Scale Model Fluctuating Pressure.

The pressures measured in the SMT system are known to be functions of flow velocity, transducer sensitivity, preamplifier gain and Data Acquisition System (DAS) characteristics. The process of determining the flow velocity that should be used in the scale model and measuring the resulting pressure oscillations generated inside the vessel consists of the following steps:

1. Determine the flow velocity in the plant, V_p, that corresponds to the power level at which pressure loads will be estimated.

2. Use the scaling laws given in [3] in order to calculate the flow velocity to be used in the scale model as follows

$$V_{m,target} = V_p \frac{C_m}{C_p} \tag{18}$$

3. Achieve the correct flow velocity in the scale model by adjusting the speed of the blowers used in the test rig. The volumetric flow in the test apparatus is calculated by considering the venturi flow calculation provided by the venturi manufacturer [6]:

$$Q_m = 0.0997 C_{D,m} Y_{1,m} d_m^2 \sqrt{\frac{\rho_m h_{w,m}}{1-\beta_m^4}} \tag{19}$$

The following equation expresses the mass flow rate in the scale model, Q_m, in terms of the average flow velocity in the main steam lines of the scale model, V_m:

$$Q_m = \pi D_{MSL,m}^2 V_m \rho_m \tag{20}$$

Substituting Eq. (20) into Eq. (19) and solving for V_m yields,

$$V_m = \frac{0.0997 C_{D,m} Y_{1,m} d_m^2}{\pi D_{MSL,m}^2} \sqrt{\frac{h_{w,m}}{\rho_m (1-\beta_m^4)}} \tag{21}$$

The flowing air density at the inlet of the venturi is calculated by:

$$\rho_m = 2.698825\frac{P_{inlet}G_i}{ZT_m} \tag{22}$$

Incorporating Eq. (22) into Eq. (21) and simplifying gives the following expression for the measured flow velocity,

$$V_{m,measured} = \frac{0.01932 C_{D,m} Y_{1,m} d_m^2}{D_{MSL,m}^2}\sqrt{\frac{Z_m T_m h_{w,m}}{P_{inlet} G_{i,m}\left(1-\beta_m^4\right)}} \tag{23}$$

4. The flow velocity in the steam lines is known to be the main driver of the pressure oscillations in the scale model. As discussed in Reference [7], the trends of fluctuating pressure amplitudes with flow velocity can be approximated by a power law or exponential curve fit depending on the frequency band of interest. The frequency content observed in the scale model test data can be grouped in four different frequency bands:

   Band A: 0 – 10 Hz.
   Band B: 10 –30 Hz.
   Band C: 30 – 100 Hz.
   Band D: 100 – 165 Hz.

   The fluctuating pressures in frequency bands A, B and C are fit with the following power law equation:

$$P_m = K \cdot V_m^X \qquad X \in [1.7,\ 2.5] \tag{24}$$

   Reference [7] also shows that the resonances in band D are reasonably well fit with an exponential expression as shown in Eq. (25).

$$P_m = K \cdot e^{X \cdot V_m} \qquad X \in [0.04,\ 0.07] \text{ and } K \in [0.019,\ 0.027] \tag{25}$$

   where K and X are the curve fit variables. The intervals for X given in Eqs. (24) and (25) are typical values based on the results given in [7].

   It is worth noting that Eqs. (24) and (25) only give a general relationship between the flow velocity in the main steam lines and the pressure fluctuations in the scale model. Even though it is true that the scale model pressure, P_m, is a function of the steam line flow velocity in the scale model, V_m; the function that relates these two variables is unknown. Equations (24) and (25) are only an approximation of this unknown function. This means that it is not possible to calculate the exact value of the scale model pressure based on the steam line flow velocity by just using Eqs. (24) or (25). Therefore, the Law of Propagation of Uncertainties cannot be applied to these equations in a truly rigorous manner. Equations (24) and (25) can only be used to obtain a general idea of how uncertainties in the flow velocity

propagate to affect the error in the scale model pressure. These equations can be used to obtain an upper bound for this error; an exact uncertainty value, however, cannot be derived from it.

5. The pressure oscillations in the scale model are measured and recorded using a data acquisition system that digitizes the analog voltage signals generated by the pressure sensors as shown in Figure 3.

Figure 2 illustrates the process described above. Step 4 is inside a dashed rectangle to clearly indicate that the function that relates steam line flow velocity, V_m, and scale model pressure, P_m, is unknown. The power and exponential laws shown in step 4 are an approximation of this unknown function and, therefore, the propagation of uncertainties through this step of the process can only be estimated.

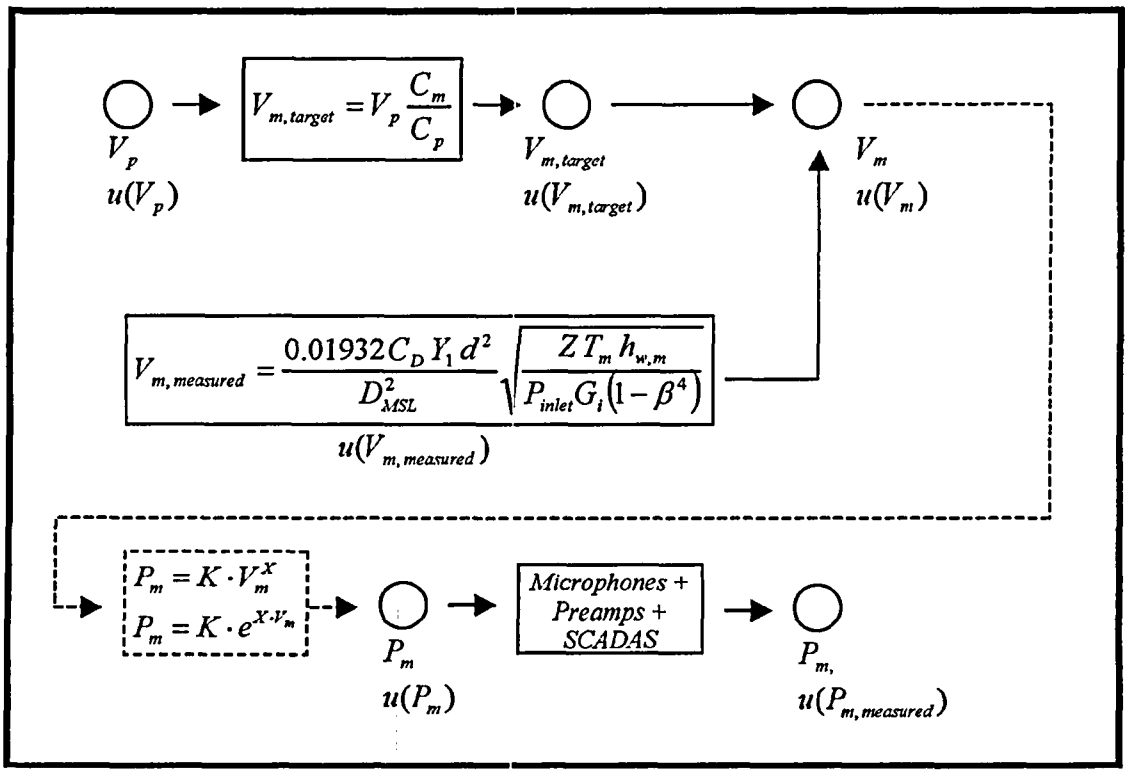

Figure 2: Schematic illustrating the propagation of uncertainties from the plant velocity measurement to the measured scale model pressure.

Expressions for the uncertainties associated with each step and variable of the process shown in Figure 2 are derived in the following sections.

Uncertainty in Full Size Plant Flow Velocity

Based on Ref. [5], page 11 (MPL No. E21-N006 through B21-N009), the uncertainty in the differential pressure high flow detection switch is ±3 psi, which corresponds to a percentage uncertainty of ±3%. Even though this uncertainty is only given for maximum flow conditions, it is safe to assume the same uncertainty for the differential pressure measurements used to calculate the plant main steam line flow under nominal steady state conditions. The general equation used to predict the flow velocity of a gaseous fluid based on the differential pressure drop across a venturi is given below:

$$V_p = \frac{Constant \cdot Y_{1,p} d_p^2}{D_{MSL,p}^2} \sqrt{\frac{Z_p T_{0,p} h_{w,p}}{P_{inlet,p} G_{i,p} \left(1-\beta_p^4\right)}} \tag{26}$$

This equation is very similar to Eq. (23) but the parameter *Constant* depends on the venturi dimensions and design and is, therefore, a plant specific parameter. However, we will prove that the accuracy of the flow velocity measurement is not affected by this parameter as long as we can assume that the uncertainty associated with it is negligible. It can be assumed that the venturi dimensions, gas compressibility factor, adiabatic expansion factor and ideal specific gravity of the gas have negligible uncertainties associated with them. Therefore, considering the terms that have non-negligible uncertainties associated with them, the measured plant velocity is a function of:

$$V_p = f(D_{MSL,p}, T_{0,p}, h_{w,p}, P_{inlet,p}) \tag{27}$$

Using the Law of Propagation of Uncertainty (Eq. 6), the uncertainty associated with the plant velocity measurement is given as:

$$u^2(V_p) = \left(\frac{\partial V_p}{\partial D_{MSL,p}}\right)^2 u^2(D_{MSL,p}) + \left(\frac{\partial V_p}{\partial T_{0,p}}\right)^2 u^2(T_{0,p}) + \ldots$$
$$\ldots + \left(\frac{\partial V_p}{\partial h_{w,p}}\right)^2 u^2(h_{w,p}) + \left(\frac{\partial V_p}{\partial P_{inlet,p}}\right)^2 u^2(P_{inlet,p}) \tag{28}$$

where

$$\frac{\partial V_p}{\partial D_{MSL,p}} = -2\frac{Constant\, Y_{1,p} d_p^2}{D_{MSL,p}^3} \sqrt{\frac{Z_p T_{0,p} h_{w,p}}{P_{inlet,p} G_{i,p} \left(1-\beta_p^4\right)}} \tag{29}$$

$$\frac{\partial V_p}{\partial T_{0,p}} = \frac{1}{2}\frac{Constant\, Y_{1,p} d_p^2}{D_{MSL,p}^2} \sqrt{\frac{Z_p h_{w,p}}{T_{0,p} P_{inlet,p} G_{i,p} \left(1-\beta_p^4\right)}} \tag{30}$$

$$\frac{\partial V_p}{\partial h_{w,p}} = \frac{1}{2} \frac{Constant\, Y_{1,p}\, d_p^2}{D_{MSL,p}^2} \sqrt{\frac{Z_p T_{0,p}}{h_{w,p} P_{inlet,p} G_{i,p} \left(1-\beta_p^4\right)}} \tag{31}$$

$$\frac{\partial V_p}{\partial P_{inlet,p}} = -\frac{1}{2P_{inlet,p}} \frac{Constant \cdot Y_{1,p}\, d_p^2}{D_{MSL,p}^2} \sqrt{\frac{Z_p T_{0,p} h_{w,p}}{P_{inlet,p} G_{i,p} \left(1-\beta_p^4\right)}} \tag{32}$$

Substituting Eqs. (29) through (32) into Eq. (28) and solving for the fractional uncertainty in the measured flow velocity yields

$$\frac{u(V_p)}{V_p} = \sqrt{4\left(\frac{u(D_{MSL,p})}{D_{MSL,p}}\right)^2 + \frac{1}{4}\left[\left(\frac{u(T_{0,p})}{T_{0,p}}\right)^2 + \left(\frac{u(h_{w,p})}{h_{w,p}}\right)^2 + \left(\frac{u(P_{inlet,p})}{P_{inlet,p}}\right)^2\right]} \tag{33}$$

Therefore, the fractional uncertainty in the measured flow velocity is given by

$$u_{\%}(V_p) = \sqrt{4\, u_{\%}^2(D_{MSL,p}) + \frac{1}{4}\left[u_{\%}^2(T_{0,p}) + u_{\%}^2(h_{w,p}) + u_{\%}^2(P_{inlet,p})\right]} \tag{34}$$

It is estimated that typical main steam line diameter tolerances are on the order of ±0.5%. The percentage uncertainties in plant temperature and pressure have been estimated based on data from Ref. [5]. Table 2 summarizes the parameters that were used to calculate the percentage uncertainty associated with the plant velocity measurement.

Table 2. Parameters for Uncertainty in Plant Velocity

$$u_{\%}(D_{MSL,p}) = 0.5\%$$
$$u_{\%}(T_{0,p}) = 1\%$$
$$u_{\%}(h_{w,p}) = 3\%$$
$$u_{\%}(P_{inlet,p}) = 1.5\%$$

Substituting the values given in Table 2 into Eq. (34) yields

$$u_{\%}(V_p) = 2\% \tag{35}$$

Uncertainty Expression for Target Flow Velocity in Scale Model

As shown in Eq. (18), the target value for the scale model flow velocity is calculated based on the ratio of sound speeds in scale model and full size plant. If steam and air are treated as perfect gases with $C^2 = kg_0RT_0$, and noting that $k_p \approx k_m$, Eq. (18) reduces to

$$V_{m,target} = V_p \sqrt{\frac{T_{0,m}}{T_{0,p}}} \tag{36}$$

Using the Law of Propagation of Uncertainty (Eq. 6), the uncertainty associated with this target value is given as:

$$u^2(V_{m,target}) = \left(\frac{\partial V_{m,target}}{\partial V_p}\right)^2 u^2(V_p) + \left(\frac{\partial V_{m,target}}{\partial T_{0,m}}\right)^2 u^2(T_{0,m}) + \left(\frac{\partial V_{m,target}}{\partial T_{0,p}}\right)^2 u^2(T_{0,p}) \tag{37}$$

where:

$$\frac{\partial V_{m,target}}{\partial V_p} = \sqrt{\frac{T_{0,m}}{T_{0,p}}} \tag{38}$$

$$\frac{\partial V_{m,target}}{\partial T_{0,m}} = \frac{V_p}{2T_{0,m}} \sqrt{\frac{T_{0,m}}{T_{0,p}}} \tag{39}$$

$$\frac{\partial V_{m,target}}{\partial T_{0,p}} = -\frac{V_p}{2T_{0,p}} \sqrt{\frac{T_{0,m}}{T_{0,p}}} \tag{40}$$

Equations (38) through (40) are substituted in Eq. (37) to get

$$u^2(V_{m,target}) = \left(\frac{T_{0,m}}{T_{0,p}}\right) u^2(V_p) + \left(\frac{V_p^2}{4T_{0,m}T_{0,p}}\right) u^2(T_{0,m}) + \left(\frac{V_p^2 T_{0,m}}{4T_{0,p}^3}\right) u^2(T_{0,p}) \tag{41}$$

Therefore, the uncertainty expression for the target flow velocity in the scale model is given by

$$u(V_{m,target}) = \sqrt{\frac{T_{0,m}}{T_{0,p}} u^2(V_p) + \frac{V_p^2}{4T_{0,m}T_{0,p}} u^2(T_{0,m}) + \frac{V_p^2 T_{0,m}}{4T_{0,p}^3} u^2(T_{0,p})} \tag{42}$$

and the fractional uncertainty in $V_{m,target}$ can be calculated as

$$\frac{u(V_{m,target})}{V_{m,target}} = \sqrt{\left(\frac{u(V_p)}{V_p}\right)^2 + \frac{1}{4}\left(\frac{u(T_{0,m})}{T_{0,m}}\right)^2 + \frac{1}{4}\left(\frac{u(T_{0,p})}{T_{0,p}}\right)^2} \tag{43}$$

From Ref. [5] the typical fractional uncertainty for plant temperature measurements is 1%. From the previous section, the tolerance associated with the plant flow velocity is

approximately 2%. According to Ref.[8], the K type Omega thermocouples used in the scale model have a tolerance of ±2.2°C or ±0.75%, whichever is greater. During operation of the scale model test apparatus, the average air temperature was around 140°F. Therefore, the average percentage uncertainty associated with the temperature measurement in the scale model is ±3.7%. The following parameters were used to determine the fractional uncertainty in the target flow velocity for the scale model:

Table 3, Parameters for Target Value of Scale Model Velocity

$$u_{\%}(V_p) = 2\%$$
$$u_{\%}(T_{0,m}) = 3.7\%$$
$$u_{\%}(T_{0,p}) = 1\%$$

for which

$$u_{\%}(V_{m,target}) = \frac{u(V_{m,target})}{V_{m,target}} \cdot 100 = 2.8\% \tag{44}$$

Uncertainty Expression for Scale Model Flow Velocity

As discussed in the previous section, Eq. (36) gives the flow velocity that needs to be achieved in the scale model in order to replicate the acoustic behavior of the steam system in the full size plant. The flow velocity in the scale model is measured using the venturi governing equation (23).

The total uncertainty in the actual flow velocity is a combination of the uncertainty in the target flow velocity and the uncertainty in the measured velocity provided by the venturi. Whether we should use quadratic or ordinary sum for combining these two uncertainties in order to obtain an estimate of the total uncertainty associated with the scale model flow velocity depends on the meaning that is given to the total uncertainty. If the uncertainty associated with the total flow velocity is understood as an upper bound, meaning that the error in the flow velocity is certainly no more than the total uncertainty, then direct addition is appropriate. On the other hand, if the uncertainty is used in statistical terms, meaning that there is a high probability that the true value of the flow velocity will lie within the range given by the reported total uncertainty, then addition in quadrature should be used. Since the variables considered here are independent and subject to many small sources of random error, and therefore follow a Gauss distribution, it is widely accepted that a quadratic sum of uncertainties is usually a more convenient approach for reporting the total uncertainty. Therefore, the total uncertainty in the scale model flow velocity will be calculated as follows

$$u_{total}(V_m) = \sqrt{u^2(V_{m,target}) + u^2(V_{m,measured})} \tag{45}$$

The uncertainty associated with the measured flow velocity is calculated by applying the Law of Propagation of Uncertainties to Eq. (23). It is worth noting that, strictly speaking, all the variables in Eq. (23) have uncertainties associated with them. However, for the purposes of this analysis, the dimensions of the venturi and the values of the ideal specific gravity, compressibility factor and adiabatic expansion factor of air have such small uncertainties associated with them that will be considered exact values as we did for determining the uncertainty associated with the plant velocity measurement. Therefore, considering the terms that have uncertainties associated with them, the measured velocity can be shown to be a function of:

$$V_{m,measured} = f(D_{MSL}, T_m, h_{w,m}, P_{inlet}) \tag{46}$$

Using the Law of Propagation of Uncertainty (Eq. 6), the uncertainty associated with the model velocity measurement is given as:

$$u^2(V_{m,measured}) = \left(\frac{\partial V_{m,measured}}{\partial D_{MSL,m}}\right)^2 u^2(D_{MSL,m}) + \left(\frac{\partial V_{m,measured}}{\partial T_m}\right)^2 u^2(T_m) + \ldots$$
$$\ldots + \left(\frac{\partial V_{m,measured}}{\partial h_{w,m}}\right)^2 u^2(h_{w,m}) + \left(\frac{\partial V_{m,measured}}{\partial P_{inlet,m}}\right)^2 u^2(P_{inlet,m}) \tag{47}$$

where

$$\frac{\partial V_{m,measured}}{\partial D_{MSL,m}} = -2\frac{0.01932 C_{D,m} Y_{1,m} d_m^2}{D_{MSL,m}^3}\sqrt{\frac{Z_m T_m h_{w,m}}{P_{inlet,m} G_{i,m}\left(1-\beta_m^4\right)}} \tag{48}$$

$$\frac{\partial V_{m,measured}}{\partial T_m} = \frac{1}{2}\frac{0.01932 C_{D,m} Y_{1,m} d_m^2}{D_{MSL,m}^2}\sqrt{\frac{Z_m h_{w,m}}{T_m P_{inlet,m} G_{i,m}\left(1-\beta_m^4\right)}} \tag{49}$$

$$\frac{\partial V_{m,measured}}{\partial h_{w,m}} = \frac{1}{2}\frac{0.01932 C_{D,m} Y_{1,m} d_m^2}{D_{MSL,m}^2}\sqrt{\frac{Z_m T_m}{h_{w,m} P_{inlet,m} G_{i,m}\left(1-\beta_m^4\right)}} \tag{50}$$

$$\frac{\partial V_{m,measured}}{\partial P_{inlet,m}} = -\frac{1}{2P_{inlet,m}}\frac{0.01932 C_{D,m} Y_{1,m} d_m^2}{D_{MSL,m}^2}\sqrt{\frac{Z_m T_m h_{w,m}}{P_{inlet,m} G_{i,m}\left(1-\beta_m^4\right)}} \tag{51}$$

Substituting Eqs. (48) through (51) into Eq. (47) and solving for the uncertainty in the measured flow velocity yields

$$u(V_{m,measured}) = \frac{0.01932 C_{D,m} Y_{1,m} d_m^2}{D_{MSL,m}^2} \sqrt{\frac{Z_m T_m h_{w,m}}{P_{inlet,m} G_{i,m} (1-\beta_m^4)}} \cdot \ldots \quad (52)$$

$$\ldots \cdot \sqrt{\left(\frac{2}{D_{MSL,m}}\right)^2 u^2(D_{MSL,m}) + \left(\frac{1}{2T_m}\right)^2 u^2(T_m) + \left(\frac{1}{2h_{w,m}}\right)^2 u^2(h_{w,m}) + \left(\frac{1}{2P_{inlet,m}}\right)^2 u^2(P_{inlet,m})}$$

Therefore, the fractional uncertainty in the measured flow velocity is given by

$$\frac{u(V_{m,measured})}{V_{m,measured}} = \sqrt{4\left(\frac{u(D_{MSL,m})}{D_{MSL,m}}\right)^2 + \frac{1}{4}\left[\left(\frac{u(T_m)}{T_m}\right)^2 + \left(\frac{u(h_{w,m})}{h_{w,m}}\right)^2 + \left(\frac{u(P_{inlet,m})}{P_{inlet,m}}\right)^2\right]} \quad (53)$$

The main steam lines in the scale model are made of 1" stainless steel piping. Measurements of these pipes gave an ID uncertainty of approximately ±0.015". Therefore, the percentage uncertainty in the main steam line diameter is 1.5%.

As discussed in previous sections, the average percentage uncertainty associated with the temperature measurement in the scale model is ±3.7%.

The transducer used to measure the differential pressure across the venturi is a Rosemount 3051CD 2A22A1A, with a percentage uncertainty of 0.15% as given in Ref. [4]. This is the same percentage uncertainty associated with the pressure measurement at the inlet.

The previous paragraphs justify the following values that were used to determine the fractional uncertainty in the measured scale model flow velocity:

Table 4, Parameters for Measured Value of Scale Model Velocity

$$u_{\%}(D_{MSL,m}) = 1.5\%$$
$$u_{\%}(T_m) = 3.7\%$$
$$u_{\%}(h_{w,m}) = 0.15\%$$
$$u_{\%}(P_{inlet,m}) = 0.15\%$$

for which

$$u_{\%}(V_{m,measured}) = \frac{u(V_{m,measured})}{V_{m,measured}} \cdot 100 = 3.5\% \quad (54)$$

We can now obtain the total uncertainty associated with the steam model flow velocity by combining the uncertainties of the target and measured velocities, given by Eqs. (44) and (54) respectively, as shown in Eq. (45):

$$u_{\%}(V_m) = \sqrt{u_{\%}^2(V_{m,target}) + u_{\%}^2(V_{m,measured})} = 4.5\% \quad (55)$$

Uncertainty in Scale Model Pressure

As discussed in previous sections, the pressure inside the scale model is a function of the flow velocity. Since this function is unknown, it was decided to approximate it by either a power law or exponential law in order to quantify how uncertainties in the scale model flow velocity propagate to the scale model pressure oscillations. Eqs. (24) and (25) express the scale model pressure in terms of the flow velocity and are shown again below for convenience:

$$P_m = K \cdot V_m^X \qquad X \in [1.7,\ 2.5] \qquad \text{for frequency bands A, B and C} \tag{56}$$

$$P_m = K \cdot e^{X \cdot V_m} \quad X \in [0.04,\ 0.07],\ K \in [0.019,\ 0.027] \quad \text{for frequency band D} \tag{57}$$

It is clear that Eqs. (56) and (57) were derived using standard curve fitting algorithms and do not have a physical meaning. Furthermore, the parameters K and X are different depending on the frequency range of interest as shown in Ref. [7] and there is relatively large variability of the measured pressure points around the proposed curves. It would be possible to evaluate the uncertainty associated with Eqs. (56) and (57) and test the goodness of fit of the proposed curves by applying the Law of Propagation of Uncertainties and considering K and X as variables. However, it is not the purpose of this document to evaluate the accuracy of Eqs. (56) and (57). Since these equations are just a tool to estimate propagation of errors from flow velocity to pressure, the parameters K and X will be considered constant and their values will be selected from the typical ranges given in Ref. [7] so that they provide an upper bound for the pressure uncertainty. Therefore, Using the Law of Propagation of Uncertainties (Eq. 6), the uncertainty associated with the model pressure within the frequency bands A, B and C is given as:

$$u^2(P_m) = \left(\frac{\partial P_m}{\partial V_m}\right)^2 u^2(V_m) \tag{58}$$

where

$$\frac{\partial P_m}{\partial V_m} = K \cdot X \cdot V_m^{X-1} \tag{59}$$

Substituting Eq. (59) into Eq. (58) and solving for the uncertainty in the scale model pressure yields

$$u(P_m) = \sqrt{K^2 \cdot X^2 \cdot V_m^{2X-2} u^2(V_m)} \tag{60}$$

Therefore, the fractional uncertainty associated with P_m is given by

$$\frac{u(P_m)}{P_m} = X\frac{u(V_m)}{V_m} \tag{61}$$

In order to obtain a conservative estimate of the pressure uncertainty, X has been assigned a value of 2.5, which is the maximum value it can take based on Eq. (56). The percentage uncertainty in the flow velocity is 4.5%, as calculated in the previous section. Substituting these values into Eq. (61) yields

$$u_{\%}(P_{m,\,Band\,A,B,C}) = 11.3\% \tag{62}$$

For the pressure oscillations in band D we have that

$$\frac{\partial P_m}{\partial V_m} = K \cdot X \cdot e^{X \cdot V_m} \tag{63}$$

Substituting Eq. (63) into Eq. (58) and solving for the uncertainty in the scale model pressure yields

$$u(P_m) = K \cdot X \cdot e^{X \cdot V_m} \cdot u(V_m) \tag{64}$$

Noting that $X = 1/V_m \cdot Ln(P_m/K)$, Eq. (64) reduces to

$$u_{\%}(P_m) = Ln\left(\frac{P_m}{K}\right) \cdot u_{\%}(V_m) \tag{65}$$

From Ref. [7], maximum RMS fluctuating pressures in the scale model are on the order of 40 Pa. The minimum value of K is 0.019 Pa as shown in Eq. (57). The percentage uncertainty in the flow velocity is 4.5%, as calculated in the previous section. Substituting these values into Eq. (65) yields

$$u_{\%}(P_{m,\,Band\,D}) = 34.4\% \tag{66}$$

Uncertainty in Measured Scale Model Pressure

The uncertainty given by Eqs. (62) and (66) show the error in the actual scale model pressure with respect to the full size plant pressure that the scale model was designed to replicate. However, the actual scale model pressure is not known until it is measured using a Data Acquisition System (DAS). Therefore, the total error in the measured scale model pressure is a combination of the uncertainty in the actual pressure and the uncertainty in the measuring system. Figure 3 shows the elements of the test system used to measure and record the scale model pressure.

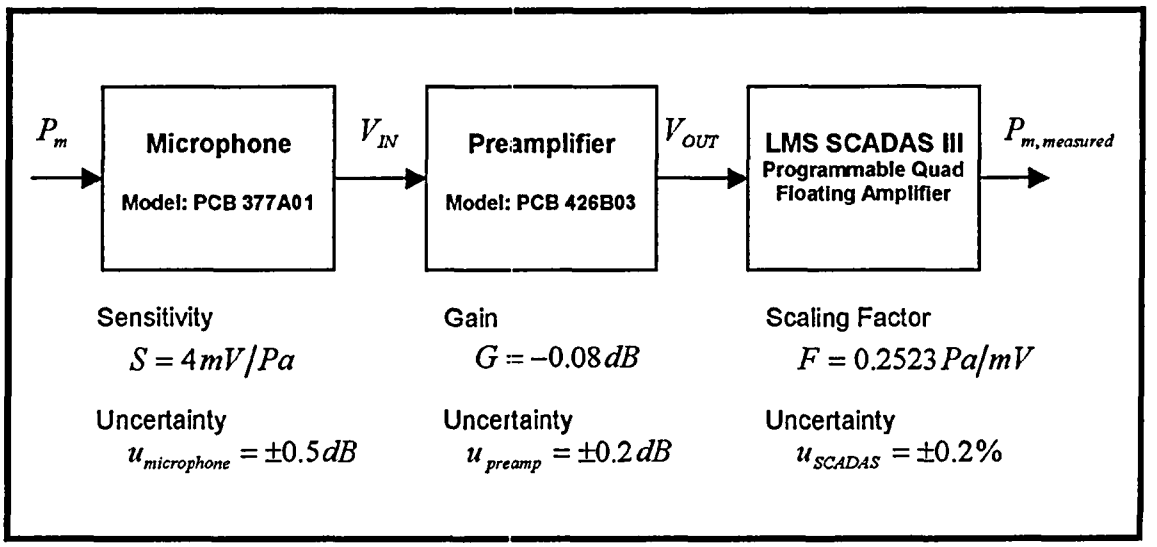

Figure 3: Schematic showing test system components and associated uncertainties.

The parameters and uncertainties shown in Figure 3 have been taken from References [9], [10] and [11].

The following equation expresses the measured pressure in terms of the actual scale model pressure, microphone sensitivity, preamplifier gain and SCADAS scaling factor:

$$P_{m,measured} = S \cdot G \cdot F \cdot P_m \tag{67}$$

So, the measured pressure is a function of the following parameters,

$$P_{m,measured} = f(S, G, F, P_m) \tag{68}$$

Using the Law of Propagation of Uncertainties (Eq. 6), the uncertainty associated with the plant pressure measurement is given as:

$$\begin{aligned} u^2(P_{m,measured}) = &\left(\frac{\partial P_{m,measured}}{\partial S}\right)^2 u^2(S) + \left(\frac{\partial P_{m,measured}}{\partial G}\right)^2 u^2(G) + \ldots \\ &\ldots + \left(\frac{\partial P_{m,measured}}{\partial F}\right)^2 u^2(F) + \left(\frac{\partial P_{m,measured}}{\partial P_m}\right)^2 u^2(P_m) \end{aligned} \tag{69}$$

Substituting Eq. (67) into Eq. (69) and solving for $u(P_{m,measured})/P_{m,measured}$ yields

$$\frac{u(P_{m,measured})}{P_{m,measured}} = \sqrt{\left(\frac{u(S)}{S}\right)^2 + \left(\frac{u(G)}{G}\right)^2 + \left(\frac{u(F)}{F}\right)^2 + \left(\frac{u(P_m)}{P_m}\right)^2} \tag{70}$$

Equation (70) can be rewritten in terms of the percentage uncertainties as follows:

$$u_{\%}(P_{m,measured}) = \sqrt{u_{\%}^2(S) + u_{\%}^2(G) + u_{\%}^2(F) + u_{\%}^2(P_m)} \tag{71}$$

Equation (71) indicates that the fractional uncertainty in the measured pressure is the quadratic sum of the original fractional uncertainties.

The absolute microphone uncertainty shown in Figure 3 can be converted to an equivalent percentage uncertainty after calculating the ratio between the reference pressure and measured pressure that corresponds to an absolute uncertainty of ±0.5 dB:

$$0.5 = 20\log\frac{P_{OUT}}{P_{REF}} \quad \Rightarrow \quad \frac{P_{OUT}}{P_{REF}} = 1.059 \tag{72}$$

Therefore, the percentage uncertainty associated with the preamplifier is ±5.9 %.

The absolute preamplifier uncertainty shown in Figure 3 can be converted to an equivalent percentage uncertainty using the same equation used for the microphone uncertainty:

$$0.2 = 20\log\frac{V_{OUT}}{V_{REF}} \quad \Rightarrow \quad \frac{V_{OUT}}{V_{REF}} = 1.023 \tag{73}$$

which gives a preamplifier uncertainty of ±2.3 %.

Table 5 summarizes the percentage uncertainties that determine the total uncertainty in the measured model pressure.

Table 5. Parameters for Uncertainty in Measured Scale Model Pressure

$$u_{\%}(S) = 5.9\%$$
$$u_{\%}(G) = 2.3\%$$
$$u_{\%}(F) = 0.2\%$$
$$u_{\%}(P_{m,\,Bands\,A,B,C}) = 11.3\%$$
$$u_{\%}(P_{m,\,Band\,D}) = 34.4\%$$

Substituting the values in Table 5 into Eq. (71) gives

$$u_{\%}(P_{m,measured,Bands\,A,B,C}) = 13\% \tag{75}$$

and

$$u_{\%}(P_{m,measured,Band\,D}) = 35\% \tag{76}$$

Table 6 provides a summary of all the uncertainties that determine the total uncertainty in the plant pressure that is predicted using scale model pressure measurements. The values in Table 6 have been obtained in previous sections and do not require further discussion.

Table 6. Parameters for Total Uncertainty in Full Size Plant Pressure

$$u_{\%}(P_{m,measured,Bands\,A,B,C}) = 13\%$$
$$u_{\%}(P_{m,measured,Band\,D}) = 35\%$$
$$u_{\%}(P_{0,p}) = 1.5\%$$
$$u_{\%}(P_{0,m}) = 0.15\%$$

It is now possible to calculate the total uncertainty in the predicted plant pressure by substituting the uncertainties shown in Table 6 into Eq. (17). Since the scale model pressure uncertainty is more than an order of magnitude greater than the other two, the total uncertainty is approximately the same as the scale model pressure uncertainty.

$$u_{\%}(P_{p,Bands\,A,B,C}) = 13.1\% \tag{77}$$

and

$$u_{\%}(P_{p,Band\,D}) = 35\% \tag{78}$$

Figure 4 summarizes the propagation of uncertainties from the initial plant velocity measurement to the final plant pressure prediction.

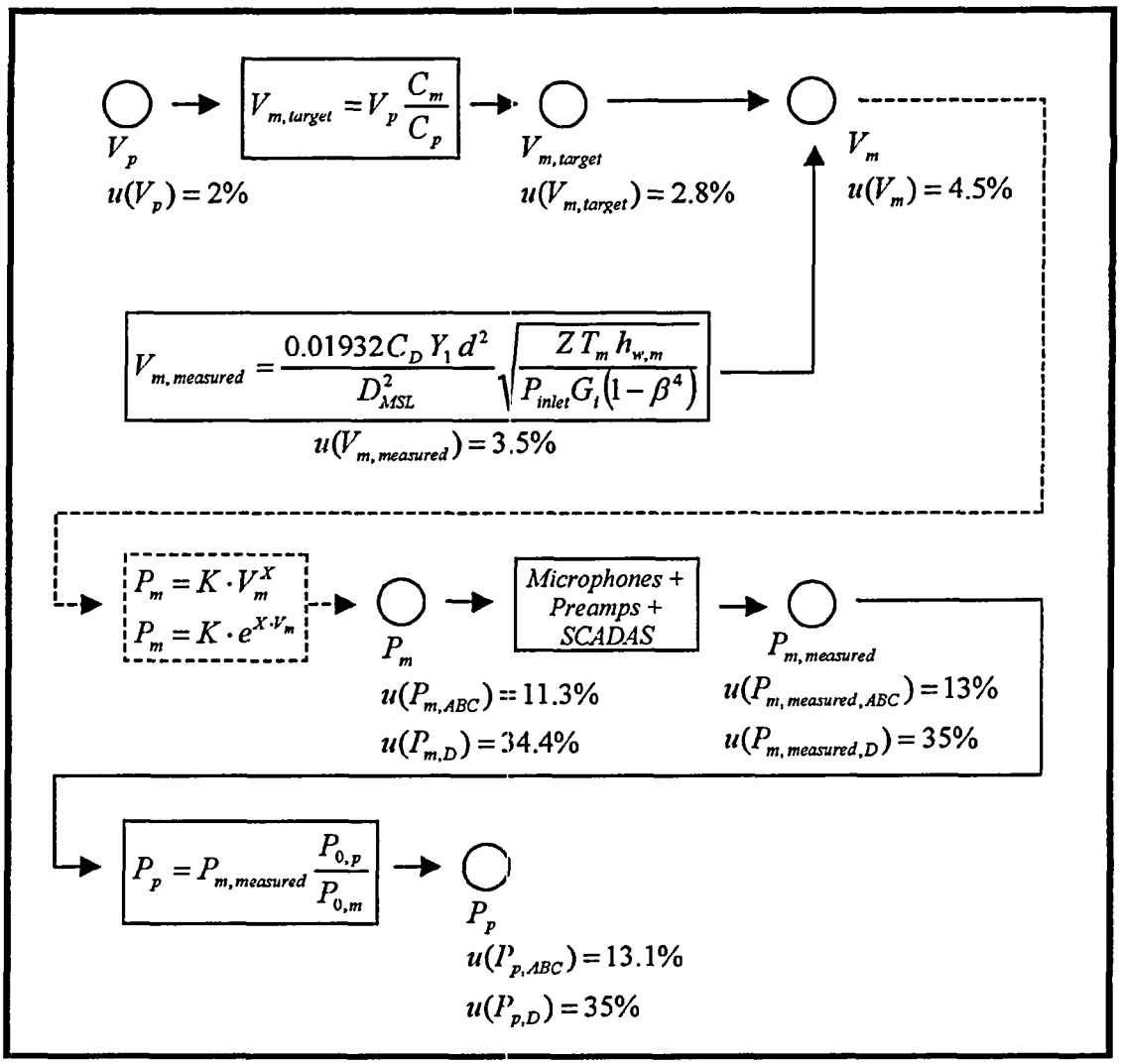

Figure 4: Schematic illustrating the propagation of uncertainties from the plant velocity measurement to the predicted plant pressure.

Uncertainty Expression for Plant Frequency Prediction:

The plant frequency estimate is given in Ref. [3] as:

$$f_p = f_m \frac{L_m}{L_p} \frac{C_p}{C_m} \tag{79}$$

If the steam and air are treated as perfect gases with $C^2 = kg_0 RT_0$, the plant frequency estimate can be written as:

$$f_p = f_m \frac{L_m}{L_p}\sqrt{\frac{k_p T_{0,p}}{k_m T_{0,m}}} \tag{80}$$

Since $k_m \approx k_p$, Eq. (80) reduces to

$$f_p = f_m \frac{L_m}{L_p}\sqrt{\frac{T_{0,p}}{T_{0,m}}} \tag{81}$$

Therefore, the plant frequency is a function of the following parameters:

$$f_p = f(f_m, L_m, L_p, T_{0,p}, T_{0,m}) \tag{82}$$

Using the Law of Propagation of Uncertainties, the uncertainty associated with the plant frequency prediction is give by:

$$\begin{aligned} u^2(f_p) = &\left(\frac{\partial f_p}{\partial f_m}\right)^2 u^2(f_m) + \left(\frac{\partial f_p}{\partial L_m}\right)^2 u^2(L_m) + \left(\frac{\partial f_p}{\partial L_p}\right)^2 u^2(L_p) + \ldots \\ &\ldots + \left(\frac{\partial f_p}{\partial T_{0,p}}\right)^2 u^2(T_{0,p}) + \left(\frac{\partial f_p}{\partial T_{0,m}}\right)^2 u^2(T_{0,m}) \end{aligned} \tag{83}$$

where

$$\frac{\partial f_p}{\partial f_m} = \frac{L_m}{L_p}\sqrt{\frac{T_{0,p}}{T_{0,m}}} \tag{84}$$

$$\frac{\partial f_p}{\partial L_m} = \frac{f_m}{L_p}\sqrt{\frac{T_{0,p}}{T_{0,m}}} \tag{85}$$

$$\frac{\partial f_p}{\partial L_p} = -f_m \frac{L_m}{L_p^2}\sqrt{\frac{T_{0,p}}{T_{0,m}}} \tag{86}$$

$$\frac{\partial f_p}{\partial T_{0,p}} = f_m \frac{L_m}{2L_p}\sqrt{\frac{1}{T_{0,p}T_{0,m}}} \tag{87}$$

$$\frac{\partial f_p}{\partial T_{0,m}} = -f_m \frac{L_m}{2L_p T_{0,m}}\sqrt{\frac{T_{0,p}}{T_{0,m}}} \tag{88}$$

Substituting Eqs. (84) through (88) into Eq. (83) and solving for the uncertainty in the plant frequency prediction gives

$$u(f_p) = f_m \frac{L_m}{L_p}\sqrt{\frac{T_{0,p}}{T_{0,m}}}\cdot\sqrt{\left(\frac{u(f_m)}{f_m}\right)^2+\left(\frac{u(L_m)}{L_m}\right)^2+\left(\frac{u(L_p)}{L_p}\right)^2+\frac{1}{4}\left[\left(\frac{u(T_{0,m})}{T_{0,m}}\right)^2+\left(\frac{u(T_{0,p})}{T_{0,p}}\right)^2\right]} \tag{89}$$

After dividing through by f_p it is possible to express the percentage uncertainty in the plant frequency prediction in terms of the percentage uncertainties associated with the other variables as follows:

$$u_{\%}(f_p) = \sqrt{u_{\%}^2(f_m)+u_{\%}^2(L_m)+u_{\%}^2(L_p)+\frac{1}{4}\left(u_{\%}^2(T_{0,m})+u_{\%}^2(T_{0,p})\right)} \tag{90}$$

The percentage uncertainty associated with the model frequency measurements is required prior to evaluating Eq. (90).

Uncertainty in Model Frequency Measurement

The model frequency uncertainty associated with the test instrumentation used to monitor the oscillating pressures in the scale model is negligible and will not be considered in this document. The main sources of frequency uncertainty in the scale model are the fabrication tolerances of the scale model components.

As discussed in previous sections, Ref. [7] shows that the frequency content observed in the scale model test data can be grouped in four different frequency bands:

Band A: 0 – 10 Hz.
Band B: 10 – 30 Hz.
Band C: 30 – 100 Hz.
Band D: 100 – 165 Hz.

The frequency content in Band A is attributable to an organ pipe mode of the main steam lines. The fundamental mode (1/2 wave) of an open – open or a closed – closed pipe is given by

$$f_{m,Band\,A} = \frac{C_m}{2L_{m,MSL}} \tag{91}$$

If air is treated as a perfect gas, the model frequency estimate can be written as a function of the air temperature as

$$f_{m,Band\,A} = \frac{\sqrt{k_m g_0 R T_{0,m}}}{2 L_{m,MSL}} \tag{92}$$

Considering the terms that have non-negligible uncertainties associated with them, the model frequency in band A can be shown to be a function of:

$$f_{m,Band\,A} = f(L_{m,MSL}, T_{0,m}) \tag{93}$$

Using the Law of Propagation of Uncertainties, the uncertainty associated with the model frequency measurement in band A is given by:

$$u^2(f_{m,Band\,A}) = \left(\frac{\partial f_{m,Band\,A}}{\partial L_{m,MSL}}\right)^2 u^2(L_{m,MSL}) + \left(\frac{\partial f_{m,Band\,A}}{\partial T_{0,m}}\right)^2 u^2(T_{0,m}) \tag{94}$$

where

$$\frac{\partial f_{m,Band\,A}}{\partial L_{m,MSL}} = -\frac{\sqrt{k_m g_0 R T_{0,m}}}{2 L_{m,MSL}^2} \tag{95}$$

and

$$\frac{\partial f_{m,Band\,A}}{\partial T_{0,m}} = \frac{\sqrt{k_m g_0 R}}{4 L_{m,MSL} \sqrt{T_{0,m}}} \tag{96}$$

Substituting Eqs. (95) and (96) into Eq. (94) and solving for the fractional uncertainty in the model frequency yields

$$\frac{u(f_{m,Band\,A})}{f_{m,Band\,A}} = \sqrt{\left(\frac{u(L_{m,MSL})}{L_{m,MSL}}\right)^2 + \frac{1}{4}\left(\frac{u(T_{0,m})}{T_{0,m}}\right)^2} \tag{97}$$

which, written in terms of percentage uncertainties gives

$$u_{\%}(f_{m,Band\,A}) = \sqrt{u_{\%}^2(L_{m,MSL}) + \frac{1}{4} u_{\%}^2(T_{0,m})} \tag{98}$$

The frequency content in the 10 – 20 Hz range (band B) is not fully understood. Assuming that the nature of the pressure oscillations in this band is similar to that of the other three bands, we would need to know the characteristic length of the resonator associated with these frequencies in order to calculate the uncertainty associated with this frequency band. Since the resonator is not known, we will assume that the uncertainty associated with this frequency band is bound by that of the other three bands.

The 30 – 100 Hz content is contributed by the steam plenum acoustic normal modes, which are excited by turbulence generated in the steam lines and vortex shedding generated as steam flows over the edge of the dryer. Since the steam cavity inside the vessel is three-dimensional, the frequencies of the pressure oscillations are hard to calculate analytically. However, as a first approximation, it can be said that the frequencies in this band will be proportional to the speed of sound and inversely proportional to the corresponding characteristic length inside the steam cavity:

$$f_{m,Band\,C} = \frac{nC_m}{4L_{m,dryer}}; \qquad n = 1, 2, \ldots, \infty \tag{99}$$

Following the same process that was used for determining the percentage uncertainty associated with the frequencies in Band A it is easy to obtain the following expression for the percentage uncertainty in the Band C frequencies:

$$u_{\%}(f_{m,Band\,C}) = \sqrt{u_{\%}^2(L_{m,dryer}) + \frac{1}{4}u_{\%}^2(T_{0,m})} \tag{100}$$

The 100 – 250 Hz frequency peaks are contributed by the S/RV standpipe ¼ wave organ pipe modes excited by vortices that are generated as boundary layer separation occurs at the edge of the S/RV standpipes. Analytically, the frequency at which this phenomenon occurs is given by

$$f_{m,Band\,D} = \frac{C_m}{4\left(L_{m,stanpipe} + 0.6\frac{d_{m,inlet}}{2}\right)} \tag{101}$$

The above equation includes an end effect correction due to the S/RV inlet diameter as described in Ref. [12].

The uncertainty associated with the frequencies in band D as a function of the uncertainties associated with the sound speed in the model and S/RV dimensions can be obtained by applying the Law of Propagation of Uncertainties to Eq. (101), which yields

$$\frac{u(f_{m,Band\,D})}{f_{m,Band\,D}} = \sqrt{\frac{u^2(L_{m,stanpipe}) + 0.09u^2(d_{m,inlet})}{(L_{m,stanpipe} + 0.3d_{m,inlet})^2} + \frac{1}{4}\left(\frac{u(T_{0,m})}{T_{0,m}}\right)^2} \tag{102}$$

Equations (98), (100) and (102) give the uncertainty expressions for the model frequency measurements. In previous sections, the percentage uncertainty in the model temperature was determined to be ±3.7%. According to Ref. [13], the absolute error in the main steam line length is approximately 0.7 inches, which gives a percentage error of 0.4% for an approximate steam line length of 16 ft. Also according to Ref. [13], the tolerance for the SR/V standpipe length is approximately ±0.005", and the average standpipe length in the

scale model is 1.75". The typical tolerance for the S/RV inlet diameters is ± 0.002" and the typical inside diameter value is 0.37" as shown in GE drawing 352B2099.

According to Ref. [14], the SLA process used to make the steam dryer holds standard tolerances of ± 0.005" for the first inch of the build and ± 0.002" for every inch thereafter. In the Z direction (shortest span of the part), standard tolerances are ± 0.010" for the first inch of the build and ± 0.002" on every inch thereafter. Where bond lines are crossed, a tolerance of ± 0.010" is added. Additionally, due to the nickel plating of these parts, an extra tolerance of ± 0.005" is added on all plated surfaces. For conservatism, we will consider that steam dryer dimensions have a tolerance of ± 0.005" per inch, or 0.5%.

All the tolerances described above are summarized in the following table.

Table 7, Parameters for Uncertainty in Scale Model Frequencies

$$u_{\%}(T_{0,m}) = 3.7\%$$
$$u_{\%}(L_{m,MSL}) = 0.4\%$$
$$u_{\%}(L_{m,dryer}) = 0.5\%$$
$$u(l_{m,stanpipe}) = 0.005"$$
$$u(d_{m,inlet}) = 0.002"$$
$$L_{m,stanpipe} = 1.75"$$
$$d_{m,inlet} = 0.37"$$

Substituting the values given in Table 7 into Eqs, (98), (100) and (102) yields

$$u_{\%}(f_{m,Band\,A}) = 1.9\%$$
$$u_{\%}(f_{m,Band\,C}) = 1.9\%$$
$$u_{\%}(f_{m,Band\,D}) = 1.9\%$$

Since all dimensional tolerances are similar and small, the main source of error in the model frequencies is the uncertainty associated with the speed of sound in the scale model, which is governed by the air temperature.

Uncertainty in Plant Frequency Prediction

The uncertainty expression for the plant frequency prediction is given by Eq. (90), which is written again below for convenience:

$$u_{\%}(f_p) = \sqrt{u_{\%}^2(f_m) + u_{\%}^2(L_m) + u_{\%}^2(L_p) + \frac{1}{4}\left(u_{\%}^2(T_{0,m}) + u_{\%}^2(T_{0,p})\right)} \qquad (103)$$

From Ref. [13], there are differences between plant drawings and actual steam line lengths of up to 3%. It is estimated that, S/RV standpipe lengths are known with a tolerance of ± 1", which corresponds to a percentage uncertainty of 3.3%. The parameters used to estimate the uncertainty in the plant frequency prediction are shown in Table 8.

Table 8, Parameters for Uncertainty in Plant Frequency Predictions

$$u_{\%}(T_{0,m}) = 3.7\% \qquad u_{\%}(T_{0,p}) = 1\%$$
$$u_{\%}(f_m) = 1.9\% \qquad u_{\%}(L_{p,MSL}) = 3.0\%$$
$$u_{\%}(L_{m,MSL}) = 0.4\% \qquad u_{\%}(L_{p,dryer}) = 0.5\%$$
$$u_{\%}(L_{m,dryer}) = 0.5\% \qquad u_{\%}(L_{p,stanpipe}) = 3.3\%$$
$$u_{\%}(L_{m,stanpipe}) = 0.3\%$$

Substituting the values given in Table 8 into Equation (103) yields

$$u_{\%}(f_{p,Band\,A}) = 4.1\%$$
$$u_{\%}(f_{p,Band\,C}) = 2.8\%$$
$$u_{\%}(f_{p,Band\,D}) = 4.2\%$$

DISCUSSION REGARDING SYSTEMATIC ERRORS

All the test instruments used in the scale model are calibrated and they do not exhibit bias or systematic errors. However, a systematic error in the plant pressure and frequency predictions may be introduced due to the simplifications and assumptions used for building the scale model. After a preliminary inspection of the QC benchmark results, it is apparent that the pressure amplitudes in bands A, B and C overestimate those in the full size plant. This difference could be caused by a systematic error introduced by a difference in damping between the plant and the model. This error could be corrected by performing a statistical analysis of the model and plant data and introducing an empirical scaling factor or bias error correction term. However, this empirical term would most likely be plant specific so this approach is not recommended because it would hamper the use of the scale model as a predictive tool.

The best approach for dealing with potential systematic errors in the scale model is to refine the boundary conditions and simplifications used for building it in order to achieve a more accurate representation of the plant behavior.

CONCLUSIONS

An uncertainty analysis of the plant pressure and frequency predictions provided by the Scale Model Test system has been performed in this document. The only uncertainties

considered for this analysis have been those associated with test instrumentation and fabrication tolerances. Systematic errors due to the simplifications and assumptions made to build the scale model can only be eliminated by checking and improving these assumptions if necessary.

Based on the results obtained in previous sections it has been determined that the most important factors that limit the precision of the scale model predictions are the uncertainties in the model sound speed, which are caused by the uncertainties in the model air temperature, uncertainties in the actual plant dimensions, especially those of the S/RV standpipes, and the highly non-linear behavior of the S/RV resonances.

The following tables summarize the results obtained in this document as well as all the uncertainties that affect the scale model predictions.

<table>
<tr><th>Uncertainties Associated with Primary Variables (Measured Variables)</th><th colspan="4">Intermediate Uncertainties (Calculated Using Law of Propagation of Uncertainties)</th><th>Uncertainty in Plant Pressure Prediction</th></tr>
<tr><td>$u(P_{0,m}) = 0.15\%$
(From Ref. [4])</td><td colspan="4" rowspan="2">⟹</td><td rowspan="15">$u(P_p)$
Bands A,B,D: 13%
Band D: 35%</td></tr>
<tr><td>$u(P_{0,p}) = 1.5\%$
(From Ref. [5])</td></tr>
<tr><td>$u(V_p) = 2\%$
(Derived based on $u(h_{w,p}) = 3\%$ as indicated in Ref. [5])</td><td rowspan="3">$u(V_{m,target})$
3%</td><td rowspan="7">$u(V_m)$
5%</td><td rowspan="7">$u(P_m)$
Bands A,B,D: 11%
Band D: 34%</td><td rowspan="12">$u(P_{m,measured})$
Bands A,B,D: 13%
Band D: 35%</td></tr>
<tr><td>$u(T_{0,m}) = 3.7\%$
(From Ref. [8])</td></tr>
<tr><td>$u(T_{0,p}) = 1\%$
(From Ref. [5])</td></tr>
<tr><td>$u(D_{MSL,m}) = 1.5\%$
(Measured)</td><td rowspan="4">$u(V_{m,measured})$
4%</td></tr>
<tr><td>$u(T_{0,m}) = 3.7\%$
(From Ref. [8])</td></tr>
<tr><td>$u(h_{w,m}) = 0.15\%$
(From Ref. [4])</td></tr>
<tr><td>$u(P_{inlet,m}) = 0.15\%$
(From Ref. [4])</td></tr>
<tr><td>$X_{Bands\ A,B,C} = 2.5$
$K_{Band\ D} = 0.019$
(From Ref. [7])</td><td colspan="2">⟹</td></tr>
<tr><td>$u(S) = 5.9\%$
(From Ref. [9])</td><td colspan="4" rowspan="3">⟹</td></tr>
<tr><td>$u(G) = 2.3\%$
(From Ref. [10])</td></tr>
<tr><td>$u(F) = 0.2\%$
(From Ref. [11])</td></tr>
</table>

Table 9: Propagation of uncertainties for plant pressure prediction.

Uncertainties Associated with Primary Variables (Measured Variables)	Intermediate Uncertainty (Calculated Using Law of Propagation of Uncertainties)	Uncertainty Associated with Plant Frequency Prediction for Band A (0 – 10 Hz)
$u(L_{m,MSL}) = 0.4\%$ (From Ref. [13])		$u(f_{p,Band\,A}) = 4\%$
$u(L_{p,MSL}) = 3\%$ (From Ref. [13])		
$u(T_{0,m}) = 3.7\%$ (From Ref. [8])		
$u(T_{0,p}) = 1\%$ (From Ref. [5])		
$u(L_{m,MSL}) = 0.4\%$ (From Ref. [13])	$u(f_{m,Band\,A}) = 2\%$	
$u(T_{0,m}) = 3.7\%$ (From Ref. [8])		

Table 10: Propagation of uncertainties for band A plant frequency prediction.

Uncertainties Associated with Primary Variables (Measured Variables)	Intermediate Uncertainty (Calculated Using Law of Propagation of Uncertainties)	Uncertainty Associated with Plant Frequency Prediction for Band C (30 – 100 Hz)
$u(L_{m,dryer}) = 0.5\%$ (From Ref. [14])	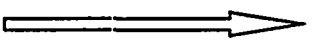	$u(f_{p,Band\,C}) = 3\%$
$u(L_{p,dryer}) = 0.5\%$ (Estimate)		
$u(T_{0,m}) = 3.7\%$ (From Ref. [8])		
$u(T_{0,p}) = 1\%$ (From Ref. [5])		
$u(L_{m,dryer}) = 0.5\%$ (From Ref. [14])	$u(f_{m,Band\,C}) = 2\%$	
$u(T_{0,m}) = 3.7\%$ (From Ref. [8])		

Table 11: Propagation of uncertainties for band C plant frequency prediction.

<table>
<tr><th>Uncertainties Associated with Primary Variables (Measured Variables)</th><th>Intermediate Uncertainty (Calculated Using Law of Propagation of Uncertainties)</th><th>Uncertainty Associated with Plant Frequency Prediction for Band D (100 – 165 Hz)</th></tr>
<tr><td>$u(L_{m,standpipe}) = 0.3\%$
(From Ref. [13])</td><td rowspan="4">⟹</td><td rowspan="8">$u(f_{p,Band\,D}) = 4\%$</td></tr>
<tr><td>$u(L_{p,standpipe}) = 3.3\%$
(Estimate)</td></tr>
<tr><td>$u(T_{0,m}) = 3.7\%$
(From Ref. [8])</td></tr>
<tr><td>$u(T_{0,p}) = 1\%$
(From Ref. [5])</td></tr>
<tr><td>$u(L_{m,standpipe}) = 0.3\%$
(From Ref. [13])</td><td rowspan="3">$u(f_{m,Band\,D}) = 2\%$</td></tr>
<tr><td>$u(d_{inlet}) = 0.5\%$
(Estimate)</td></tr>
<tr><td>$u(T_{0,m}) = 3.7\%$
(From Ref. [8])</td></tr>
</table>

Table 12: Propagation of uncertainties for band D plant frequency prediction.

REFERENCES

[1] Taylor, B.N. and Kuyatt, C.E. "Guidelines for Evaluating and Expressing the Uncertainty of NIST Measurement Results". NIST Technical Note 1297.

[2] Taylor, J.R. "An Introduction to Error Analysis. The Study of Universities in Physical Measurements". University Science Books. Second Edition, 1997.

[3] Lynch, J. "Scaling of the Miniature Steam Dome". GENE-0000-0026-1669-05. December 2, 2002. GENE Document. San Jose, CA.

[4] Rosemount 3051 Product Data Sheet. Data Sheet 00813-0100-4001, Rev FA. August 2004.

[5] Nuclear Boiler System Design Spec. Data Sheet. FMF: Susquehanna. MPL: B21-4020. GENE Document 22A2925AD.

[6] CEESI Technical Note TN-014. August 1992. Colorado Engineering Experiment Station. Nunn, CO.

[7] Sommerville, D. "General Electric Boiling Water Reactor Steam Dryer Scale Model Test Based Fluctuating Load Definition Methodology – January 2006 Benchmark Report". GENE-0000-0045-9086-01. January 2006. GENE Document. San Jose, CA.

[8] Omega Thermocouple website. http://www.omega.com/guides/thermocouples.html.

[9] Certificates of Calibration and Compliance for Microphone model 40BE. Manufacturer : Grass. Serial numbers 58153 through 58174. Calibration performed by PCB Piezotronics Vibration Division. June 2005.

[10] Microphone Preamplifier Spec. Sheet. Model Number 426B03. PCB Piezotronics Vibration Division. Spec. Number 22760. ECN # 21214. December 2004.

[11] "LMS SCADAS III Programmable Quad Floating Amplifier (PQFA) Product Information". LMS International. October 2004.

[12] Elmore, W.C., Heald, M.A. "Physics of Waves". Dover Publications. 1969.

[13] "Uncertainty Analysis Inputs", e-mail from Matthew O'Connor, GENE Project Manager to David Galbally, GENE Engineer. January 16, 2006.

[14] "Question on GE Model Dryers", e-mail from Adam Kincaid, Area Representative of QuickParts Inc. to Matthew O'Connor, Project Manager of GE Nuclear Energy. January 16, 2006.